Generic Superheat Control of Evaporators using One Sensor and One Actuator

Master Thesis in Intelligent Autonomous Systems

Written by:
Casper Hillerup Lyhne
Erik Baasch Sørensen

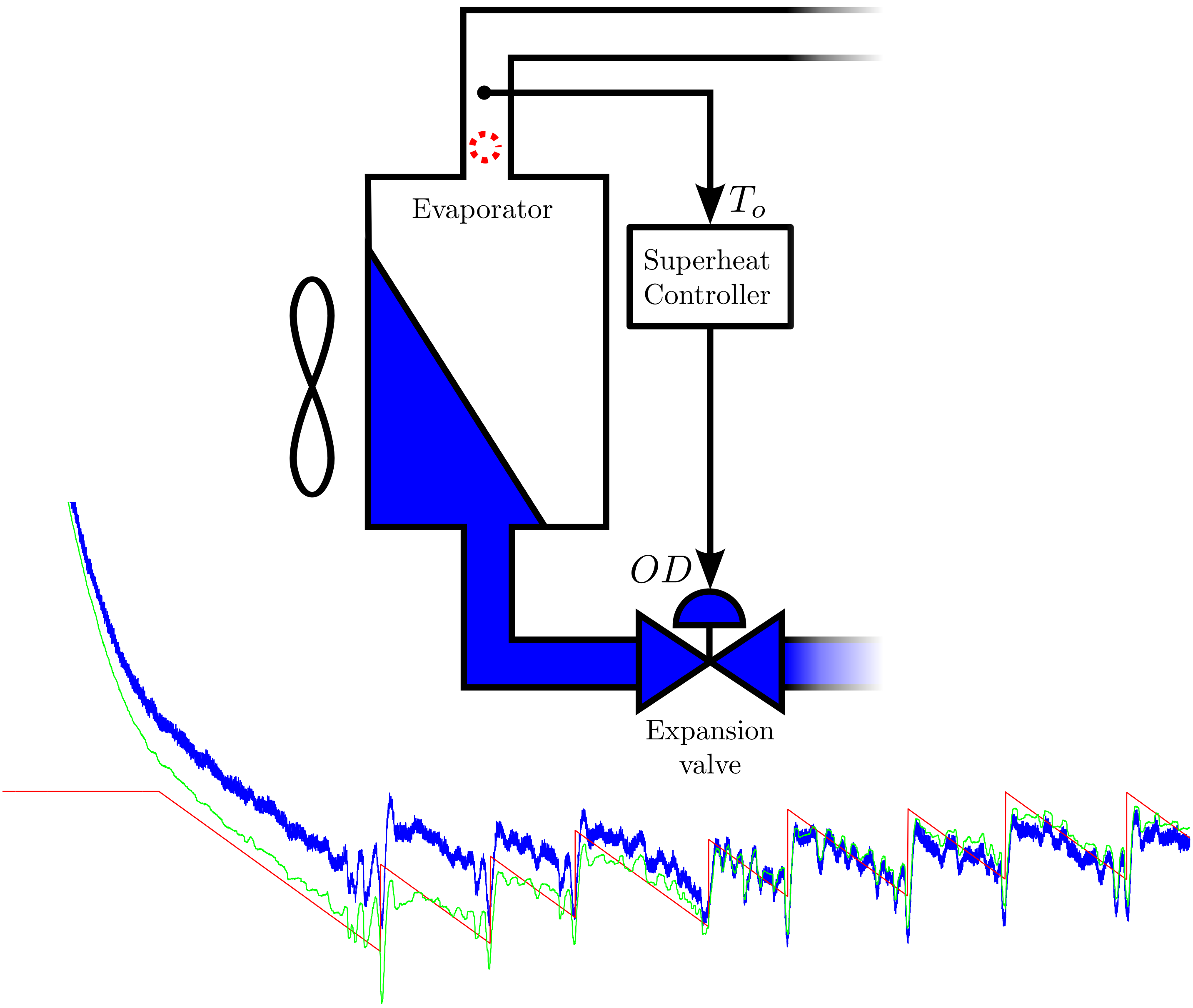

Section of Automation and Control
Department of Electronic Systems
Aalborg University
May 31st 2011

AALBORG UNIVERSITET

Department of Electronic Systems
Electronical Engineering
Frederik Bajers vej 7a
9220 Aalborg Øst
Tlf. 99 40 99 40
http://es.aau.dk

Title: Generic Superheat Control of Evaporators using One Sensor and One Actuator

Theme: Control Engineering

Project period: 1/9 2010 – 31/5 2011

Project group:
1034

Members of the group:
Casper Hillerup Lyhne
Erik Baasch Sørensen

Supervisor:
Henrik Rasmussen
Kasper Vinther
Roozbeh Izadi-Zamanabadi

Synopsis:

This master thesis deals with generic superheat control of an air conditioning system using one sensor and one actuator.

The system is analyzed and a model of the evaporator is derived that extends a conventional evaporator model. The extended model improves the understanding of superheat phenomenon in evaporators, which are unevenly filled.

A model based superheat controller, which utilizes all parameter knowledge, is constructed and tested on the test setup. The controller showed positive results, and showed the feasibility of the control structure.

The superheat controller was simplified to a generic controller that only measures the output temperature of the evaporator, and does not need knowledge of the system parameters beforehand. The controller was tested on two different test systems and showed positive results on both systems.

Feed forward was also included in the controller to help improve the performance of the controller with regard to disturbance rejection.

Number of copies: 6
Number of pages: 131
Appendices and attachments: Four appendices in the report, 1 CD enclosed
Project completed: 31/5 - 2011

Preface

This report is the documentation of a master thesis written by Casper Hillerup Lyhne and Erik Baasch Sørensen from the Section of Automation and Control under the Department of Electronic Systems at Aalborg University. The thesis was written during the fall semester 2010 and the spring semester 2011. For the master thesis it was chosen to work with the project "Generic Superheat Control of Evaporators using One Sensor and One Actuator". The report is addressed to censor and supervisors and other master students at Aalborg university.

The report is structured to represent the chronological order in which we worked with the project. To get an overview of the report, please turn to Section 1.4 on page 16.

References to external material are marked with an author and year of publication e.g. (Skovrup, 2000) throughout the report. A list of all the references can be seen in the end of the report.

A nomenclature of all the symbols used on the report can be found in Appendix C. The nomenclature can be folded out for easy access during reading.

With the report is a CD with the following content: all measurements from the experiments that were performed, the simulink models used to perform the experiments and some of the references used in this report and a digital copy of the report.

We would like to use this opportunity to thank Associate Professor Henrik Rasmussen from Aalborg University for his help and support, and his truly great technical insight and intuition into refrigeration systems. We would also like to thank Ph.D. student Kasper Vinther from Aalborg University for his help and support, his help with the alternative test setup and with writing the article about some of the methods developed in this thesis. Furthermore we would like to thank Associate Professor, Ph.D. EE. Roozbeh Izadi-Zamanabadi, and Danfoss in general, for disclosing initial ideas about possible approaches and giving us the opportunity to work with a very industry relevant project.

Casper Hillerup Lyhne

Erik Baasch Sørensen

Contents

Chapter 1

Introduction

Vapor-compression cycle cooling technologies are widely used in Heating Ventilation and Air Conditioning (HVAC), and the market is subject to intense competition. Any manufacturer able to reduce the production cost or increase the value of its vapor-compression cycle based products therefore has a significant advantage over the other manufacturers. Traditionally the evaporator of these systems has been controlled using a Thermostatic Expansion Valve (TEV). TEVs are cheap and reliable. They work with a broad range of systems, and they can be adjusted on site by a technician with no prior knowledge of the system parameters.

However, TEVs only allow one mode of control and their performance varies with the load on the system. On the contrary an algorithmic controlled valve allows more advanced types of control, such as distributed control of multiple systems e.g. refrigerators in supermarkets, control of special valves like the Danfoss EcoFlow^{TM} valve, or more efficient control using more sensors. Many of the more advanced algorithmic controllers are model based, and requires extensive knowledge of the model parameter, e.g. the method used in (Rasmussen and Larsen, 2011). Those methods lack the merits of the TEV, which can be implemented on different systems with minimal effort.

Therefore we develop a digital algorithmic controller which is generic like the TEV, while still allowing implementation of the features which are known from other digital algorithmic controllers. To make the system cheaper and more generic, we develop a digital algorithmic controller which does not use a pressure sensor, but only a temperature sensor. The temperature sensor can be surface mounted on the system. The algorithmic digital controller needs to interface with a digital Electric Expansion Valve (EEV).

We have not found any descriptions of controllers, which does not use at least two sensors for control. Therefore we investigate the possibilities ourselves, and develop a mathematical model of the system in order to gain a thorough understanding of the non-linear phenomena in the system. The knowledge is then exploited to make the controller.

The experiments used for the development of both the mathematical model and the controller were all conducted using an vapor-compression cycle air conditioning system as a test setup. The general principle of a vapor-compression cycle systems is described next.

1.1 Principle of a Vapor-compression Cycle Refrigeration System

In a vapor-compression cycle refrigeration system heat is removed from one area and expelled into another. It uses a refrigerant which is used to both absorb heat from the area that is to be cooled, and to release the heat to another area, i.e. the surroundings.

The system uses a pressure difference to adjust the boiling point of the refrigerant to make it either absorbs energy by evaporating, or lose heat by condensing. The refrigerant evaporates in the area to be cooled and condenses in the area where the heat should be disposed of; making the cold area colder and the warm area warmer. The basic refrigeration system consists of four components: a condenser (A), a valve (B), an evaporator (C) and a compressor (D). The four components are connected as shown in Figure 1.1.

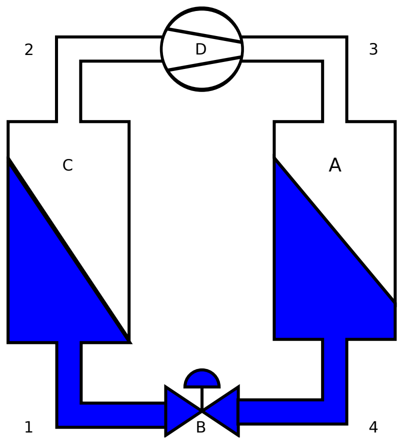

Figure 1.1: *The liquid refrigerant exits the condenser through the valve into the evaporator. Here it evaporates before it is compressed by the comressor and expelled into the condenser, where it cools and becomes liquid again.*

The pressure, enthalpy, and phase changes of the refrigerant are shown in Figure 1.2, where the letters correspond to the letters in Figure 1.1.

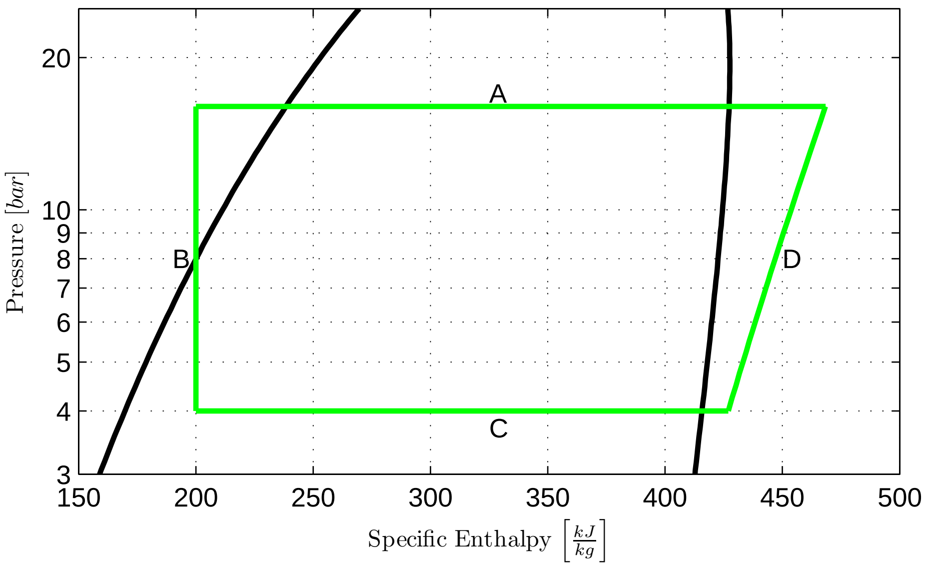

Figure 1.2: *Pressure-Enthalpy diagram with the vapor compression cycle indicated. The hot refrigerant is cooled under high pressure in the condenser (A) and looses energy. Through the valve it is released into the low pressure of the evaporator (B). Here it evaporates and takes energy from the surroundings thus cooling them (C). The refrigerant is compressed again (D) and released into the condenser.*

The refrigerant enters the evaporator as a mixture of gas and liquid at low pressure and low temperature (1). The pressure in the evaporator is so low that the boiling point of the refrigerant is lower than the ambient temperature of the evaporator. This causes the liquid to boil and evaporate, absorbing heat from the environment (C), thus cooling it. At the outlet of the evaporator the refrigerant has absorbed enough heat to change phase and consist of gas only. It is then heated beyond teh boling point or it becomes superheated (2).

After evaporating the low pressure gas enters the compressor. The compressor increases the pressure of the gas and heats it up in the process (D). The pressure is increased enough so its condensation temperature is higher than the ambient temperature in the warm area.

The high pressure and high temperature gas from the compressor enters the condenser (3), and cools until it reaches its dew point, where it begins to condense (A). As the refrigerant passes through the condenser it ejects heat to the environment. At the outlet of the condenser the refrigerant has ejected enough heat to change phase and consists of liquid only (4).

Before the refrigerant re-enters the evaporator it flows through an adjustable valve (B). The valve is used to adjust the pressure in the evaporator and thus adjust the boiling temperature. As the refrigerant flows through the valve it is subject to a sudden pressure drop. This pressure drop causes the temperature of the refrigerant to drop, and some of the refrigerant evaporates. The refrigerant exits the valve at low pressure and low temperature.

1.1.1 Performance

The performance of any vapor compression cycle depends on many variables (Larsen, 2005), of which many are mutually dependent. One of them is the pressure difference between the condenser and the evaporator. If the pressure difference is high, the compressor needs to do more work, thus using more energy. (Duprez et al., 2007) So to keep the efficiency high it is important to keep the maximum cooling effect at the lowest possible pressure difference. The way to do this is to maximize the heat transfer from the ambient air to and from the evaporator and the condenser, respectively. This can be done partly by proper ventilation of the two components. The efficiency can also be improved by optimizing the amount of refrigerant in the system, ensuring the subcooled zone of the condenser is as short as possible at the set point, to maximize the length of the two phase zone, and thereby the heat transfer. The balance between these variables cannot be uniquely expressed and may be optimized online as shown in (Larsen, 2005).

The performance parameter central to this study is to keep the heat transfer of the evaporator as high as possible along the entire length of the evaporator. This can be done by controlling the amount of refrigerant entering the evaporator by choosing the opening degree of the valve, which makes liquid refrigerant present in the entire evaporator, but not in the compressor. As the system always consumes the least energy in this state.

The required opening degree to achieve this varies as the load of the system varies, and therefore it needs to be controlled. This is one of the most important aspects of maximizing energy efficiency of vapor compression cycle plants.

Measurements of the fraction of the evaporator which is not efficiently utilized are needed, to control the process. Typically the measurements are of the output temperature of the evaporator, T_o and the boiling point in the evaporator T_e. The latter either by direct temperature measurement, or by conversion from a pressure measurement. The difference between the measurements are called the superheat temperature of the evaporator denoted T_{sh} in this thesis, as it expresses how much the gas has heated up after it evaporated. This in turn is also an expression of how much of the evaporator is efficiently utilized. The higher superheat temperature, the less efficient the evaporator is.

A controller must therefore try to minimize the superheat in order to maximize the efficiency of the system. This research traeats methods on how to do that, even without a measurement of the boiling point. The next section describes the specific vapor compression cycle test setup available for this research.

1.2 The Test Setup

This section describes the specific test setup available for the research. Figure 1.3 shows the test setup and the actuators and sensors mounted on the setup.

The evaporator and the condenser of the system are mounted in two different rooms, the cold room and the warm room. The warm room with the condenser can be ventilated with air from the outside to simulate a situation where the condenser is located outside. This is shown in Figure

1.3 as the fan controlled by f_{hvac}.

The cooling capacity of the system is so high that it would quickly cool the cold room with the evaporator to a low temperature that is out of range of a normal air conditioning system. Therefore the system is artificially loaded by ventilating air from the warm room into the cold room. This is shown in Figure 1.3 as the fan controlled by f_{room}. The evaporator is ventilated to create air flow around the evaporator. The fan used for this is controlled manually, and during this research it is always set to full speed to give consistent measurements. There is also a fan, which ventilates the condenser, this fan can be controlled automatically by the f_{con} signal, contrary to that of the evaporator.

The system has a Danfoss EcoFlow^{TM} valve, which is a special electronic expansion valve which allows digital control of the flow of refrigerant into each pipe of the evaporator. The opening degree of this valve can be controlled automatically.

The compressor compresses the superheated refrigerant from the outlet of the evaporator and releases it under high pressure into the condenser. The speed of the compressor can be digitally controlled, however it has a minimum speed.

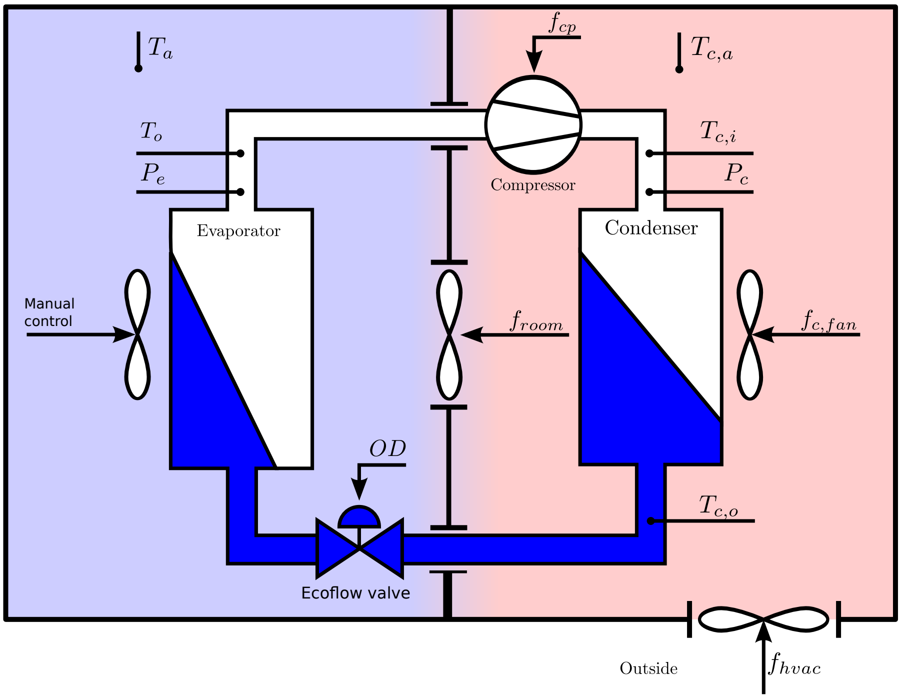

Figure 1.3: *Overview of the sensors and actuators connected to the test setup.*

There are seven sensors in the system, where five of them are temperature sensors. The temperature of the room with the evaporator and the condenser is measured by T_a and $T_{c,a}$ respectively. The plant itself has three temperature sensors; T_o, $T_{c,i}$ and $T_{c,o}$. They measure the temperature out of the evaporator, into the condenser and out of the condenser respectively. The plant has two pressure sensors: P_e and P_c, which measure the pressure in the evaporator and the condenser respectively. All the sensors of the plant are shown in Figure 1.3.

1.2.1 Common Setup

The test setup provides an array of sensors meant to be used for research in air conditioning technologies. However, the air conditioning units of commercial products are usually equipped with only two sensors and a valve, for superheat control. Often in the form of a TEV, but also as a separate digital algorithmic controller in conjunction with an EEV. This is shown in Figure 1.4.

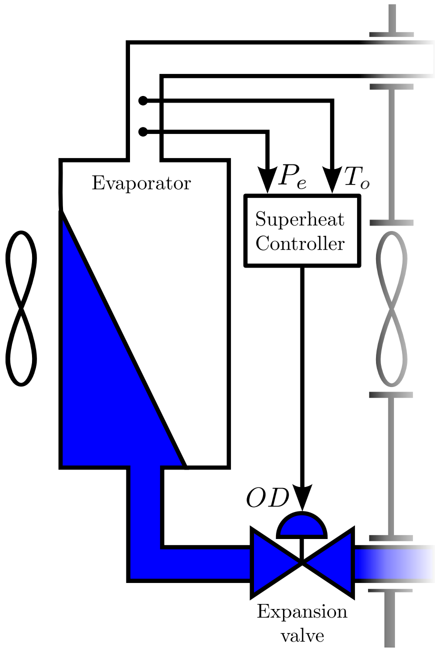

Figure 1.4: *Overview of the sensors, actuators and controller connected in a common system.*

The sensors available for control typically measure the pressure of the evaporator, P_e and the output temperature of the gas in the evaporator T_o, as described in Section 1.1. An algorithmic controller uses the available sensors and actuators to keep the superheat low without overflowing the evaporator. However, it is desirable to save the pressure sensor, as it would reduce the overall cost of the system.

1.2.2 Desired Setup

The system described in Section 1.2.1 uses a pressure sensor. It is desirable to make a digital algorithmic superheat controller without the use of the pressure sensor, which is still generic like a TEV. Saving the pressure sensor reduces the production cost of an air conditioning system. The advantage of using a digital algorithmic controller is to allow for advanced modes of control such as distributed control of refrigerators in supermarkets. The desired setup is shown in Figure 1.5.

The temperature of the gas as it leaves the evaporator is the only measurement available for control, when the pressure sensor is removed. As the valve in the setup makes it possible to precisely control the flow of each pipe of the evaporator, this is used as the control actuator over the compressor. In most systems the temperature of the room to be cooled is controlled. This can be done in an outer control loop using the compressor, and the T_a sensor. However, the focus of this research lies in superheat control.

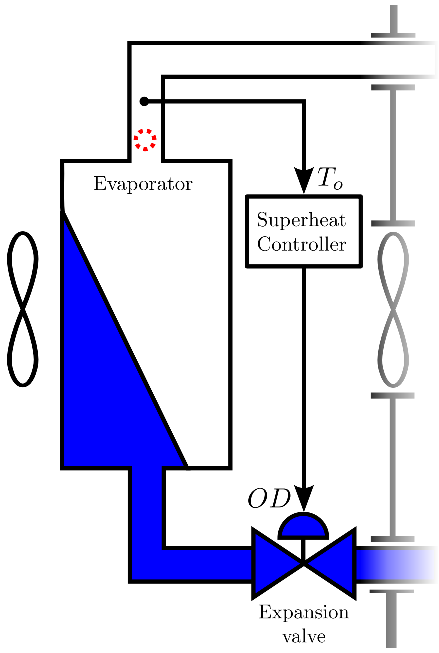

Figure 1.5: *Overview of the sensors and actuators connected in a desired system. The P_e sensor is no longer used, which makes T_o the only available sensor for control.*

The output temperature of the evaporator apparently carries no information about the superheat temperature, which should be minimized in order to optimize performance of the system. If the controller must be generic, it should adapt itself to the system it has been implemented on. In this thesis we investigate the possibilities for superheat control without a pressure sensor.

1.3 Challenges

Since the controller should only use the measurement of T_o for superheat control, it is necessary to gain a better understanding of the phenomenon related to the superheat temperature, and use the knowledge to estimate the superheat. Therefore a mathematical model of the evaporator of the test setup should be developed which is particularly good at explaining superheat related phenomenon, in the hope that the knowledge is usable in designing the desired controller. Then a controller should be developed, which uses all the available knowledge from the specific system. If this controller is successful, it should be simplified, generalized, and made adaptive in order to make it generic like a TEV. In order to verify that the controller is indeed generic, it should be tested on different systems. The challenges to be undertaken can be summarized as follows

- Understand the system in general, and particularly phenomenon related to the superheat.
- Use the gained understanding to estimate the superheat from T_o alone.
- Develop a controller, which is independent of a P_e measurement.
- Generalize the controller to make it work on different systems.
- Show that it works on different systems.

The challenges are undertaken in the same order as they are presented. In Section 1.5 there is a summary of contributions made during the research. The next section is a thesis outline, where the structure of the thesis is summarized.

1.4 Thesis Outline

The next sections treat the understanding, verification and improvement of the conventional models of the components of an air condition system. Then a model based controller is developed, which uses all the obtained knowledge of the system, while only using the T_o sensor. The controller is then simplified, generalized, and made adaptive. The result is a generic controller with similar performance to the system specific controller. Finally the disturbance rejection of the controller is improved using feed forward. A short description of each chapter in the thesis follows.

- In Chapter 2 mathematical models of the compressor and the EcoFlow^{TM} valve are developed to estimate the mass flows, and their parameters are estimated. This is important, because if the mass flows are not correct, it obscures the results of the evaporator model.
- In Chapter 3 a conventional low order model of the evaporator based on known models from the literature is derived. Its parameters are estimated, and the results are evaluated in conjunction with the new models for the valve and the compressor.
- A new model is developed in Chapter 4 using the experience gained from the conventional model. The model explains phenomenon related to the superheat temperature better than the conventional model. Especially phenomenon related to different heat transfer coefficients in different parts of the evaporator are investigated and incorporated into the model. In the process a new phenomenon of oscillating output temperatures in the evaporator is discovered and described.
- In Chapter 5 a controller is developed, which only uses one temperature sensor for superheat control. The controller is based on the knowledge gained from the improved model of the system. It uses a linearized version of the model in an observer. The controller is tested and evaluated. Even though this is not a generic controller, it serves as a starting point for a more general version.
- In Chapter 6 the previously developed controller is simplified, generalized, and made independent of model parameters. This allows it to be used without prior knowledge of the target system model parameters. The controller is tested and evaluated.
- In Chapter 7 the simplified controller is tested using another test setup with a different behavior. This is to study the ability of the controller to function on different systems.
- In Chapter 8 a feed forward signal is introduced to the controller to increase its performance in tracking a varying reference signal.

1.5 Contributions

Several new discoveries and model developments were made during the research, while other parts are known material. Our contributions are summarized here, for clarity.

A new way of estimating the intake volume of the compressor in the system, and thereby its mass flow, was developed. This is described in Subsection 2.1.5. The method uses the ideal enthalpy difference, the actual enthalpy difference, and the power consumption to calculate the mass flow. The method has yet to be verified using a flow meter, but its results are plausible, and make expected predictions.

The new EcoFlow^{TM} valve allows the flow into each pipe of the evaporator to be controlled. A mathematical model of the Ecoflow^{TM} valve, not found in literature, has been developed. The model is an extension of the conventional model of an expansion valve based on the Bernoulli equation. However, it incorporates the pulse width modulation like effects of the Ecoflow^{TM} valve, and its ability to control the flow into each pipe individually. This is described in Subsection 2.2.3.

A new model of the evaporator was developed. The model accounts for the underlying physical phenomenon responsible for the uneven filling of pipes in the evaporator by introducing a separate state for the length of the two-phase zone in each pipe, and one extra parameter which captures the uneven load on each pipe. The model captures phenomenon related to the superheat temperature, and makes the model fit very well to the measurements. This is described in Chapter 4.

A new surprising phenomenon was discovered. At low superheat temperatures, the output temperature of the evaporator began to exhibit oscillatory behavior, when expected to be steady. This new phenomenon is described in Section 4.3, and later used in the control algorithm for the superheat control.

A new controller was developed. The controller utilizes the oscillatory behavior at low superheat to save the pressure sensor. The controller is simplified and generalized to fit other systems without prior system knowledge. The controller and its simplified version are described in Chapter 5 and 6 respectively.

A scientific paper about the simplified controller was written together with Kasper Vinther and Henrik Rasmussen. The draft of the article can be found in Appendix D.

Chapter 2

Compressor and Valve Models

A mathematical model of the air conditioning system is derived to gain an understanding of the behavior of the system ans as a foundation for simulations of the system. The purpose of the model is to give an understanding of the system, and to be used in the design of a controller, whcih is based on the changes in output temperature from the evaporator.

For the purpose of modeling, the system is divided into four components: The Scroll Compressor, the EcoFlow^{TM} Valve, the Evaporator and the Condenser. The division of the system can be seen in Figure 2.1, where the component borders are marked with red lines.

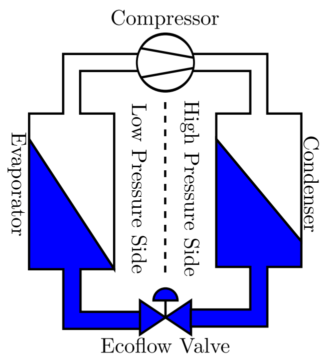

Figure 2.1: *Illustration of the entire system. The system is divided into four components: the condenser, evaporator valve and compressor. This chapter covers the model of the valve and compressor.*

In this chapter the models of the compressor and the valve are derived. The parameters of the models are found from experiments conducted using the test setup. A model for the evaporator is derived in the next chapter

2.1 Compressor

The compressor in the test setup is a scroll compressor. It works by moving a spiral in circles inside a stationary spiral. The circulating movement creates closed pockets of gas, which becomes continuously smaller. This compresses the trapped gas. The principle is shown in Figure 2.2.

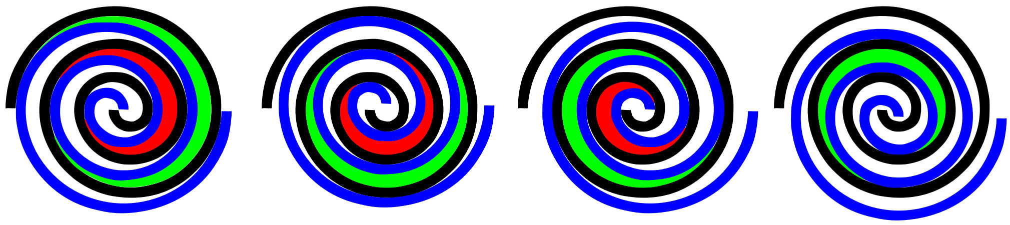

Figure 2.2: *Principle of how gas is compressed inside a scroll compressor. Two pockets of gas are present. The pockets are being pushed in a spiral towards the middle, where the gas is expelled. The pockets are reduced in size during the movement, thus compressing the gas.*

Figure 2.2 shows a complete cycle at quarter cycle intervals. The leftmost figure shows the beginning of a cycle where a volume of gas, marked with green, has just been closed off from the inlet. As the spiral cycles, the green pocket of gas is pushed inwards between the two spirals, as shown in the following three figures. The green pocket is reduced in size during the cycle, thus compression the refrigeratn. The gas has not been pushed all the way through the compressor in one revolution. In the following revolution the gas is further compressed, as shown with the volume marked with red. When the gas reaches the center of the spirals, the compression is done, and the gas leaves the compressor.

From the description of the scroll compressor it is shown, that the mass flow through the compressor is proportional to the size of the intake volume of the compressor. This is the volume marked with green in the leftmost figure in Figure 2.2. Furthermore, the mass flow is proportional with the density of the gas and the speed of the compressor. As the compressor compresses the refrigerant, work is done on the refrigerant, which leads to an increase in its internal energy.

To model the behavior of the compressor, a model for the mass flow through the compressor is needed. Furthermore, an expression of the temperature out of the compressor has to be derived.

In this section a model of the temperature is shown based on (He et al., 1998). After the derivation of the model, it is compared to measured data from the test setup. After the test, the model of the temperature is modified based on the data and refitted to achieve a more precise model.

After the derivation of the temperature model, the model of the mass flow is derived and fitted to test data. The mass flow model is also based on (He et al., 1998).

2.1.1 Adiabatic Temperature Model

During the compression of the refrigerant in the compressor work is done on the refrigerant. This leads to an increase in temperature. With the assumption that the process is an adiabatic process, i.e. there is no heat transfer in the refrigerant during the compression; the enthalpy chance must follow a line of constant entropy.

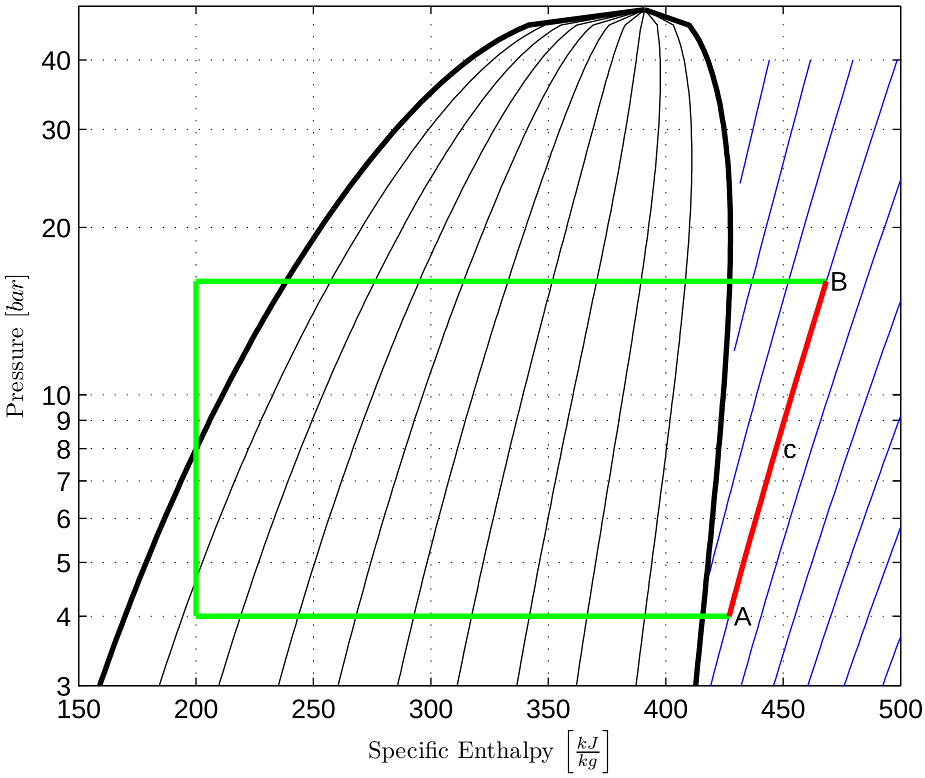

Figure 2.3: *Illustration of the movement of the refrigerant on a P-h diagram. The movement in the compressor is marked with red.*

Figure 2.3 shows a pressure-enthalpy diagram for the refrigerant. The point A on the figure shows the point where the refrigerant exits the evaporator. As the entropy of the refrigerant does not change in the compressor, the refrigerant follows the line c, marked with red on the figure, which follows a line of constant entropy. The point B is the point on the line, where the pressure corresponds to the condenser pressure.

With the assumption that the refrigerant is an ideal gas and the assumption of an adiabatic process, the change in temperature can be calculated by

$$\frac{T_{c,i}}{T_o} = \left(\frac{P_c}{P_e}\right)^{\frac{C_p - C_v}{C_p}} \qquad [-] \qquad (2.1)$$

where T_o and $T_{c,i}$ are the temperature of the refrigerant in to and out of the compressor respectively, P_c and P_e are the pressure in the condenser and in the evaporator respectively and C_p and C_v are the molar specific heat at constant pressure and volume respectively. The equation is based on the ideal gas law and the first law of thermodynamics. The full derivation of the equation can be found in Appendix A.

Alternatively, the temperature can be calculated using an advanced model of the specific gas, which does not assume that the gas is ideal. This model has been implemented in a software library called RefrigEquations (Skovrup, 2000). The difference between the results of an adiabatic compression calculated by RefrigEquations and the model of an ideal gas is shown in Figure 2.4

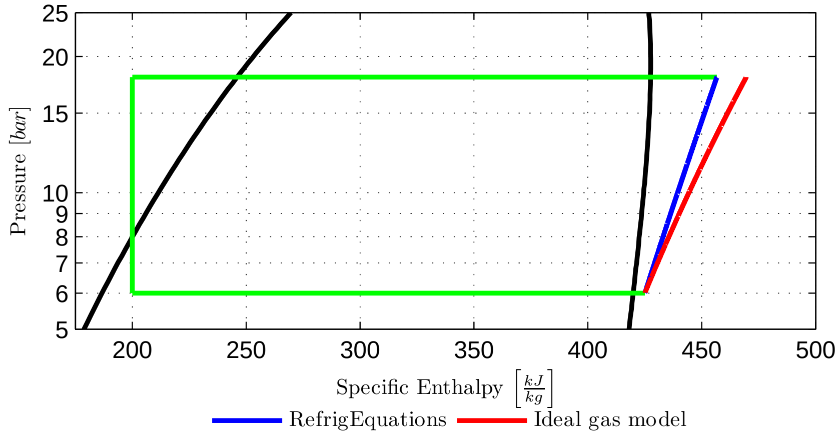

Figure 2.4: *Predictions of $T_{c,i}$ in RefriqEquations compared to ideal gas model. The compression is simulated for a typical operating pressure range with P_e set to 6 bar and P_c to 18 bar with 5 degrees superheat.*

It is noted that the model of an ideal gas predicts the output temperature out of the compressor to be significantly higher that the advanced model of the refrigerant. Therefore, the RefrigEquations is used to calculate the output temperature of the compressor.

2.1.2 Evaluation of the Temperature Model

The model was compared to a dataset measured from an experiment with the system. The experiment was designed to excite the pressure of both the condenser and the evaporator. This was done by making steps in both the speed of the compressor, and in the opening degree of the valve, as seen in Figure 2.5.

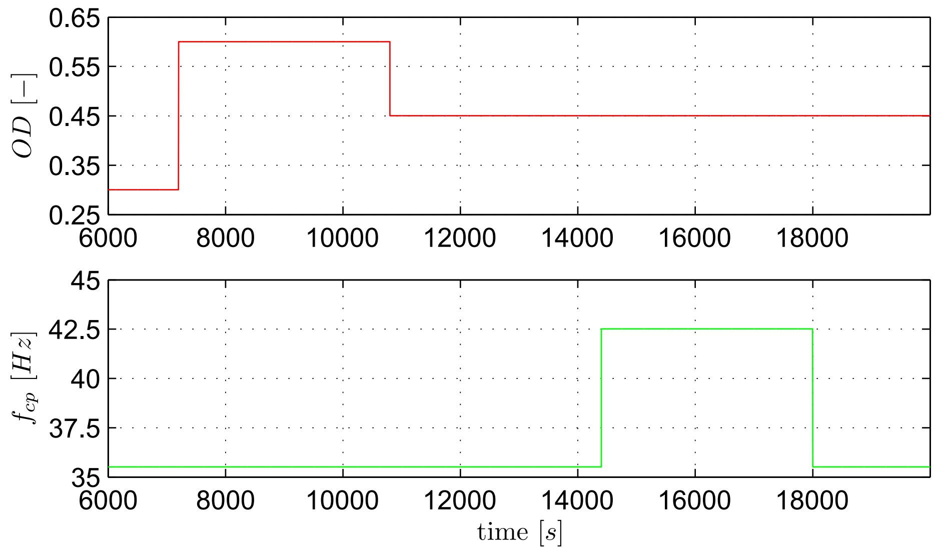

Figure 2.5: *Input signals from the experiment used to estimate the parameters. OD is the opening degree of the valve and f_{cp} is the speed of the compressor.*

The result of the experiment compared to the simulated temperature is shown in Figure 2.6.

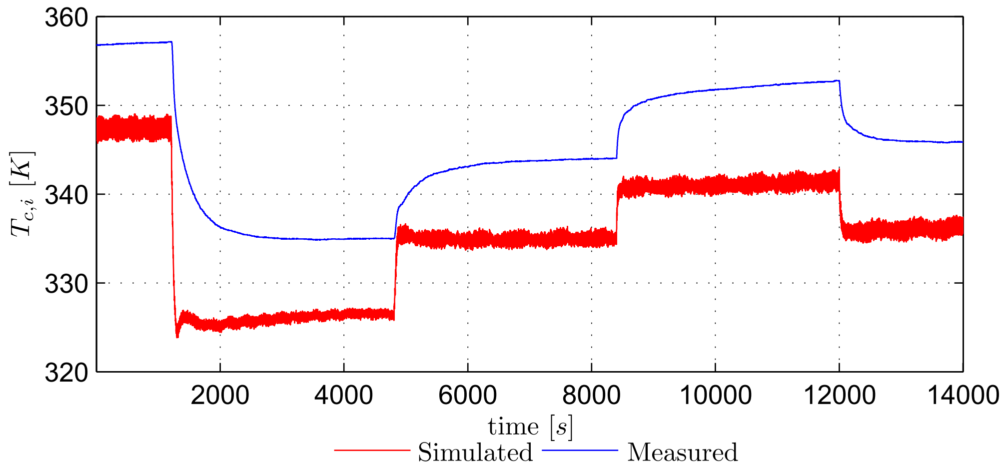

Figure 2.6: *Simulation versus measurements of $T_{c,i}$. The actual temperature of the refrigerant is higher than the one predicted with the adiabatic model. Also the adiabatic model does not have dynamics, which the actual system does. The noise in the simulation comes from the pressure measurements it is based on.*

It is shown in Figure 2.6, that the model does not capture the measurements accurately. It looks like there is both an offset and a time constant that the model does not account for. A good model of the compressor must capture the steady state temperature and the dynamics better. An improved model is derived in the next subsection.

2.1.3 Modification of the Temperature Model

The fitting of the model to the measured data shows two problems. The calculated model shows an offset error from the measured $T_{c,i}$, and there are dynamics in the measured data that does not exist in the model.

The measurements show that the gas is about 10 degrees hotter than that predicted by the simulation. One possible reason for this may be that the excess heat from the electric motor of the compressor heats the refrigerant, and thereby causes what looks like an offset error.The compression process is therefore seen as an adiabatic compression of the non-ideal gas, but where the extra enthalpy from the loss of the compressor is added afterwards. The loss in the compressor is assumed to be proportional to the work done in the adiabatic compression, and can be described in terms of a coefficient of efficiency of the compressor. Since the gas is not ideal, RefrigEquations is used to calculate the compression. In the following equations the calculation of compression with the extra enthalpy due to loss is shown:

$$\begin{aligned} S &= STP\left(T_o, P_e\right) \\ \Delta h_{cp} &= h\left(S, P_c\right) - h\left(S, P_e\right) \\ \Delta h'_{cp} &= \frac{\Delta h_{cp}}{e_{cp}} \end{aligned} \tag{2.2}$$

where S is the entropy of the gas as it enters the compressor, Δh_{cp} is the increase in specific enthalpy from adiabatic compression and e_{cp} is the coefficient of efficiency of the compressor. The result of the equations is the change of specific enthalpy during the compression, when the power loss in the compressor is included.

The resulting temperature of the refrigerant after the compression can be calculated as

$$\begin{aligned} \bar{h}_{c,i} &= h_o + \Delta h'_{cp} \\ \bar{T}_{c,i} &= T\left(\bar{h}_{c,i}, P_c\right) \end{aligned} \tag{2.3}$$

where h_o is the specific enthalpy of the refrigerant at the input of the compressor, $\bar{h}_{c,i}$ is the enthalpy at the input of the condenser when in steady state and $\bar{T}_{c,i}$ is the corresponding temperature. This model of the compression was fitted to the measurements in an experiment. The result from the experiment is shown in Figure 2.7.

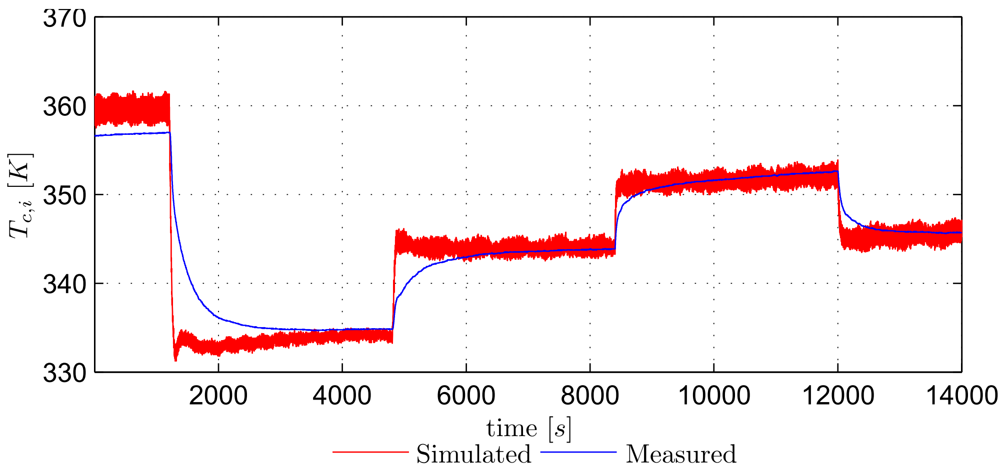

Figure 2.7: *Predictions of output temperature of the compressor using RefrigEquations and the extra enthalpy from heating, compared to the measured temperature. Note that the steady state level fits well, but the dynamics does not.*

It is observed that the steady state values of the output temperature now fit the data reasonably well. The coefficient of efficiency was estimated to 76% which seems reasonable. The fit of the steady state temperature is considered good enough. However, the dynamics of the compressor still needs to be modeled.

The data shows that the output temperature has dynamics, and it has been shown that excess heat from the motor of the compressor does indeed enter the refrigerant. During the compression the refrigerant flows along a large surface area of metal belonging to the compressor. Therefore a heat transfer between the refrigerant and the metal of the compressor occurs. Based on this, it is assumed that the mass of the compressor acts as a heat capacitor, accounting for the dynamics of the systems shown in the measurements.

This effect is considered as a low pass filtering of the temperature of the refrigerant out of the compressor. When the gas is compressed it is heated, but because of the large surface area of the walls the gas leaves the compressor at a temperature close to that of the compressor walls. In time the walls are heated by the gas, until they have the same temperature as the adiabatic compressed gas. Under the assumption that the gas leaves the compressor at exactly the same temperature as the walls of the compressor, a first order model was derived.

The walls of the compressor are considered as the control volume. When it is assumed that the only energy transfer is the heat transfer between the refrigerant and the wall, the energy balance of the wall can be expressed as

$$\dot{Q}_{cp,w} = \alpha_{cp} \cdot A_{cp} \cdot (\bar{T}_{c,i} - T_{cp,w}) \qquad [J/s] \qquad (2.4)$$

where $\dot{Q}_{cp,w}$ is the energy change in the wall, α_{cp} is the heat transfer coefficient, A_{cp} is the surface area and $T_{cp,w}$ is the temperature of the wall. Based on the energy balance, the change in temperature of the wall can be expressed as

$$\dot{T}_{cp,w} = \frac{\alpha_{cp} \cdot A_{cp}}{c_{cp,w} \cdot M_{cp,w}} \cdot (\bar{T}_{c,i} - T_{cp,w}) \qquad [K/s] \qquad (2.5)$$

where $\dot{T}_{cp,w}$ is the change in temperature of the compressor wall, $c_{cp,w}$ is the heat capacity of the wall and $M_{cp,w}$ is the mass of the wall. The assumption that the gas, which leaves the compressor, has the same temperature as the walls of the compressor, leads to the output equation

$$T_{c,i} = T_{cp,w} \qquad [K/s] \qquad (2.6)$$

where $T_{c,i}$ is the temperature at the inlet of the condenser. The first order system is illustrated in Figure 2.8.

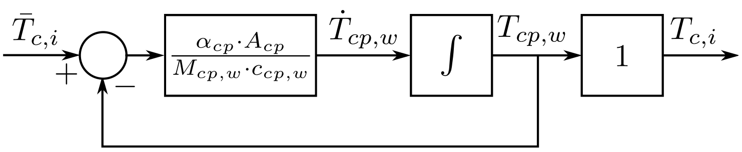

Figure 2.8: *Block diagram of the first order filter effect of the compressor walls.*

The new model was fitted to the data set as well. The result is shown in Figure 2.9.

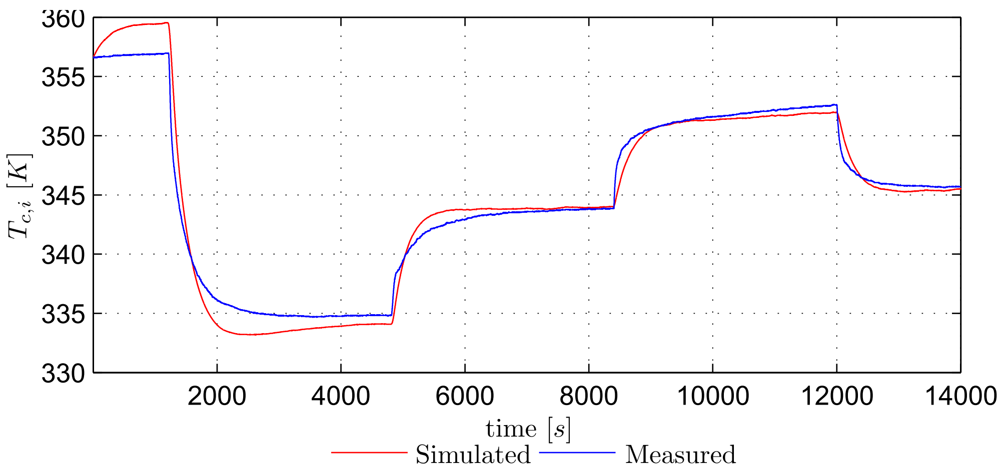

Figure 2.9: *Simulation versus measurements of $T_{c,i}$ when both the additional enthalpy from heating, and the first order filter is included in the model.*

When compared to the result shown in Figure 2.7, it is seen, that the fit has improved. The time constant introduced has been estimated to about 198 seconds or 3 minutes and 18 seconds. The model of the temperature follows the measured temperature, although there are some higher order effects, which are not captured by the model.

An advanced model of the refrigerant, implemented in a software library called RefrigEquations, was used to predict the temperature of the adiabatic compression process. This was about 10 degrees inaccurate compared to the data. This leads to the inclusion of the coefficient of efficiency of the compressor, and its effect on the output temperature. Furthermore the data displayed characteristics that indicated a filtering effect from the metal walls of the compressor. This was approximated as a first order low pass filter. The new model of the temperature leads to an extra state in the model of the refrigeration system, and two extra parameters to be estimated. These were the time constant of the filtering effect, and the coefficient of efficiency of the compressor.

2.1.4 Model of the Mass Flow

From the description of the scroll compressor it is seen, that the volume flow through the compressor is the size of the inlet volume of the compressor multiplied with the speed of the compressor. The equation

$$\dot{V}_{cp} = V_{cp,i} \cdot f_{cp} \qquad \left[{}^{m^3}\!/\!{}_{s}\right] \qquad (2.7)$$

describes the volume flow through the compressor, when $V_{cp,i}$ is the intake volume and f_{cp} is the speed of the compressor.

The mass flow of the compressor can be calculated from Equation (2.7) by multiplying with the density of the gas, ρ_g, which leads to the equation

$$\dot{m}_{cp} = \rho_g \cdot V_{cp,i} \cdot f_{cp} \qquad \left[{}^{kg}\!/\!{}_{s}\right] \qquad (2.8)$$

The density is dependent on the pressure in the inlet of the compressor, which is assumed to be the same pressure as in the evaporator.

The speed of the compressor has to be calculated from the control signal to the compressor. The control signal to the compressor is a number between zero and ten. A control signal of zero corresponds to the minimum speed of the compressor, $f_{cp,min}$. A control signal of ten corresponds to the maximum speed, $f_{cp,max}$. The speed of the compressor is linear in between the minimum and maximum. Based on this, the speed of the compressor can be calculated by

$$f_{cp} = f_{cp,min} + f_{cp,cont} \cdot \frac{f_{cp,max} - f_{cp,min}}{10} \qquad [Hz] \qquad (2.9)$$

where $f_{cp,cont}$ is the control signal to the compressor.

2.1.5 Fitting of the Mass Flow Model

The only unknown parameter in the mass flow equation is the intake volume of the compressor. The mass flow of the system could not be measured directly since there is no flow meter in the system. Therefore a new approach for estimating the intake volume was needed. The idea is that the power consumption of the compressor and the temperature change of the refrigerant through the compressor can be used to estimate the mass flow. This was done by reading the power consumption from the display of the inverter of the compressor. With the assumption that there is no heat loss from the compressor to the air, the enthalpy gain of the refrigerant during the compression must equal the power consumption of the compressor. As the temperature before and after the compressor, and the enthalpy gain was known, $\dot{m}_{cp}$ was calculated by the equation

$$\dot{m}_{cp} = \frac{P_{cp,meas}}{h_{c,i} - h_o} \qquad [kg/s] \qquad (2.10)$$

where $P_{cp,meas}$ is the measured power consumption of the compressor and $h_{c,i}$ is the specific enthalpy of the refrigerant as it enters the condenser. With m_{cp} and f_{cp} known, the intake volume of the compressor, $V_{cp,i}$, was fitted to match the mass flow. This way of estimating the mass flow has not been found in the literature.

The intake volume was estimated based on four operating points. The measured power consumption and the calculated power consumption based on the estimated intake volume, is shown in Table 2.1.

f_{cp} $[Hz]$	$P_{cp,meas}$ $[kW]$	$P_{cp,sim}$ $[kW]$	$\dot{m}_{cp}$ $[g/s]$	$P_{cooling}$ $[kW]$
35.5	1.21	1.2072	38.1	7.375
39.0	1.37	1.3788	41.4	7.902
46.0	1.66	1.6584	45.2	8.799
49.5	1.81	1.8057	48.0	9.323

Table 2.1: *Table of predicted and measured power consumption at different compressor speeds when $V_{cp,i}$ has been fitted.*

As it is shown in the table, the measured and calculated power consumptions fit at all four operating points. The estimated intake volume is

$$V_{cp,i} = 39.34 \cdot 10^{-6} \qquad [m^3] \qquad (2.11)$$

This is in the expected region, since it predicts cooling powers between 7.375 and 9.323 $[kW]$ as shown in Table 2.1. This range is the expected for this particular system. The cooling powers have been calculated using the formula

$$P_{cooling} = \dot{m}_{cp} \cdot (h_i - h_o) \qquad [W] \qquad (2.12)$$

The cooling power is the specific enthalpy change in the evaporator multiplied with the mass flow. Based on this, the mass flow is thought to be accurate. A flow meter should be used if the mass flow is to be estimated more accurately.

2.2 EcoFlow Valve

The valve mounted in the system is an Danfoss EcoFlow^{TM} valve. The valve is used in conjunction with an evaporator which has four parallel pipes for refrigerant. The valve can dose the amount of refrigerant entering each individual pipe. The distribution of refrigerant into the four pipes can be set by a control signal. The Ecoflow^{TM} valve does this with a stepper motor, which directs the flow into one pipe at the time, with a closed position in between each period. The ratio between the time the valve is letting refrigerant enter the pipes and the time it does not, is controlled by an opening degree signal to the valve. This corresponds to the opening degree of a traditional EEV.

The modeling of the EcoFlow^{TM} valve is divided into two parts. First a model of the mass flow through the Ecoflow^{TM} valve, which is based on Bernoulli's equation also used in (He et al., 1998), is derived. Its parameters are then fitted to make the mass flow of the valve match that of the compressor when the system is in steady state. The fit is evaluated and it is decided to modify the model to better describe the Ecoflow^{TM} valve. It is then refitted to the data.

The second part of the model of the EcoFlow^{TM} valve treats the special characteristics and timings of the mass flows in each of the four pipes.

2.2.1 Model Based on Bernoulli's Equation

Traditionally the valves of refrigeration systems have been expansion valves, and have been modeled as such. The valve of this system can be seen as an expansion valve that is pulse width modulated between fully open and completely closed. An expansion valve can be seen as a tube which changes diameter. This is shown in Figure 2.10.

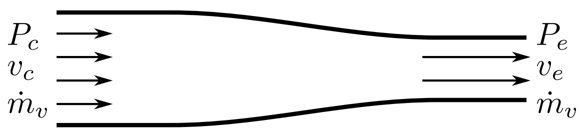

Figure 2.10: *The flow must satisfy Bernoulli's equation throughout the valve. The flow has low speed in the beginning and high speed in the end.*

It is assumed that the flow through the valve is laminar, non-viscous and that the liquid refrigerant is incompressible. This means that the motion of the fluid is governed by Bernoulli's equation (Raymond A. Serway, 2004, p. 434) given as

$$\frac{1}{2} \cdot v^2 + g \cdot z + \frac{p}{\rho} = c \qquad [J/kg] \qquad (2.13)$$

Where v is the speed of the fluid, z is the elevation and g is the gravitational constant. The equation is applied to the input from the condenser and the output to the evaporator to get.

$$\frac{1}{2} \cdot v_c^2 + g \cdot z + \frac{P_c}{\rho_l} = \frac{1}{2} \cdot v_e^2 + g \cdot z + \frac{P_e}{\rho_l} \qquad [J/kg] \qquad (2.14)$$

Where P_e and P_c is the pressure of the evaporator and the condenser respectively. Also v_e and v_c

are the speed of the fluid in and out of the valve. The constant ρ_l is the density of the fluid. The speed of the fluid v_e and v_c can be expressed as.

$$v_c = \frac{\dot{m}_v}{A_c \cdot \rho_l} \qquad [m/s] \qquad (2.15)$$

$$v_e = \frac{\dot{m}_v}{A_e \cdot \rho_l} \qquad [m/s] \qquad (2.16)$$

Where A_c and A_e are the cross section area of the pipe before and after the valve. $\dot{m}_v$ are the mass flow through the valve. When Equation (2.15) and (2.16) are substituted into Equation (2.14), the elevation terms are neglected, and $\dot{m}_v$ is isolated you get

$$\dot{m}_v = \sqrt{P_c - P_e} \cdot \frac{\sqrt{\rho_l}}{\sqrt{\frac{1}{2}\left(\frac{1}{A_e^2} - \frac{1}{A_c^2}\right)}} \qquad [kg/s] \qquad (2.17)$$

$$\dot{m}_v = \sqrt{P_c - P_e} \cdot \frac{\sqrt{\rho_l}}{\sqrt{R_v}} \qquad [kg/s] \qquad (2.18)$$

Where R_v is a constant that describes the resistance in the valve. This applies to the system when the valve is fully open. However, the flow through the EcoFlow^{TM} valve can be controlled via the *OD* input signal. *OD* is a number between one and zero, and the flow is assumed to be linear with respect to *OD*. In reality *OD* corresponds to the proportion of the time the valve is fully opened. Otherwise the valve is closed. With the assumption that the pulse frequency is sufficiently short, the flow can be assumed to be the average over one period. The model of the flow through the valve can therefore be described as

$$\dot{m}_v = OD \cdot \sqrt{P_c - P_e} \cdot \frac{\sqrt{\rho_l}}{\sqrt{R_v}} \qquad [kg/s] \qquad (2.19)$$

2.2.2 Fitting of the Model

The model has been implemented in the simulation software and R_v has been fitted to make the best possible fit to the measurements. The flow was measured by estimating the flow through the compressor, $\dot{m}_{cp}$, and then assuming the flow through the valve and compressor to be the same in steady state. Figure 2.11 shows the ratio between the flow of the compressor and that of the valve, when R_v is fitted.

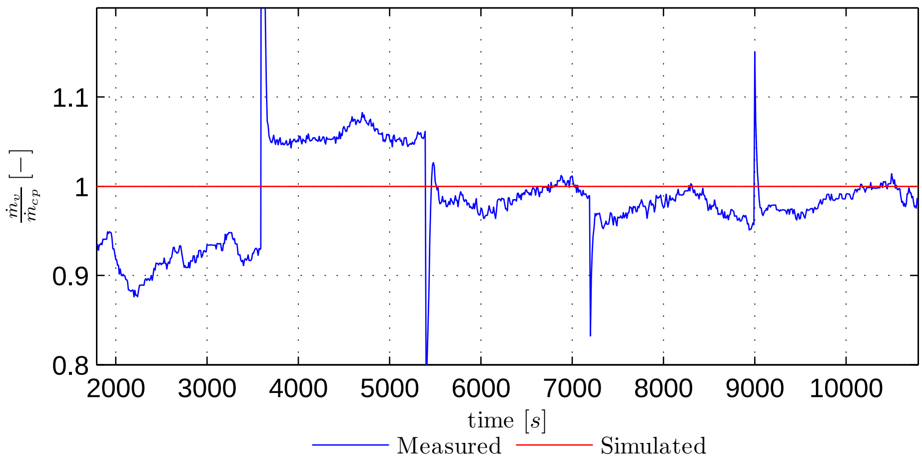

Figure 2.11: *Fitting of the valve model. The estimation is nearly 10% off at low flows. Note that the transients are expected since they occur just when the compressor changes its speed and P_e and P_c has not yet reached steady state.*

Figure 2.11 shows that the flow through the valve is not accurately represented by the model at different values for *OD*. This suggests that the flow is not linear with respect to *OD* as first assumed. Therefore a modification of the model that takes the non-linearity of *OD* into account is needed. This is described in the next section.

2.2.3 Modifications of the Model

It has been shown that the model of the mass flow of the valve is not linear with respect to *OD*. In the model it is assumed that the transition from fully open to fully closed and vice versa is instantaneous. However as the stepper motor rotates it takes time to move from a fully closed position to a fully open position. To capture this non-linearity in the model, a constant was introduced as a power of the opening degree, so that the modified model of the mass flow through the valve becomes

$$\dot{m}_v = OD^{1+\varepsilon_v} \cdot \sqrt{P_c - P_e} \cdot \frac{\sqrt{\rho_l}}{\sqrt{R_v}} \qquad [kg/s] \qquad (2.20)$$

where ε_v is a constant that is fitted to match the measurements. ε_v should be a somewhat small number as the previous model did capture the effects seen in the measurements to some degree. Since *OD* is a number between 0 and 1 the model of the valve still has the same flow range.

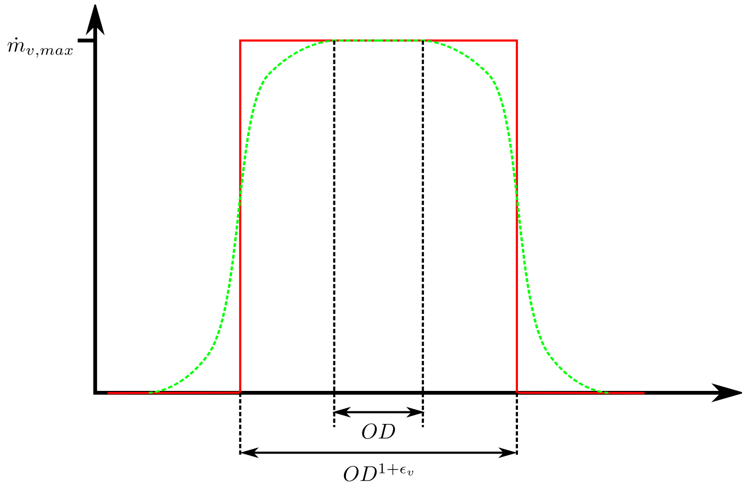

Figure 2.12: *Diagram showing the effect of the valve not being able to open and close instantly.*

Figure 2.12 shows how *OD* is compensated so the model of the valve can be viewed as either completely closed or fully open.

2.2.4 Fitting of the Modified Model

The new model was fitted to the same dataset as the previous model. It is seen that the model fits the data significantly better than the previous one, as it captures the correct flow in a wider range of opening degrees.

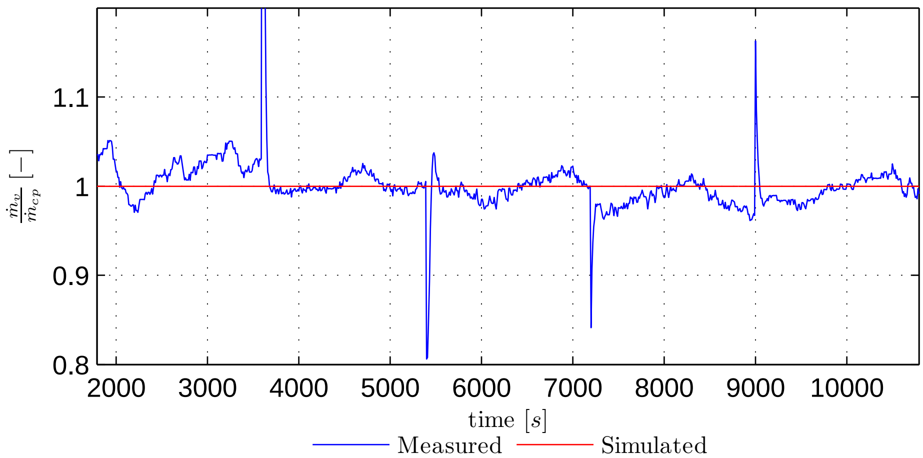

Figure 2.13: *Fitting of ε_v and R_v in the valve model. The transients are expected since they occur just when the compressor changes its speed and P_e and P_c has not yet reached steady state. Their effect on the fitting is so small that it is ignored. Note that the gain error is corrected compared to the old fit seen in Figure 2.11.*

The new model improves the fit of the average flow over one period of the pulse width modulation. The new model is extended to cover the mass flow through the individual pipes in the next section.

2.2.5 Division of Flow into Pipes

The evaporator model has four pipes in which the valve injects refrigerant individually, and the EcoFlow^{TM} valve allows the distribution of the opening times between the pipes to be set individually. The valve can be seen as a rotating disc with four holes. When the holes are aligned with the outlets refrigerant flows through, and when they are not there is no flow. There are one big hole and three small ones in the rotating disc. When the big hole in the rotating disc is aligned with one of the outlets, a relatively large flow is produced in this outlet. This is shown in Figure 2.14. When a small hole is aligned with an outlet a relatively small flow is produced. The distribution of time the big hole is aligned with the respective outlets during one cycle controls the average flow into each outlet.

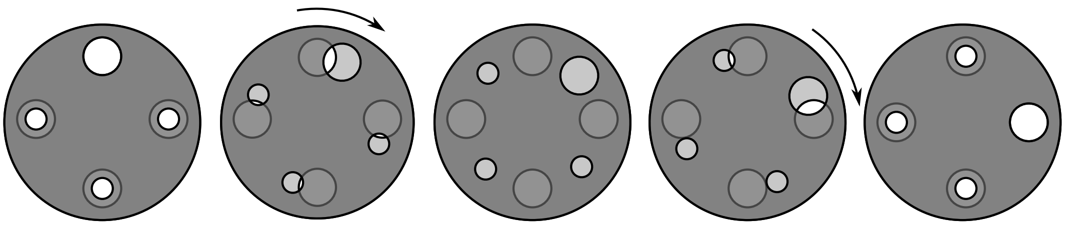

Figure 2.14: *First the top outlet is fully open, and the others less so. Then the disc rotates to the closed position where no outlets receive flow. The disc stays for a given time, defined by the opening degree. The disc then rotates again to allow a large flow in the outlet, to the right, and a smaller in the others.*

As a result each outlet receives either no flow, a high flow or a low flow. When one outlet receives a high flow all the others receive a low flow. When one outlet is closed all outlets are closed. The proportion of time where all outlets are closed is $1 - OD^{1+\varepsilon_v}$. An example of the flow in each individual pipe is shown in Figure 2.15.

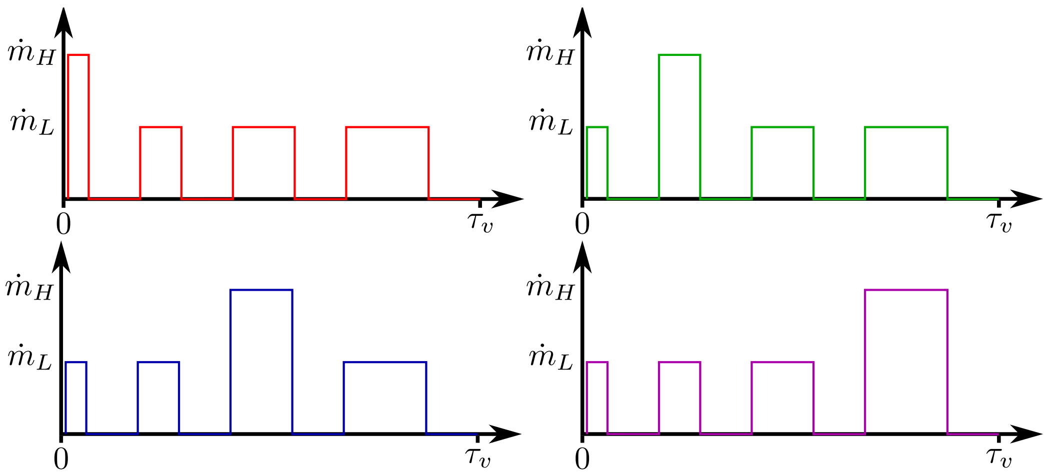

Figure 2.15: *The individual flows of each outlet of the valve. Note the duration of each opening is not the same, this allows one outlet to receive more flow than the others on average. This is encoded in a distribution vector which is an input to the valve.*

In Figure 2.15 $\dot{m}_H$ and $\dot{m}_L$ are unknown because it is unknown how large the holes in the rotating disc are compared to each other. However it is known that when the valve is not closed, it is fully open yielding maximum flow. This implies that one outlet receives $\dot{m}_H$ and the others $\dot{m}_L$, and gives the following relation with $\dot{m}_{v,max}$

$$\dot{m}_{v,max} = \dot{m}_H + 3 \cdot \dot{m}_L \qquad [kg/s] \qquad (2.21)$$

The relative time an outlet receives $\dot{m}_H$ compared to the combined opening time is

$$\tau_v[j] = \frac{\tau_v}{N_{pi}} \cdot OD^{1+\varepsilon_v} \cdot D[j] \qquad [s] \qquad (2.22)$$

where τ_v is the cycle time of the valve and N_{pi} is the number of outputs and $D[j]$ modifies the time the j'th output is open. To ensure that the total mass flow through the valve is equal to Equation (2.20) in a period, the distribution factor must satisfy the condition $\frac{1}{N_{pi}} \sum_{j=1}^{N_{pi}} D[j] = 1$. The time the valve is closed between switching $\dot{m}_H$ from one outlet to the next can be calculated as

$$\tau_{cl} = \frac{\tau_v}{N_{pi}} \cdot \left(1 - OD^{1+\varepsilon_v}\right) \qquad [s] \qquad (2.23)$$

The offset time each outlet begins to receive $\dot{m}_H$ during the rotation period τ_v can then be calculated as the sum of opening and closing times before that.

$$t_{v,0}[j] = (j-1) \cdot \tau_{cl} + \sum_{k=1}^{j-1} t_{v,0}[k] \qquad [s] \qquad (2.24)$$

where $j = \{1, \cdots, N_{pi}\}$.

The effects of the opening and closing of different outlets of the valve has now been modeled in a way that is still consistent with the standard model based on the Bernoulli's equation. This concludes the model of the EcoFlow^{TM} valve. In the next chapter a conventional model of the evaporator is derived.

Chapter 3

Conventional Evaporator Model

To gain an understanding of the superheat phenomenon of the evaporator a conventional evaporator model is derived, fitted to measurements, and evaluated. The model is conventional in the sense that very similar models has served as a basis for controller design in both (He et al., 1998) and (Rasmussen and Larsen, 2011). The purpose of the conventional model is to serve as a basis for an improved model. It allows us to understand its shortcomings with respect to superheat phenomenon and uneven filling of the pipes of the evaporator. With the understanding of the shortcomings, a new and improved model is derived in the following chapter.

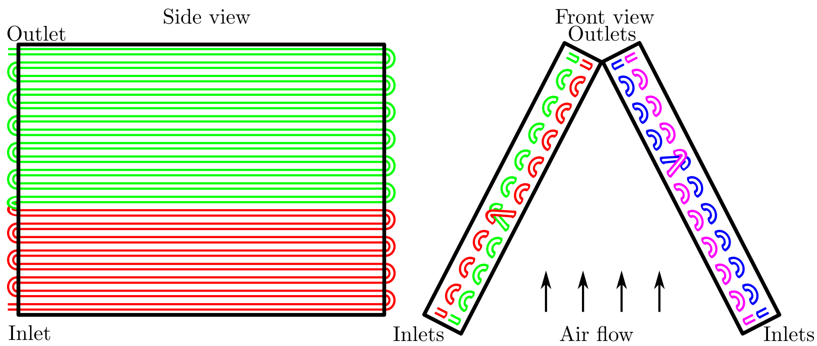

Figure 3.1: *Illustration of the evaporator used in the test setup. The figure shows how the evaporator is placed in the airflow and how the individual pipes are placed.*

The evaporator operates at low pressure and temperature of the refrigerant. The temperature of the refrigerant in the evaporator is lower than its ambient temperature, which results in a heat transfer from the surrounding air to the refrigerant inside the evaporator. When the refrigerant enters the evaporator, from the outlet of the EcoFlow^{TM} valve, it is in a two-phase state, a mixture of gas and liquid. When energy is added to the refrigerant from the heat transfer, more of the gas evaporates, until, if enough energy is added, all the gas has changed phase and the refrigerant is in gas form only. As further energy is added to the gas, the temperature of the gas increases, and the gas becomes superheated.

Figure 3.1 shows an illustration of the evaporator used in the test setup. The evaporator has four pipes in parallel, all with fins to increase the heat transfer. As seen in the illustration the four pipes are separated in pairs on either side of the evaporator, and the pair of pipes are crossed. The crossing of the pipes is done to help make sure that the heat transfer in both pipes are even. At the end of the evaporator the four parallel pipes are connected in a manifold, from where the refrigerant flows in a single pipe to the compressor.

3.1 Evaporator Model

To reflect the phase change occurring through the evaporator, the evaporator is split up into two zones. The first zone of the evaporator, where the refrigerant is in both liquid and gas phase, is called the two-phase zone. The second zone, where the refrigerant is in gas phase, is called the superheated zone.

For the purpose of modeling, the following assumptions were made:

- The drop in pressure along the evaporator is insignificant, and it is therefore neglected.
- No heat is stored in the tubes. The tubes of the system are very thin, so the heat they can store is very low compared to the cooling power of the system. Therefore their heat capacity is ignored.
- There is no heat exchange between the refrigerant and the ambient air in the tubes between the evaporator, compressor, condenser and valve. Since the tubes are isolated with foam, and therefore very little heat is dissipated through these. Therefore the heat exchange is neglected.
- The ambient temperature is constant for the entire length of the evaporator.
- No heat is generated from friction between the refrigerant and the inside of the tube or the outside of the tube and the airflow around it. This assumption is connected with the assumption that there are no pressure drop in the evaporator. If there is no pressure drop, no energy can be converted to heat.
- There are no delays in the system. This assumption was made because the speed of the wave of pressure change in a particular part of the system is much faster than the other dynamics of the system.
- All four pipes are filled evenly with refrigerant, and the pipes are modeled as one large pipe.

For the purpose of modeling, the evaporator is split into two control volumes, the first is the liquid in the evaporator and the second is the gas in the evaporator. The liquid control volume is used to describe the movement of the boundary between the two control volumes. The gas control volume is used to describe the changes in pressure in the evaporator.

The changes in pressure and the position of the boundary between the two zones are introduced as states in the model.

3.1.1 Two-phase Zone Length Model

The model of the length of the two-phase zone is based on the energy balance of the control volume illustrated in Figure 3.2, which represents the liquid refrigerant in the evaporator.

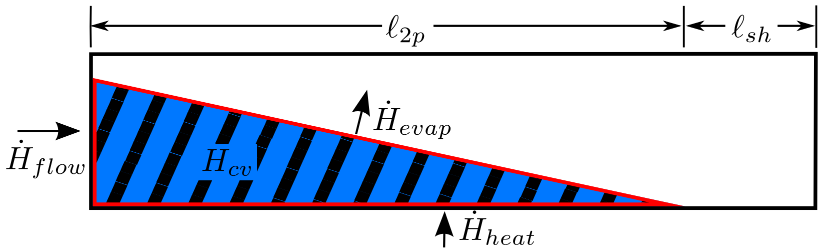

Figure 3.2: *Illustration of the control volume used to calculate the model of the length of the two-phase zone.*

The change in enthalpy in the control volume can be represented as the sum of the energy of the liquid which flows into the evaporator from the valve, the loss of energy in the control volume from the refrigerant which evaporates and the energy transferred to the control volume by heat transfer from the air surrounding the evaporator. This gives the equation

$$\dot{H}_{cv} = \dot{m}_{v,l} \cdot h_l - \dot{m}_{v,l} \cdot h_g + \alpha_{2p} \cdot O_e \cdot \ell_{2p} \cdot (T_a - T_e) \qquad [J/s] \qquad (3.1)$$

where the first term on the right hand side of the equation is the energy flow into the control volume, $\dot{H}_{flow}$, the second term is the energy lost due to evaporation, $\dot{H}_{evap}$, and the third term is the heat transfer through the wall of the evaporator, $\dot{H}_{heat}$. h_l and h_g are the specific enthalpy of the refrigerant in liquid and gas phase respectively. α_{2p} is the heat transfer coefficient in the two-phase zone, O_e is the circumference and ℓ_{2p} is the length of the two-phase zone. T_a and T_e are the temperature of the ambient air and the refrigerant respectively. $\dot{m}_{v,l}$ is the mass flow of liquid in the valve. It is equal to the fraction of the total mass flow in the valve, $\dot{m}_v$, given by

$$\dot{m}_{v,l} = \dot{m}_v \cdot \frac{h_g - h_i}{h_g - h_l} \qquad [kg/s] \qquad (3.2)$$

where h_i is the specific enthalpy of the refrigerant as it enters the evaporator.

As the length of the two-phase zone is not constant, the volume of the control volume is not constant either. Therefore the change in energy of the control volume can also be represented as the change in energy due to change in volume. This is represented by the follwing equation.

$$\dot{H}_{cv} = -A_e \cdot (1 - \gamma_{2p}) \cdot \rho_l \cdot (h_g - h_l) \cdot \frac{d(\ell_{2p})}{dt} \qquad [J/s] \qquad (3.3)$$

where A_e is the cross section area of the evaporator, γ_{2p} is the volume fraction of gas in the two-phase zone and ρ_l is the density of the liquid refrigerant. The expression is negative as an increase in energy in the control volume leads to increased evaporation and thus a decrease in volume.

By combining Equation (3.1), (3.2) and (3.3) the equation

$$A_e \cdot (1-\gamma_{2p}) \cdot \rho_l \cdot (h_g - h_l) \cdot \frac{d(\ell_{2p})}{dt} = \dot{m}_v \cdot (h_g - h_i) - \alpha_{2p} \cdot O_e \cdot \ell_{2p} \cdot (T_a - T_e) \qquad [J/s] \tag{3.4}$$

which describes changes in length of the two-phase zone, is derived. The equation has the mass flow through the valve as an input. It depends on the length of the two-phase zone and the pressure in the evaporator, as the specific enthalpy of the refrigerant at the dew and boil points depends on the pressure. As a result of this dependence, a model of the pressure in the evaporator is derived.

3.1.2 Pressure Model

To model the pressure in the evaporator, a control volume consisting of the gas in the evaporator is used. The control volume is shown in Figure 3.3.

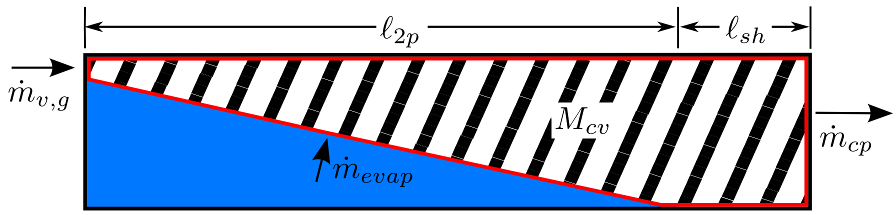

Figure 3.3: *Illustration of the control volume used to calculate the model of the pressure in the evaporator.*

The change in mass in the control volume can be described as the sum of the mass flow of gas into the volume, the flow of evaporating gas and the loss of mass due to the flow out of the volume. The sum of the flows describe the mass balance of the control volume, as described in the equation

$$\dot{M}_{cv} = \dot{m}_{v,g} + \frac{\alpha_{2p} \cdot O_e \cdot \ell_{2p} \cdot (T_a - T_e)}{h_g - h_l} - \dot{m}_{cp} \qquad [kg/s] \tag{3.5}$$

where the first term on the right side of the equation represents the mass flow of gas into the control volume. The second term is the evaporation, $\dot{m}_{evap}$, represented by the heat transfer divided by the energy needed to evaporate the refrigerant. The third term, $\dot{m}_{cp}$, is the mass flow out of the control volume, which is assumed to be equal to the mass flow through the compressor. The variable $\dot{m}_{v,g}$ is the mass flow of gas through the valve, which is equal to

$$\dot{m}_{v,g} = \dot{m}_v \cdot \frac{h_i - h_l}{h_g - h_l} \qquad [kg/s] \tag{3.6}$$

The change of mass in the control volume manifests itself as a change in the density of the refrigerant in the control volume. This is shown in the follwoing equation.

$$\dot{M}_{cv} = A_e \cdot (\ell_{2p} \cdot \gamma_{2p} + \ell_{sh}) \cdot \frac{d(\rho_g)}{dt} \qquad [kg/s] \tag{3.7}$$

where ℓ_{sh} is the length of the superheated zone. By combining Equation (3.5) and (3.7) and applying the chain rule on the derivative of the density, the equation

$$A_e \cdot (\ell_{2p} \cdot \gamma_{2p} + \ell_{sh}) \cdot \frac{d(\rho_g)}{dP_e} \frac{d(P_e)}{dt} = \dot{m}_{v,g} - \dot{m}_{cp} + \frac{\alpha_{2p} \cdot O_e \cdot \ell_{2p} \cdot (T_a - T_e)}{h_g - h_l} \quad [kg/s] \tag{3.8}$$

is derived. This equation describes the derivative of the evaporator pressure, and is used as a state equation. Next the temperature out of the evaporator is calculated.

3.1.3 Superheat Temperature Model

The length of the superheated zone is determined by the length of the two-phase zone, as the sum of the two lengths is the total length of the evaporator. As the refrigerant enters the superheated zone, it is gas at the dew temperature of the refrigerant corresponding to the pressure in the evaporator. In the superheated zone further heat is transferred to the refrigerant, which leads to an increase in temperature and thus the refrigerant becomes superheated.

The relation between the length of the superheated zone and the outlet temperature is based on the energy balance of the superheated zone. A control volume corresponding to the gas in the superheated zone is therefore used to calculate the output temperature. The control volume is illustrated in Figure 3.4.

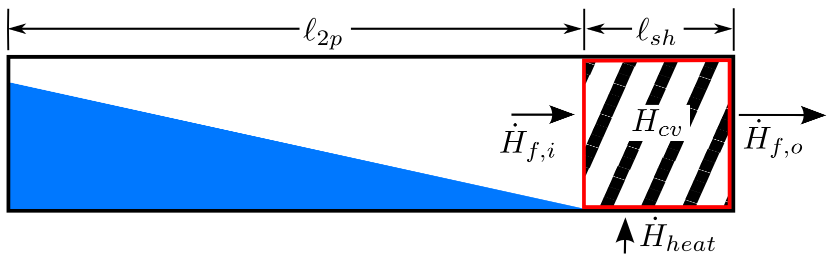

Figure 3.4: *Illustration of first idea for a control volume to calculate the output temperature from the evaporator. The control volume consists of the gas in the superheated zone.*

The change in energy in the superheated zone is equal to the energy difference of the refrigerant which flows through the zone added with the heat which enters through the wall of the evaporator in the zone.

The energy which enters and exits the superheated zone is equal to the mass flow multiplied with the specific enthalpy at the inlet and outlet of the zone respectively. It is assumed that both mass flows are equal to the mass flow through the compressor.

The energy which enters the control volume from heat transfer depends on the temperature difference between the refrigerant and the ambient air. But as the temperature of the refrigerant changes, as it flows through the control volume, the control volume is changed so the temperature is constant. The length of the control volume is changed from ℓ_{sh} to Δx, a distance so small it is assumed that the temperature of the refrigerant is constant. The new control volume is illustrated in Figure 3.5.

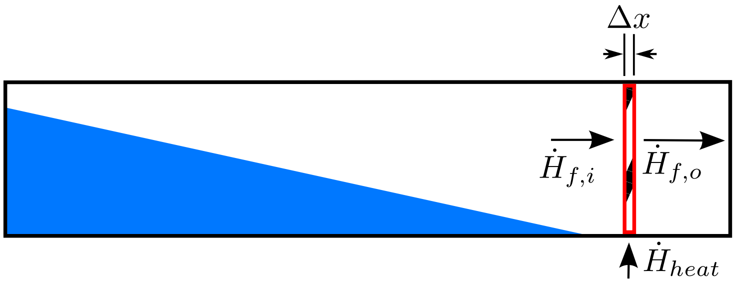

Figure 3.5: *Illustration of the new control volume. The length of the control volume is modified so the internal temperature is constant.*

The changes in internal energy in the new control volume can be expressed by

$$\begin{aligned}\dot{H}_{cv} &= \dot{m}_{cp} \cdot h(x) - \dot{m}_{cp} \cdot h(x+\Delta x) \\ &\quad + \alpha_{sh} \cdot O_e \cdot \Delta x \cdot (T_a - T(x)) \qquad [J/s] \end{aligned} \tag{3.9}$$

where α_{sh} is the heat transfer coefficient in the superheated zone, $h(x)$ is the specific enthalpy at the point x and $T(x)$ is the temperature of the refrigerant inside the control volume.

As the energy change of the refrigerant in the superheated zone is much less than that in the two-phase zone, the change of the energy is neglected. Furthermore, as the refrigerant is in the gas phase in the entire control volume, the specific enthalpy is replaced by the temperature of the refrigerant multiplied with the heat capacity at constant pressure, $c_{p,sh}$. The equation

$$\begin{aligned}0 &= \dot{m}_{cp} \cdot c_{p,sh} \cdot (T(x) - T(x+\Delta x)) \\ &\quad + \alpha_{sh} \cdot O_e \cdot \Delta x \cdot (T_a - T(x)) \qquad [J/s] \end{aligned} \tag{3.10}$$

can therefore be used to calculate the output temperature of the refrigerant. Introducing a constant β_e and rearranging Equation (3.10) to

$$\begin{aligned}\beta_e &= \frac{\dot{m}_{cp} \cdot c_{p,sh}}{\alpha_{sh} \cdot O_e} \qquad [m] \\ \frac{T(x+\Delta x) - T(x)}{\Delta x} &= \frac{1}{\beta_e} \cdot (T_a - T(x)) \qquad [K/m] \end{aligned} \tag{3.11}$$

gives a difference equation. The difference equation is transformed into a differential equation by letting $\Delta x \to 0$.

$$\begin{aligned}\lim_{\Delta x \to 0} \left(\frac{T(x+\Delta x) - T(x)}{\Delta x} \right) &= \frac{dT(x)}{dx} \qquad [K/m] \\ \frac{dT(x)}{dx} &= \frac{1}{\beta_e} \cdot (T_a - T(x)) \qquad [K/m] \end{aligned} \tag{3.12}$$

The differential equation, Equation (3.12), is solved to get the temperature of the refrigerant. The temperature of the refrigerant, as it enters the superheated zone, corresponding to a distance of zero, is equal to the temperature of the gas in the two-phase zone. The solution to the differential equation

$$T(x) = T_a - (T_a - T_e)\, e^{-\frac{x}{\beta_e}} \qquad [K] \qquad (3.13)$$

describes the temperature at a distance x from the start of the superheat zone.

The superheat temperature, T_{sh}, is defined as the change in temperature of the refrigerant in the superheated zone. To find the temperature at the outlet of the superheated zone, Equation (3.13) is evaluated at the length of the superheated zone. The equation for the superheat temperature is shown in Equation (3.14).

$$T_{sh} = T(\ell_{sh}) - T_e \qquad [K]$$

$$T_{sh} = (T_a - T_e)\left(1 - e^{-\frac{\ell_{sh}}{\beta_e}}\right) \qquad [K] \qquad (3.14)$$

The equation is used to calculate the increase in temperature in the superheated zone.

This concludes the conventional model of the evaporator in the system. Two state equations, one for pressure and one for the length of the two-phase zone, has been derived. Furthermore an output equation has been calculated. In the next section the model is fitted against data from the test setup.

3.2 Fitting of the Model

In the model of the evaporator, the parameters A_e, γ_{2p}, α_{2p}, O_e, L_e and α_{sh} has to be estimated for the model to fit the test setup. The parameters A_e and L_e can me measured directly on the test setup, so those two parameters does not have to be estimated. The parameter O_e can be measured as well, but as it is always multiplied with either α_{2p} or α_{sh}, it is included in those parameters.

3.2.1 Void Fraction

Based on (Wedekind et al., 1978) the void fraction, γ_{2p}, can be calculated directly from the other variables in the evaporator. The void fraction for the entire two-phase zone can be expressed as the average of the area mean void fraction, which is the void fraction of a cross-section area of the evaporator. As the void fraction is the volume of the gas compared to the total volume, this can be calculated from the mass of the gas at a cross section compared to the total mass.

The mass flow of gas at the inlet of the evaporator is expressed in Equation (3.6). At the end of the two-phase zone the mass flow of gas is equal to the total mass flow in the valve. As the heat transfer from the start of the two-phase zone to the end is constant, the mass flow of gas at a point along the two-phase zone can be expressed as the straight line

$$\dot{m}_g(x) = \dot{m}_{v,g} + \frac{x}{\ell_{2p}}\left(\dot{m}_v - \dot{m}_{v,g}\right) \qquad [{}^{kg}/_{s}] \qquad (3.15)$$

where $\dot{m}_g$ is the mass flow of gas at the point x and x is a number from 0 to ℓ_{2p}. The equation can be seen in Figure 3.6 as the blue line.

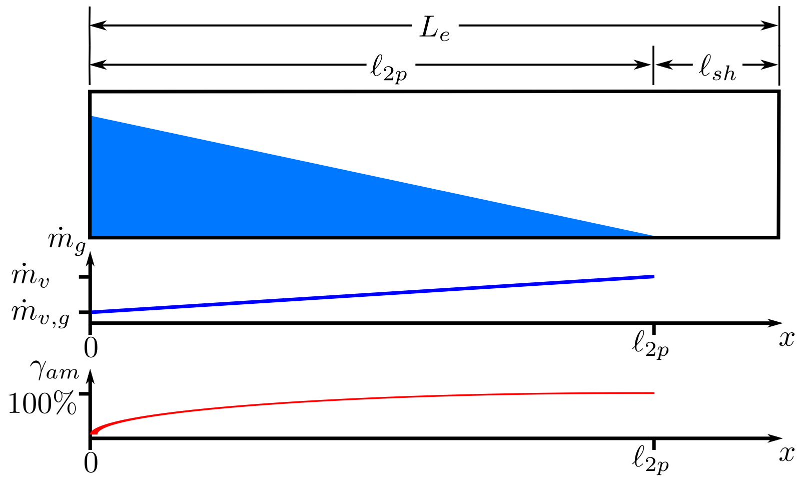

Figure 3.6: *The figure illustrates the mass flow of gas and the area mean void fraction during the length of the two-phase zone.*

To calculate the area mean void fraction, the mass flow of gas has to be multiplied with the specific volume. As the void fraction is the volume fraction of gas, the area mean void fraction is the volume of gas divided by the total volume

$$\gamma_{am}(x) = \frac{v_g \cdot \dot{m}_g(x)}{v_g \cdot \dot{m}_g(x) + v_l \cdot (\dot{m}_v - \dot{m}_g(x))} \qquad [-] \qquad (3.16)$$

where v_g and v_l are the specific volume of the gas and the liquid in the evaporator respectively. The equation can be seen as the red line in Figure 3.6.

The void fraction for the entire two-phase zone is calculated as the mean of the area mean void fraction

$$\gamma_{2p} = \frac{1}{\ell_{2p}} \int_0^{\ell_{2p}} \gamma_{am}(x) dx \qquad [-] \qquad (3.17)$$

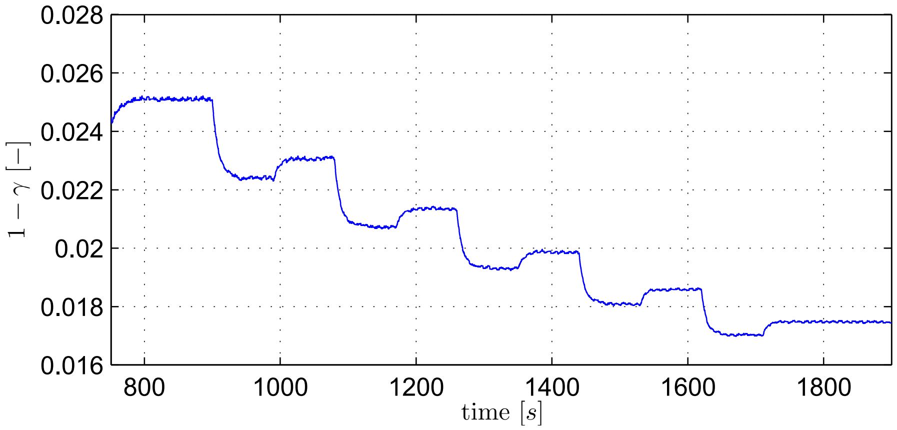

Figure 3.7: *The opening degree of the valve and the compressor speed are varied, which yields different mass flows in the evaporator. This results in changes in $(1-\gamma_{2p})$. It varies almost 50 %, which makes the speed of the ℓ_{2p} dynamics vary just as much.*

Figure 3.7 shows the calculated value of $(1-\gamma_{2p})$, which is a part of Equation (3.4). The value is different during different mass flows, which indicates that the value should be calculated using Equation (3.17) and not considered a constant.

As the void fraction can be calculated at all time intervals, the only parameters left to estimate are the heat transfer coefficients in the two-phase zone and in the superheated zone.

3.2.2 Heat Transfer in the Two-phase Zone

From the equation for the length of the two-phase zone, Equation (3.4), it is seen that if the length of the two-phase zone is in a steady state, the only unknown parameters are the heat transfer coefficient and the circumference. As they are multiplied, they will be estimated as a single parameter.

To estimate the parameter, an experiment was conducted, where the test setup was run in three different situations, all in a steady state and where $\ell_{2p} = L_e$. The inputs can be seen in Figure 3.8. As the length of the two-phase zone has to be in a steady state, the crossed out areas was not used in the estimation.

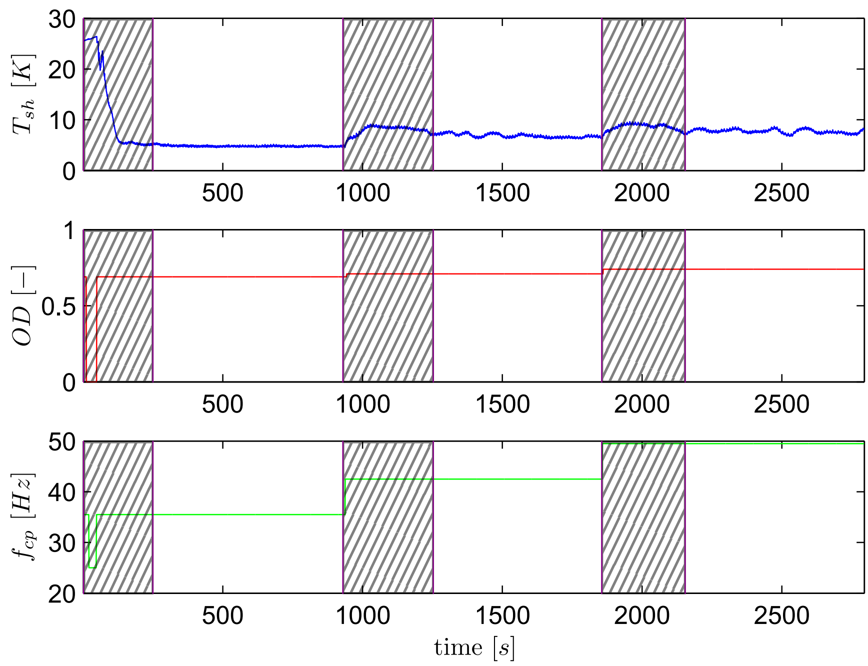

Figure 3.8: *Inputs for the experiment used to estimate the heat transfer in the two-phase zone. The grayed out areas was not used in the estimation*

The parameter $\alpha_{2p} \cdot O_e$ was estimated so the error in the length of the two-phase zone was minimized in a least square sense. The parameter was estimated to be

$$\alpha_{2p} \cdot O_e = 38.08 \qquad [J/s{\cdot}K{\cdot}m] \qquad (3.18)$$

which gave the fit shown in Figure 3.9.

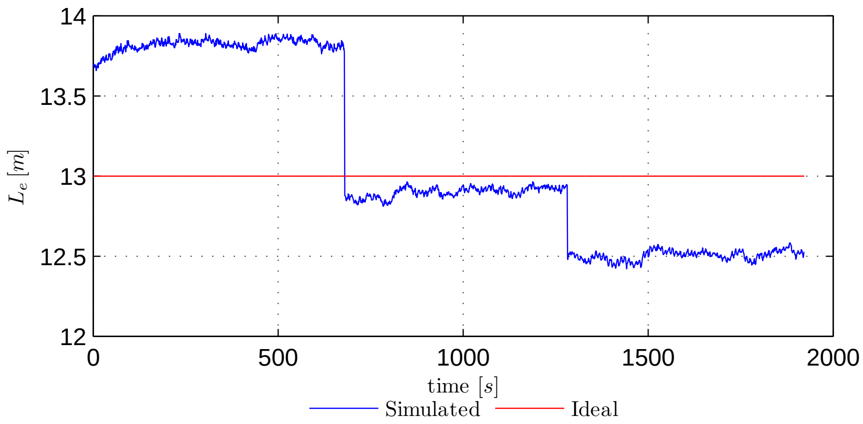

Figure 3.9: *Result of the fitting of* $\alpha_{2p} \cdot O_e$. *The result is shown as the calculation of* ℓ_{2p} *during the experiment. Ideally this should be equal to 13 meters, which is the length of the evaporator. The measurements of* P_e *are filtered to reduce high frequency oscillations due to the opening and closing of the EcoFlow*^{TM} *valve.*

The estimated length of the two-phase zone is not equal to the ideal length, but it is assessed that the result is sufficiently close for the purpose of the model. The average error in the estimated length is 3.74%. With the heat transfer coefficient in the two-phase zone estimated the only parameter left to estimate is the heat transfer in the superheated zone.

3.2.3 Heat Transfer in the Superheated Zone

The heat transfer in the superheated zone was estimated by making an experiment where the opening degree of the valve were slowly opened until there was overflow of liquid refrigerant in the evaporator. The control signal can be seen in Figure 3.10. The opening degree was only changed every five minutes to ensure that the system was in a steady state at all intervals. By making a sweep of the opening degree the gain in the superheat was tested against a wide range of operating points.

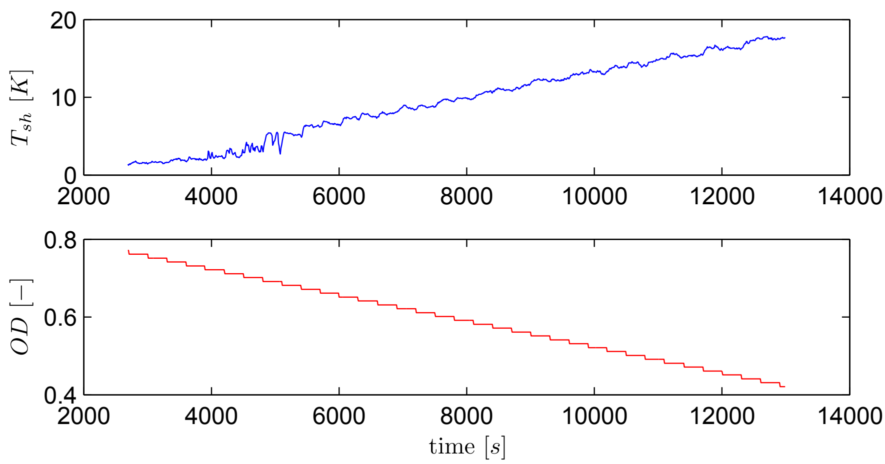

Figure 3.10: *Opening degree, OD, and superheat temperature,* T_{sh}, *in the experiment used to find the heat transfer coefficient in the superheated zone.*

The heat transfer coefficient is multiplied with the circumference of the evaporator in the equation for the output temperature of the evaporator. Therefore they are estimated as a single parameter. By fitting the output temperature the parameter was found to be

$$\alpha_{sh} \cdot O_e = 10.46 \qquad [J/s{\cdot}K{\cdot}m] \tag{3.19}$$

Figure 3.11 shows the result of the fitting. The line marked with red is the measured output temperature and the blue line is the simulated output temperature. The model captures the measurements to some degree. However, it is clear that even though the mean squared error is not particularly high, there are effects which are clearly not captured by the model.

The model predicts T_o, the output temperature from the evaporator, to reach the ambient temperature at high superheat. This is clearly not the case. Also the model predicts T_o to drop sharply to the evaporation temperature, T_e, when the evaporator overflows, while it actually converges in a smooth way.

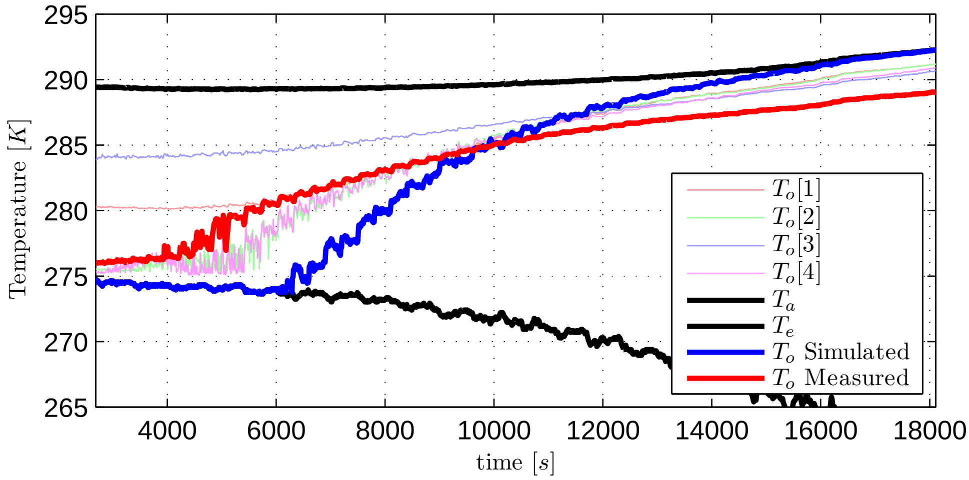

Figure 3.11: *Result from the fitting of the heat transfer coefficient in the superheated zone. The figure shows the simulated output temperature from the evaporator calculated with the estimated heat transfer coefficient.*

The two effects are not covered in the model, and indicate that a better understanding of the phenomenon related to superheat is needed. The model is therefore modified to explain the phenomenon. The reader should pay particular attention to Figure 3.11, as the similar fit is significantly improved in the improved model.

3.2.4 Pressure

With all the parameters estimated, the model of the pressure changes in the evaporator, Equation (3.8), is simulated to see if the model fits the dynamics of the system. The pressure is simulated using the dataset from an experiment where the *OD* and f_{cp} was changed rapidly to see the dynamics of the system. The inputs during the experiment can be seen in Figure 3.12.

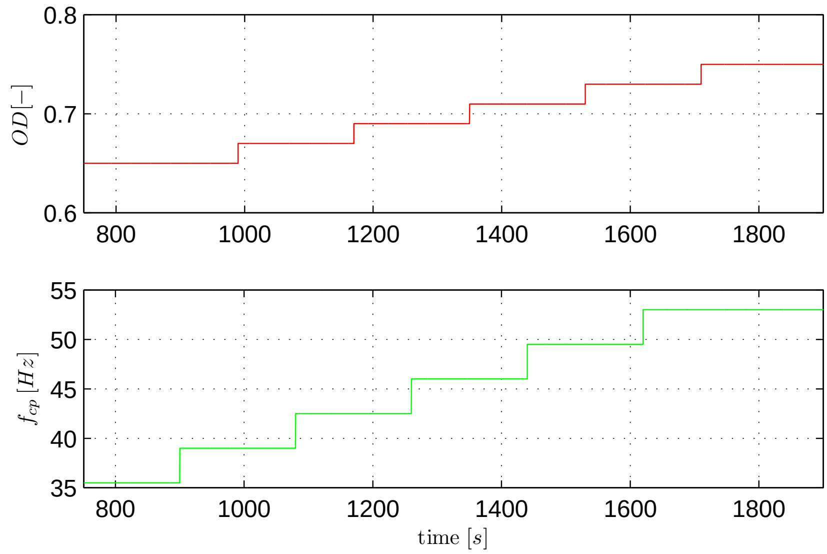

Figure 3.12: *Inputs for the experiment used to verify the dynamics of the system.*

The result of the simulated pressure compared to the measured pressure is shown in Figure 3.13.

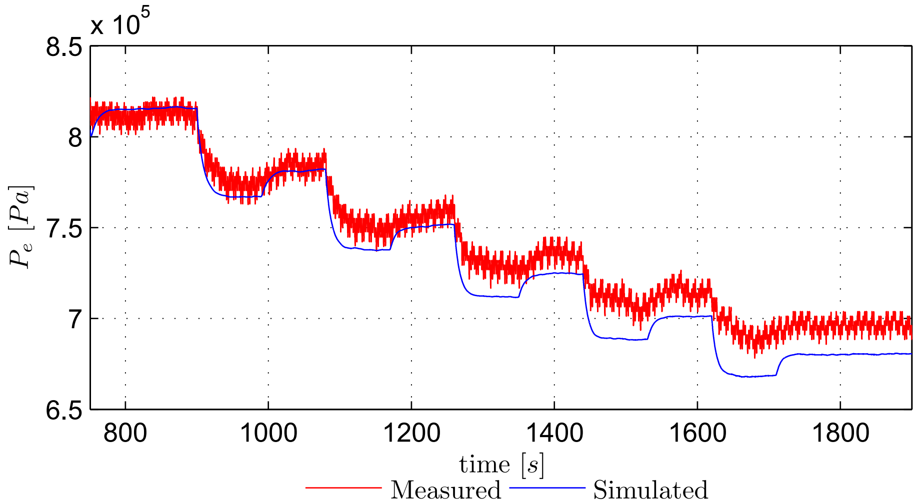

Figure 3.13: *The simulated and the measured pressure in the evaporator. The simulation has a small deviation in the steady state error, but follows the changes in pressure.*

The simulated pressure follows the changes in the measured pressure, but the dynamics of the simulation are too fast and there is a small error in the steady state values.

To correct the steady state values, the parameter $\alpha_{2p} \cdot O_e$ has to be changed. The parameter is a part of the steady state value of the length of the two-phase zone too. The simulated value of the length is shown in Figure 3.14. The length of the two-phase zone can not be measured directly, but the length is assessed to be reasonable. If $\alpha_{2p} \cdot O_e$ is altered to achieve a better steady-state pressure fit, the length of the two-phase zone becomes longer than the total length of the evaporator.

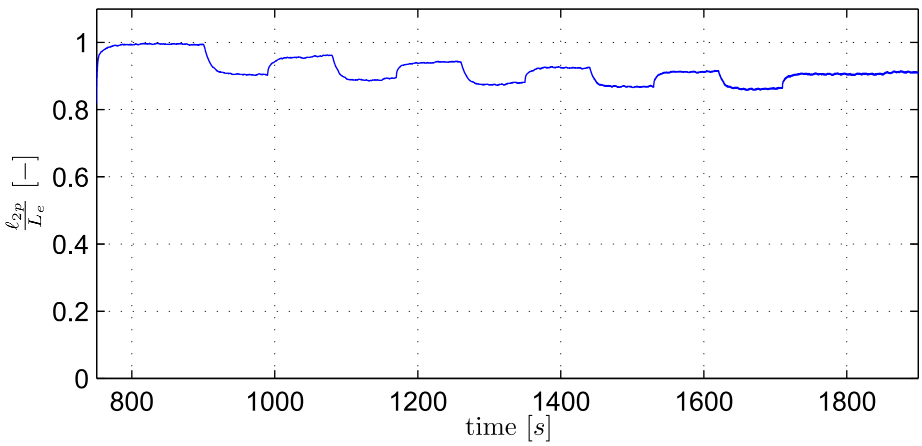

Figure 3.14: *Estimated length of the two-phase zone. The estimation shows reasonably results, as the evaporator is almost full without overflowing.*

The difference in the time constant indicates that the cross-section area used to calculate the pressure is wrong. As this can be measured, it indicates that the volume used to calculate the pressure changes is wrong. We think this is because the manifold and some of the tubes are not considered in the volume. This is included in the improved model, which is derived in the next chapter.

Chapter 4

Improved Evaporator Model

The model is modified to explain the differences between the conventional model and the measured data. The conventional model is based on the assumption that all four pipes in the evaporator are filled evenly with refrigerant, so that the length of the two-phase zone is the same in all four pipes. On Figure 3.11 it is seen that this assumption does not always hold.

Figure 4.1 illustrates the evaporator. It is constructed from four pipes running in parallel in the evaporator, and joined together afterwards in a manifold. The ambient air flows perpendicular to the pipes. This causes the air to cool, and the refrigerant in the pipes to evaporate. However, because the air cools, it is not as warm when it reaches the second pipe as it were when it reached the first. As a consequence the heat transfer to the second pipe is less than for the first, causing less evaporation, and thus an uneven filling of the two pipes. It is suspected that this unbalanced load of each pipe is responsible for some of the superheat effects unaccounted for in the conventional model.

As seen in the figure, some of this effect has been compensated by making the pipes cross, so not only one pipe receives all the warm air. The figure shows the length a given pipe is in front, is different from pipe to pipe. For example the pipe marked with red is in front longer than the pipe marked with blue.

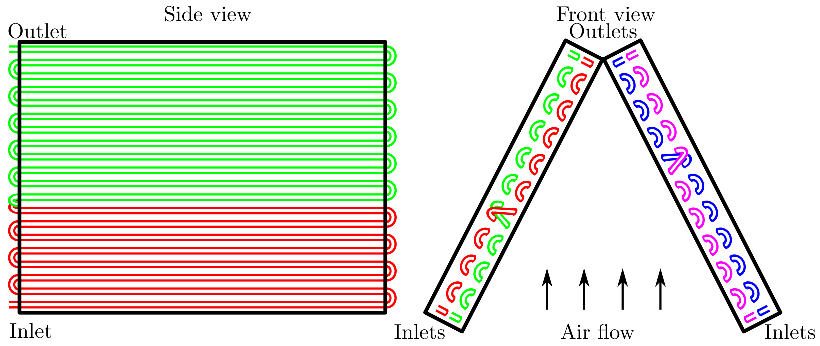

Figure 4.1: *Illustration of the evaporator used in the test setup. Note that a pipe crosses from being in front of another pipe to be behind it or reverse, as seen in the direction of the airflow.*

Because of this, the imbalance between heat transfers between two pipes is still present, which causes the evaporation in the four pipes to be uneven. This causes the length of the two-phase zone in the four pipes to be different, and thus also the temperature of the refrigerant at the output. The effect varies, with the length of the two-phase zone as this changes the relative crossing of the two phase zones of the pipes. It also varies with changing air ventilation of the evaporator, as this changes the load balance between pipes in front and pipes in the back of the airflow.

The effect on the output temperature T_o is largest when the length of the superheat is low, as the increase in temperature raises fastest in the beginning of a superheated zone.

4.1 Evaporator Model

In this section our modifications to the conventional model are developed. The conventional model is modified to incorporate the effect of different air temperature around the pipes. To incorporate the effect, and to explain the effects it has on the output temperature, the four pipes are modeled separately. Each pipe is divided into two parts. The first part of a pipe is from the beginning, to the point it crosses another, and the second part of a pipe is from the crossing to the end. In this way each part of each pipe can seen as having a constant ambient air temperature.

4.1.1 Summary of Improvements

The new evaporator model incorporates several improvements. To stress the points of improvement the results are summarized here to aid the reader in following the model derivation of the improved evaporator model.

The result of the fitting of the superheat curve in the conventional model, Figure 3.11, is reprinted here as Figure 4.2 along side the result the similar fit of the improved model, Figure 4.3.

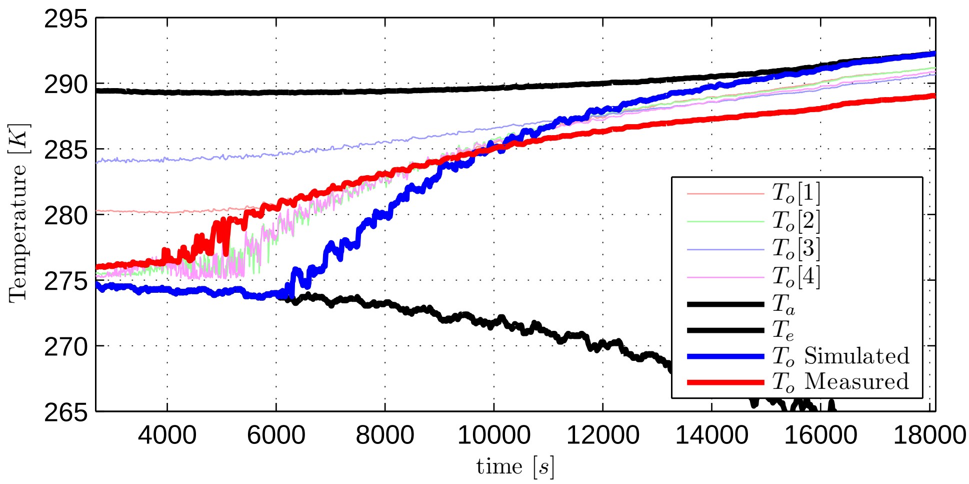

__Figure 4.2:__ Result from the fitting of the heat transfer coefficient in the superheated zone of the conventional model. The figure shows the simulated output temperature from the evaporator calculated with the estimated heat transfer coefficient. T_a is the ambient temperature, T_e is the evaporation temperature, $T_o[j]$ is the output temperature from pipe j and T_o is the combined output temperature

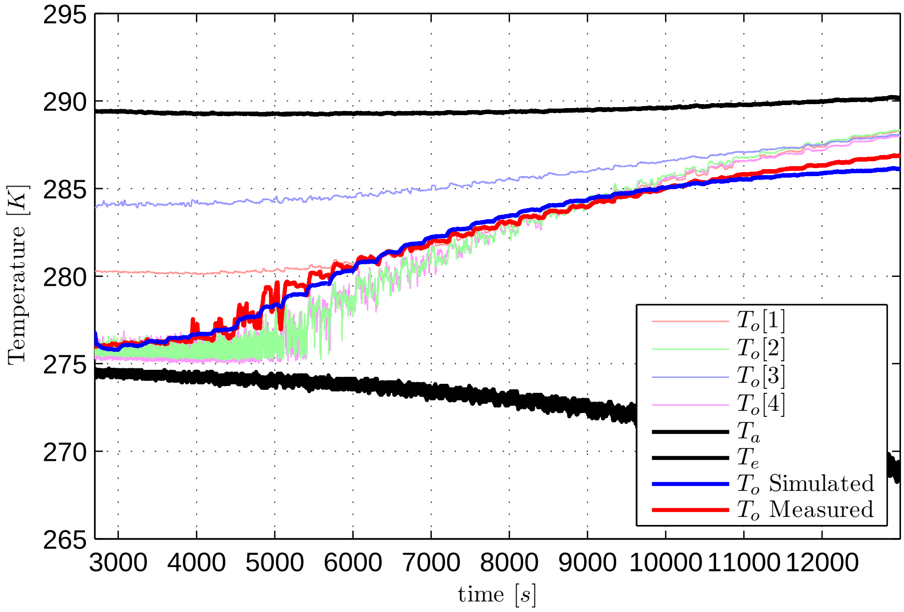

Figure 4.3: *Result from the estimated heat transfer coefficient for the two-phase zone and the superheated zone of the improved model. The system is simulated with the found parameters and compared to the measurements.*

As seen from the figures, the improved model address phenomenon not described by the conventional model. It explains why the superheat does not drop sharply to the evaporation temperature, but smooth as more and more pipes overflow. It also explains how the superheat temperature does not reach the ambient air temperature, even with very long superheat zones.

The effects are all due to the effect of different air temperatures around the pipes. Which is shown to have profound, yet simple effects on the heat transfer of each pipe. The implications of the effect are carried on to the new models for the length of a two-phase zone and the pressure. The effect is derived in the next subsection.

4.1.2 Different Air Temperatures around the Pipes

The change of air temperature at different parts of a single pipe is central to the improved model, as its consequences motivates the improvements made to the rest of the model.

If a pipe is located behind another in the flow of air, the temperature of the air when it reches the second pipe is not equal to the room temperature as it has been cooled by the pipe in front. It turns out that the drop in temperature can be modeled by multiplying the temperature difference between the ambient temperature and the evaporation temperature with a constant to get the air temperature around the second pipe. Figure 4.4 shows the change in air temperature as it flows past the two pipes of one side of the evaporator.

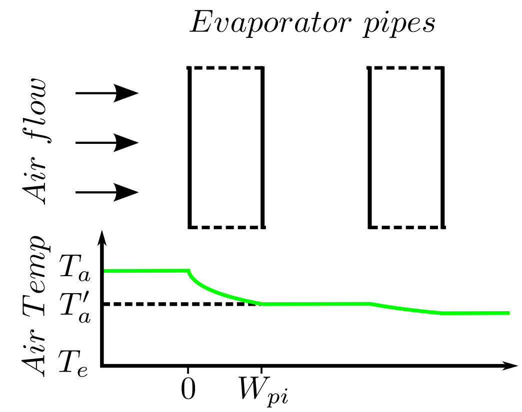

Figure 4.4: *Illustration of the temperature change of the ambient air as it flows by the evaporator pipes. The air temperature drops as it delivers energy to the refrigerant inside each pipe.*

To simplify the evaporation model, it is assumed that the temperature of the air around a part is equal to the ambient temperature, if it is first in the air flow. For a part that is behind another, the air temperature is called T'_a. The air temperature drop from the first to the second pipe is described by a constant, η, which denotes the fraction

$$\eta = \frac{T'_a - T_e}{T_a - T_e} \qquad [-] \qquad (4.1)$$

In this section it is shown that η for all parts can be found, and can indeed be approximated by a constant.

The temperature of the air is found by the same principle as the temperature of the refrigerant in the superheated zone in the evaporator. If the change in internal energy is neglected, the energy balance of a small section of the air, as it passes the first evaporation pipe, is equal to

$$0 = \dot{m}_a \cdot c_{p,a} \left(T(x) - T(x + \Delta x)\right) - \alpha_{2p} \cdot O_{pi} \cdot \Delta x \left(T(x) - T_e\right) \qquad [J/s] \qquad (4.2)$$

where $\dot{m}_a$ is the mass flow of air, $c_{p,a}$ is the heat capacity of the air, α_{2p} is the heat transfer coefficient and O_{pi} is the circumference of the evaporator pipe.

By letting Δx go towards zero, the difference equation is transformed to a differential equation with the solution

$$T(x) = T_e + (T_a - T_e)\, e^{-x/\beta_a} \qquad [K] \qquad (4.3)$$

where the length constant is equal to

$$\beta_a = \frac{\dot{m}_a \cdot c_{p,a}}{\alpha_{2p} \cdot O_{pi}} \qquad [m] \qquad (4.4)$$

Equation (4.3) expresses the temperature of the air as it passes the first refrigeration pipe. To find the temperature at the start of the second pipe, Equation (4.3) is evaluated at the end of the first pipe. The temperature of the air at the second pipe is therefore equal to

$$T_a' = T_e + (T_a - T_e)\, e^{-w_{pi}/\beta_a} \qquad [K] \qquad (4.5)$$

where w_{pi} is the width of a pipe.

In a part of a pipe that is in the back of the air flow the temperature difference between the air and the refrigerant should be expressed as $T_a' - T_e$, as this is the actual temperature difference. This is estimated by $(T_a - T_e)\,\eta$. By comparing the estimation and the value of T_a' found in Equation (4.5), η is found to be

$$\eta = e^{-W_{pi}/\beta_a} \qquad [-] \qquad (4.6)$$

The value of η for at part that is behind another is therefore a constant.

In this section it was found, that the constant η, for a part that is first in an air flow is equal to 1. For a part that is behind another, the value of the air temperature constant η is equal to Equation (4.6). It is also noticed that η is dependent on β_a, which inversely proportional to the mass flow of the air. This means that η changes when the mass flow of the air changes. This means that if the pipes of the evaporator is evenly filled at one mass flow of air. They will not be at another. With the air temperature constant found, the model for change in length of the two-phase zone in a single pipe is derived next.

4.1.3 Two-phase Zone Length Model

In the previous subsection we have shown, that the air temperature around each pipe is different. As a consequence we can no longer consider the four pipes of the evaporator as one, as we now know that the length of their respective two-phase zones cannot be the same as they do not have the same temperature difference to drive the heat transfer. We therefore split the model into four individual pipes with their own separate two-phase zones.

The model of the length of the two-phase zone has to be derived for each individual pipe in contrast to a single model for the entire pipe. The model of the two-phase zone is only derived once, as it is the same in the four pipes.

Even though the evaporator used in this study only has one crossover per pipe, the model is derived to accommodate an arbitrary number of crossovers of each pipe. However, it is assumed that superheated zone is always confined to the last part, and therefore does not reach the crossover point.

The new model of the length of the two-phase zone in a single pipe is based on the conventional model for the whole evaporator, see Equation (3.4). Some alterations has to be made to the conventional model to fit a single pipe.

In the conventional model the mass flow of refrigerant is equal to the mass flow of the valve. This is no longer the case, as the mass flow in a single pipe is only a fraction of the total mass flow. Furthermore the heat transfer in the conventional model assumes that the temperature of the refrigerant and the ambient air is constant for the entire length of the two-phase zone. This is no longer the case. The pipes cross each other, so a single pipe can be both in front and behind another pipe during the two-phase zone, so the temperature of the ambient air is no longer constant, as shown in Subsection 4.1.2. This leads to a change in rate of evaporation of refrigerant, as this is related to the temperature difference. This is illustrated in Figure 4.5.

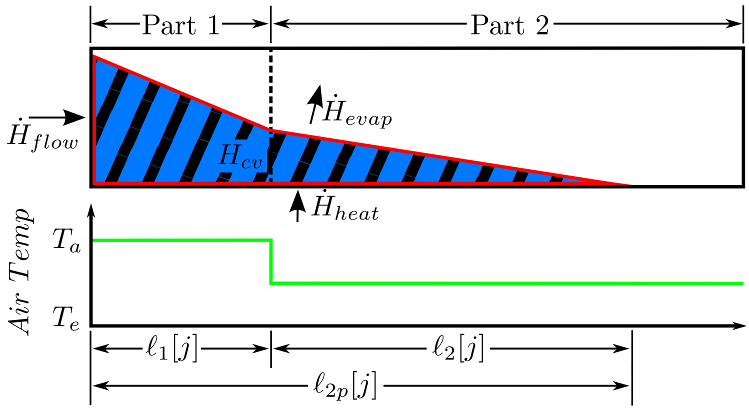

Figure 4.5: *The control volume used to model the length of the two-phase zone. Note that the temperature of the ambient air is no longer constant for the entire length of the two-phase zone.*

To model the temperature of the surrounding air, the temperature of the air at each part, and the lengths of each part, is used to calculate a mean temperature difference between the air and the refrigerant. The evaporation rate of a pipe is proportional to the mean temperature difference of the pipe. The mean temperature difference is different for each pipe and can be calculated for the j'th pipe as

$$\Delta T'[j] = \frac{T_a - T_e}{\ell_{2p}[j]} \sum_{i=1}^{N_{pa}} (\eta_i[j] \cdot \ell_i[j]) \qquad [K] \qquad (4.7)$$

where N_{pa} is the total number of parts and $\eta_i[j]$ is equal to 1 if the part is in front of the air flow and equal to Equation (4.6) if it is in the back. $\ell_i[j]$ is the length of the two-phase zone in the i'th part of the j'th pipe. For all parts except the last, this is equal to the length of the part. The sum of these lengths equals the length of the two-phase zone, as illustrated in Figure 4.5.

With the modified evaporation rate of refrigerant, and the modified temperature the model for the length of the two-phase zone in a single pipe becomes

$$\begin{aligned} &A_{pi} \cdot (1 - \gamma_{2p}[j]) \cdot \rho_l \cdot (h_g - h_l) \cdot \frac{d(\ell_{2p}[j])}{dt} \\ &= \dot{m}_v[j]\,(h_g - h_l) - \alpha_{2p} \cdot O_{pi} \cdot \ell_{2p}[j] \cdot \Delta T'[j] \qquad [J/s] \qquad (4.8) \end{aligned}$$

where $\ell_{2p}[j]$ and $\dot{m}_v[j]$ is the length of the two-phase zone in and the mass flow into the j'th pipe respectively. The fraction of gas, $\gamma_{2p}[j]$ is also different from pipe to pipe. A_{pi} and O_{pi} are the cross-section area and the circumference of a single pipe respectively.

An equation which describes the change in length of the two-phase zone in a single pipe, has now been derived. The pressure enters the equation, as the specific enthalpy for liquid and gas in the two-phase zone is determined by the pressure. Equation (4.8) is the state equation for the length of a two phase zone in one of the pipes in the evaporator. It is noteworthy, that the the dynamics of the different pipes are different.

With the equation describing the length of the two-phase zone in a single pipe derived, the equation describing the pressure is derived next.

4.1.4 Pressure Model

The pressure in the evaporator is related to the volume of refrigerant in gas phase. The liquid in the two-phase zones is assumed to be incompressible; therefore it does not change density with changes of pressure.

The control volume for the calculation of the pressure changes is set to enclose the total volume of gas in the evaporator, in the manifold and the pipe connecting the evaporator to the compressor. This is different compared to the conventional model. In the conventional model only the volume of gas in the evaporator is included in the model. However, it was concluded to be inaccurate.

In the improved model the volume of the manifold and pipe from evaporator to the compressor are included as well, as pressure changes in the evaporator leads to a pressure change in these volumes as well. However, the presence of liquid refrigerant is ignored as it only occupies between 1.7 % and 2.5 % of the volume of the evaporator, depending on mass flow, as seen from the result shown in Figure 3.7.

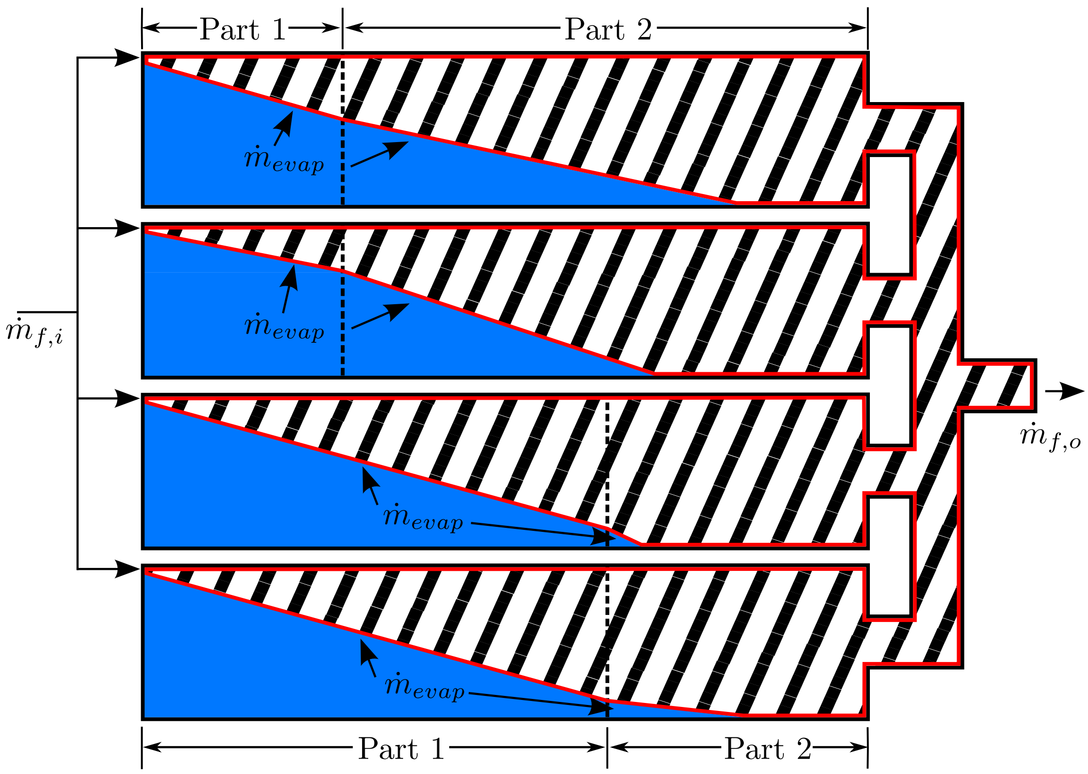

Figure 4.6: *Illustration of the control volume used to calculate the changes in pressure in the evaporator. The control volume consists of the gas in the evaporator, manifold and outlet tube combined.*

The volume in the evaporator is equal to the volume of gas in all the two-phase zones and the volume of all the superheated zones in the evaporator. The control volume is illustrated in Figure 4.6. The model of the pressure is based on the conventional model, see Equation (3.8).

The mass flow of gas into and out of the control volume is unchanged compared to the conventional model, as the sum of flow of gas into the control volume is equal to the mass flow through the valve, and the sum of flow out of the control volume equals the flow through the compressor.

The total flow from evaporation is different from the conventional model. The flow has to be expressed as the sum of evaporation in all pipes. In the calculation of the evaporation in a single pipe, the temperature difference between the air and the refrigerant is calculated by Equation (4.7).

The total volume of the control volume is equal to the combined volume of the gas in the evaporator, the gas in the manifold and the gas in the pipe. The volume of the gas in the evaporator is equal to the sum of the volume of gas in all the evaporator pipes. Since we do not consider the volume of the liquid refrigerant, the total volume of gas can be considered constant. It is expressed by the following equation.

$$V' \approx \sum_{j=1}^{N_{pi}} (V_g[j]) + V_{mf} + V_{pipe} \qquad [m^3] \qquad (4.9)$$

where N_{pi} is the number of pipes and V' is a constant that approximates the volume of the gas in the evaporator pipes, the manifold and the tube from the evaporator to the compressor combined. These changes are applied to the equation for pressure change, to get the equation

$$V' \cdot \frac{d(\rho_g)}{dP_e} \frac{d(P_e)}{dt} = \dot{m}_{v,g} - \dot{m}_{cp} + \frac{\alpha_{2p} \cdot O_{pi}}{h_g - h_l} \sum_{j=1}^{N_{pi}} \ell_{2p}[j] \cdot \Delta T'[j] \qquad [{}^{kg}/_{s}] \qquad (4.10)$$

where N_{pi} is the total number of pipes in the evaporator.

When the equation is compared to the differential equation that describes the pressure in the conventional model, see Equation (3.8), it is seen, that the only difference between the two equations is that in the new equation, the volume and modified evaporation rate to incorporate the individual pipes.

An equation that describes the pressure change has now been derived. The equation has the mass flow through the valve and the mass flow through the compressor as inputs. The length of the two-phase zones and the pressure in the evaporator enters as states in the equation.

Equation (4.10) is the state equation for the pressure in the evaporator. With the equation describing the pressure in the evaporator derived, the output temperature of the superheated gas from each pipe is calculated next.

4.1.5 Superheat Temperature Model

The length of the two-phase zones in each pipe has been shown to be different, and therefore the lengths of the superheat zones are also inherently different, and are modeled individually. The model of the output temperature of each pipe is based on the model for the output temperature of the evaporator in the conventional model, see Equation (3.14). With the assumption that the superheated zone is always confined to the last part in a pipe, the conventional model of the superheat temperature is valid for each pipe, with the following alterations: The temperature of the surrounding air is specific to each pipe and the length constant, β_e, has to be modified to each pipe. The temperature of the air around the last part of a pipe can be expressed by

$$T'_a[j] = T_e + (T_a - T_e) \cdot \eta_{N_{pa}}[j] \qquad [K] \qquad (4.11)$$

where $\eta_{N_{pa}}[j]$ is the air temperature constant for the last part of the j'th pipe.

A part of the length constant of the temperature is the mass flow and the circumference. Both have to be modified to apply to a single pipe. The mass flow in the superheated zone in a single pipe can be expressed as the sum of the mass flow of gas into and the evaporation in the two-phase zone. This is expressed by the equation

$$\dot{m}_{sh}[j] = \dot{m}_{v,g}[j] + \frac{\alpha_{2p} \cdot O_{pi} \cdot \ell_{2p}[j] \cdot \Delta T'[j]}{h_g - h_l} \qquad [kg/s] \qquad (4.12)$$

The modified length constant is equal to

$$\beta'_e[j] = \frac{\dot{m}_{sh}[j] \cdot c_{p,sh}}{\alpha_{sh} \cdot O_{pi}} \qquad [m] \qquad (4.13)$$

and the superheat temperature in the j'th pipe is equal to

$$T_{sh}[j] = \left(T'_a[j] - T_e\right)\left(1 - e^{-\frac{\ell_{sh}[j]}{\beta'_e[j]}}\right) \qquad [K] \qquad (4.14)$$

where $\ell_{sh}[j]$ is the length of the superheated zone in the j'th pipe.

The model of the superheat temperature describes the increase in temperature in a single pipe, but it is not valid if a pipe overflows with liquid refrigerant. In that situation, the enthalpy of the refrigerant, as it exits the pipe, is less than the dew point. For the model to be able to cover this situation a model of the enthalpy flow out of each pipe is needed.

When a pipe does not overflow, the enthalpy flow out of the pipe is equal to the enthalpy at the dew point plus the enthalpy added in the superheated zone. Both multiplied with the mass flow.

When a pipe overflows the enthalpy flow out is equal to the enthalpy flow into the pipe plus the heat transfer. This is less than the dew point.

To cover both situations, the enthalpy flow out of a pipe is expressed as

$$\begin{aligned}\dot{H}_e[j] = {} & \dot{m}_{v,g}[j] \cdot h_i + \alpha_{2p} \cdot O_{pi} \cdot \ell_{2p}[j] \cdot \Delta T'[j] + \\ & + c_{p,sh} \cdot T_{sh}[j] \cdot \dot{m}_{sh}[j] \qquad [J/s] \qquad (4.15)\end{aligned}$$

In the case where there is no overflow, the first two terms equals the enthalpy at the dew point multiplied with the mass flow and the last term equals the enthalpy flow from the superheated zone. In the case where there is overflow, the first two terms equals the enthalpy flow. The last term equals zero, as the length of the superheated zone is zero.

From the derived equation, the enthalpy flow out of a single pipe can be calculated. This is used to calculate the temperature out of the manifold, which is calculated next.

4.1.6 Manifold Model

The outputs of the individual pipes are connected together in the manifold. The manifold mixes the flows together to one output. A model of the combined output temperature is needed, as this is the temperature at the inlet of the compressor. Equation (4.15) is the enthalpy flow out of a single pipe. As the manifold mix the flow from each pipe together, it is assumed that the enthalpy flow out of the manifold is the mean of the flows out of the pipes.

$$\dot{H}_o = \frac{1}{N_{pi}} \sum_{j=1}^{N_{pi}} \dot{H}_e[j] \qquad [J/s] \qquad (4.16)$$

To get the output temperature, the enthalpy flow is divided by the mass flow and the heat capacity. From this the superheat temperature can be calculated by

$$T_{sh} = \frac{\dot{H}_o}{\dot{m}_{cp} \cdot c_{mf}} - T_e \qquad [K] \qquad (4.17)$$

when it is assumed that the mass flow in the manifold is equal to the mass flow in the compressor.

4.2 Fitting of the Model

The modified model introduces new variables in the model, and is therefore refitted to the test setup. The parameters that needs to be estimated are η, A_{pi}, γ_{2p}, O_{pi}, $\ell_i[j]$ and V'. α_{2p} and α_{sh} has to be estimated as well, as the introduction of η changes the parameters. To estimate the constants, a series of experiments are conducted.

4.2.1 Estimation of the Air Temperature Constant

To estimate the air temperature constant η, an experiment is conducted. Recall when the air flows past the evaporator the temperature drops from the first pipe to the second. Similarly, the temperature drops from the second pipe to the end, as shown in Figure 4.7.

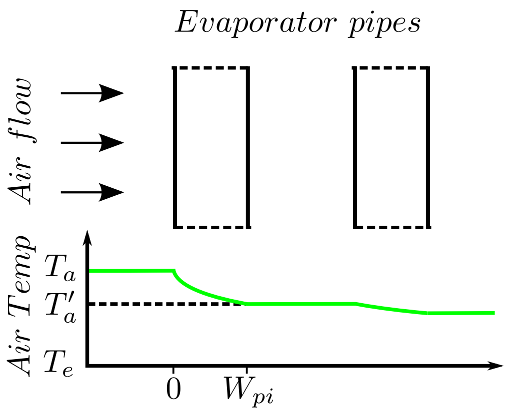

Figure 4.7: *Illustration of the temperature change of the ambient air as it flows by the evaporator pipes.*

The temperature change of the air during passage of the evaporator can be calculated as

$$T(x) = T_e + (T_a - T_e)\, e^{-x/\beta_a} \qquad [K] \qquad (4.18)$$

and recall that

$$\eta = e^{-W_{pi}/\beta_a} \qquad [-] \qquad (4.19)$$

It is seen, that if Equation 4.18 is calculated with twice the width of a pipe, the resulting temperature from the equation is equal to the temperature after the last pipe, and therefore equal to the temperature of the air after the evaporator.

By measuring the temperature of the air before and after the evaporator, and calculating the evaporation temperature, the only free parameter is η, which is then obtained by fitted it to the data.

The experiment was designed so the test setup was in steady state at two different evaporator pressures, and thus two different evaporation temperatures. Both operating points were chosen so the length of the superheated zone was small. Figure 4.8 shows the inputs used in the experiment. As η is constant, the fit should equally good in both operating points.

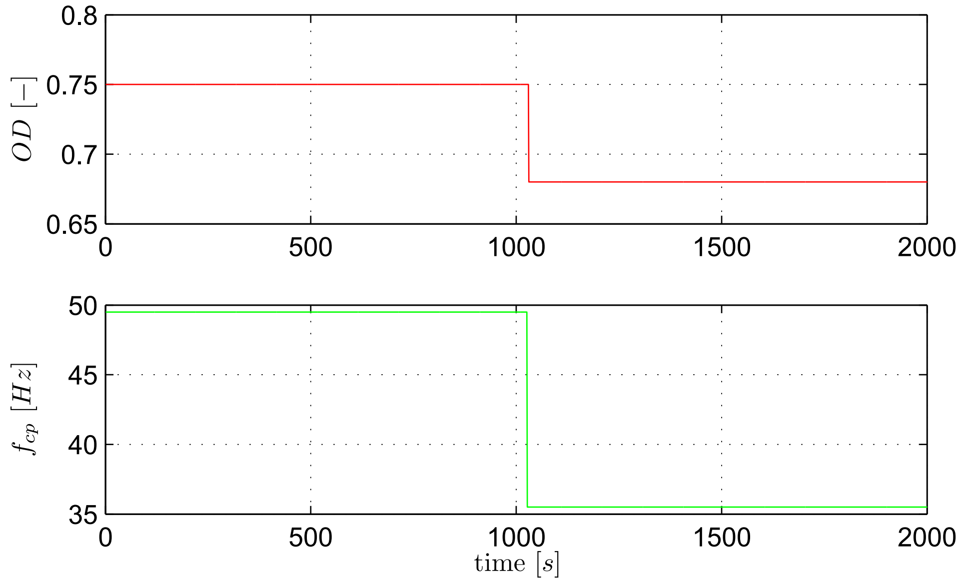

Figure 4.8: *Inputs used in the experiment to estimate η for a pipe that is behind another.*

From the test data obtained in the experiment, the output temperature was calculated. η was estimated so the difference between the calculated and the measured output air temperature was minimized in a least squares sense. Figure 4.9 shows the measured and the calculated output air temperature.

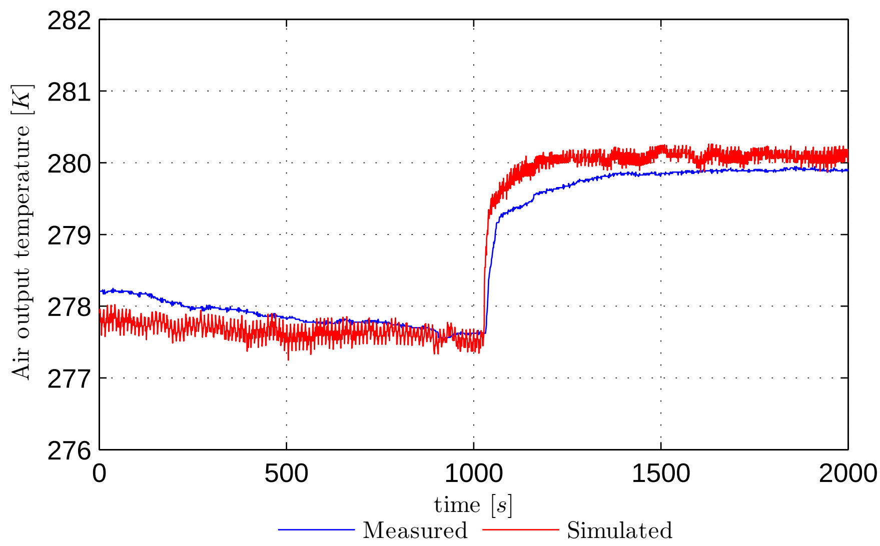

Figure 4.9: *The predicted air temperature after the evaporator when η is fitted to the measurements. The fit is very good, and supports the theory that η is indeed a constant, if the air flow is held constant.*

The estimated air temperature fits the measurements in both operating points. From the estimated constant in the experiment η was found, for which only a single pipe width was used in the calculation. The constant was found to be

$$\eta = 0.674 \qquad [-] \tag{4.20}$$

Based on the estimated η and measured lengths of the parts in all pipes, an overview of $\eta_i[j]$ and $\ell_i[j]$ can be seen in Table 4.1.

			Pipe			
			1	2	3	4
Part	1	$\ell_1[j]$ $[m]$	7.8	7.8	5.2	5.2
		$\eta_1[j]$ $[-]$	1	0.674	0.674	1
	2	$\ell_2[j]$ $[m]$	5.2	5.2	7.8	7.8
		$\eta_2[j]$ $[-]$	0.674	1	1	0.674

Table 4.1: *Length and air temperature constant η, for all parts in all pipes. η is equal to 1 if a part is the first part in the flow of ambient air and equal to 0.674 if the part is behind another.*

From the experiments we see that η is indeed constant as long as the airflow of the evaporator is held constant, and the superheat is kept constant. This explains the different evaporation rates in the different pipes of the evaporator.

4.2.2 Calculation of the Void Fraction

The void fraction in a single pipe in the new model is calculated by the same principle as the void fraction for the entire evaporator, see Subsection 3.2.1. The void fraction for a two-phase zone in a pipe can be expressed as the average of the area mean void fraction, which is the void fraction of a cross-section area of the evaporator. As the void fraction is the volume of the gas compared to the total volume, this can be calculated from the mass of the gas at a cross section compared to the total mass.

In the calculation in the conventional model, it is assumed that the mass flow of gas increase linearly between the start and the end of the two-phase zone. This assumption is only valid if the rate of evaporation is the same throughout the pipe. However, the model proposed in this thesis incorporates different rates of evaporation in different parts of the pipe. Therefore a modification to the calculation of γ is needed.

The rate of evaporation with respect to length, and thereby the gas flow in a part with respect to length depends on the value of η in the part. This is illustrated in Figure 4.10 for two different pipes. Both pipes have the same length and gas flow in, but the volume of gas is different because the rates of evaporation in their corresponding parts are different. The combined rates of evaporation in their correspondent two-phase zones are the same. Therefore the lengths of their two-phase zones are also the same.

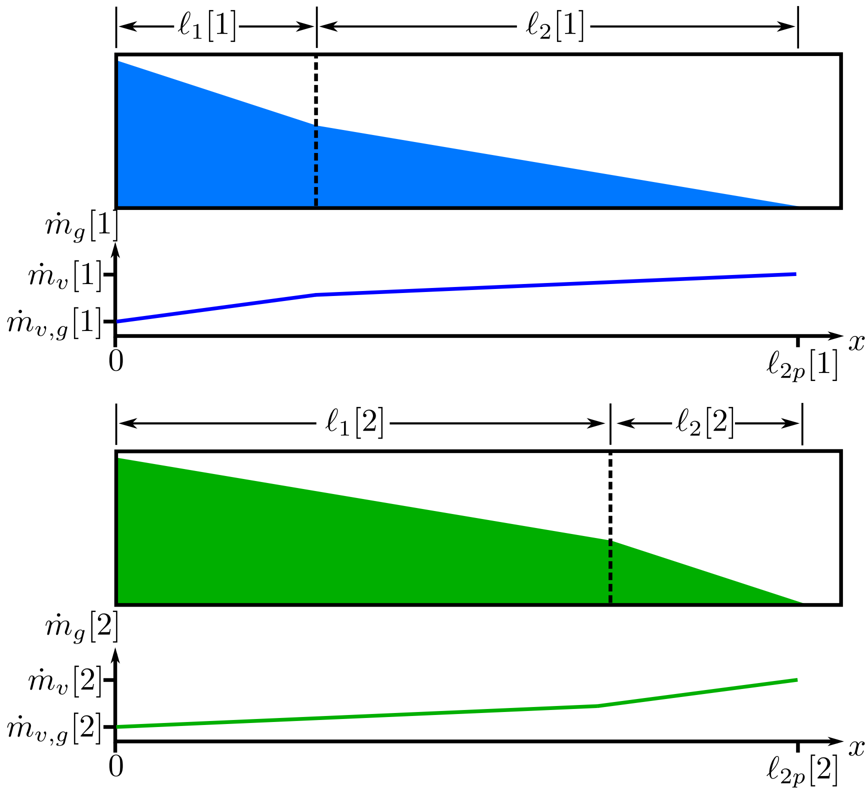

Figure 4.10: *Mass flow of gas in two different pipes. Even through the length of the two-phase zones in the two pipes are the same, the volume of gas is different, which gives different void fractions.*

To calculate the ratio of gas flow versus liquid flow at any point of the pipe, it is calculated backwards from the end of the two-phase zone. By the end of the two-phase zone, it is known that the entire flow in the pipe has gas form. Moving back towards the inlet the flow of refrigerant consists more and more of liquid as it has not yet had time to evaporate. This difference of gas flow between the end of the two-phase zone to anywhere before is equal to the refrigerant that evaporate between these two points. This can be expressed as

$$\dot{m}_{g,border}[j] = \dot{m}_v[j] - \frac{\alpha_{2p} \cdot O_{pi} \cdot (T_a - T_e) \cdot \ell_2[j] \cdot \eta_2[j]}{h_g - h_l} \qquad [^J/_s] \qquad (4.21)$$

which is the gas flow out of the pipe minus the evaporated gas in the last part. The mass flow of gas at the start of the pipe is calculated by the mass flow into the pipe minus the total evaporation

$$\dot{m}_{g,i}[j] = \dot{m}_v[j] - \frac{\alpha_{2p} \cdot O_{pi} \cdot \ell_{2p}[j] \cdot \Delta T'}{h_g - h_l} \qquad [^J/_s] \qquad (4.22)$$

Because the rate of evaporation within a part is assumed to be linear, the mass flow of gas at any point in the second part can be calculated by

$$\dot{m}_{g,2}(x_2) = \dot{m}_{g,border}[j] + \frac{x_2}{\ell_2[j]} \left(\dot{m}_v[j] - \dot{m}_{g,border}[j]\right) \qquad [^{kg}/_s] \qquad (4.23)$$

where x_2 is a number between 0 and $\ell_2[j]$. And similarly in the first part the mass flow at any point x_1 can be calculated by

$$\dot{m}_{g,1}(x_1) = \dot{m}_{g,in}[j] + \frac{x_1}{\ell_1[j]}\left(\dot{m}_{g,border}[j] - \dot{m}_{g,in}[j]\right) \qquad [kg/s] \tag{4.24}$$

where x_1 is a number between 0 and $\ell_1[j]$.

Now that the fraction between gas and liquid at any point of the two-phase zone has been calculated, it is converted to volume fraction by scaling with the specific volumes of gas and liquid. This yields the area mean void fraction in the two parts at any point x_1 and x_2 for the first and second part respectively. This is calculated based on Equation (3.16) as

$$\begin{aligned}\gamma_{am,1}(x_1) &= \frac{v_g \cdot \dot{m}_{g,1}(x_1)}{v_g \cdot \dot{m}_{g,1}(x_1) + v_l \cdot (\dot{m}_v - \dot{m}_{g,1}(x_1))} && [-]\\ \gamma_{am,2}(x_2) &= \frac{v_g \cdot \dot{m}_{g,2}(x_2)}{v_g \cdot \dot{m}_{g,2}(x_2) + v_l \cdot (\dot{m}_v - \dot{m}_{g,2}(x_2))} && [-]\end{aligned} \tag{4.25}$$

Now that the mean area void fraction at any point in the entire two-phase zone is known, the void fraction for the entire two-phase zone is calculated as the mean of the area mean void fractions

$$\gamma_{2p} = \frac{1}{\ell_{e,1}[j]}\int_0^{\ell_{e,1}[j]} \gamma_{am,1}(x_1)dx_1 + \frac{1}{\ell_{e,2}[j]}\int_0^{\ell_{e,2}[j]} \gamma_{am,2}(x_2)dx_2 \qquad [-] \tag{4.26}$$

These integrals can be calculated explicitly, and are therefore computationally easy to calculate. The explicit equation is omitted in this report.

4.2.3 Estimation of the Heat Transfer Coefficients

With the air temperature constant, η, estimated, the heat transfer in the two-phase zone and the superheated zone can be estimated. By conducting an experiment where the system is in many different steady state situations, a dataset for estimation of the heat transfer coefficients is obtained. By conducting the experiment with long intervals between steps in *OD*, the fit of the system is dominated by the steady state error and not the dynamics of the system.

By ramping the *OD* slowly from high to low flow, the system is fitted in a wide range of different operating points. The input signal can be seen in Figure 4.11.

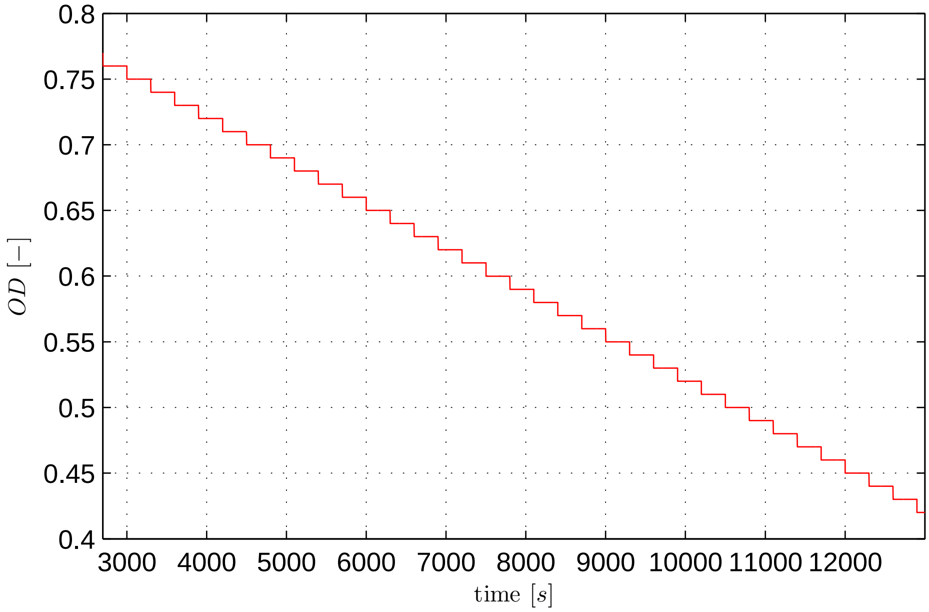

Figure 4.11: *Input signal in the experiment used to find the heat transfer in the two-phase and superheated zone. The compressor was held constant at $35.5Hz$ for the entire experiment.*

The parameters $\alpha_{2p} \cdot O_{pi}$ and $\alpha_{sh} \cdot O_{pi}$ are estimated by minimizing the function

$$error = \sum_{n=1}^{N} \left(10^{10} \cdot \left(T_o[n] - \hat{T}_o[n]\right)^2 + \left(P_e[n] - \hat{P}_e[n]\right)^2\right) \qquad [-] \qquad (4.27)$$

The function is chosen to weight the temperature and the pressure measured in bar evenly. The calculated values for the heat transfers is

$$\alpha_{2p} \cdot O_{pi} = 13.08 \qquad [J/s{\cdot}K] \qquad (4.28)$$

$$\alpha_{sh} \cdot O_{pi} = 3.8 \qquad [J/s{\cdot}K] \qquad (4.29)$$

For convenience the result of the fitting of the same experiment using the conventional model, shown in Figure 3.11 is reprinted in Figure 4.12. Notice the sharp drop in superheat temperature predicted by the conventional model. This is not in agreement with the measurements. The conventional model predicts $T_o = T_e$ when the superheat has dropped, which is clearly not the case. Also the conventional model predicts $T_o = T_a$ when the superheat is very high. This is not the case either.

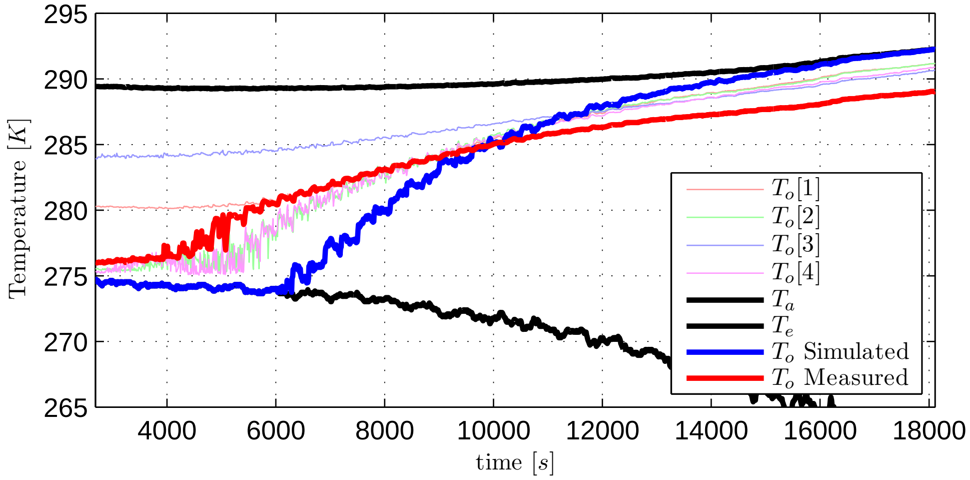

Figure 4.12: *Result from the fitting of the heat transfer coefficient in the superheated zone of the conventional model. The figure shows the simulated output temperature from the evaporator calculated with the estimated heat transfer coefficient.*

The improved model of the evaporator explains these effects very well. The result of the fit is shown in Figure 4.13.

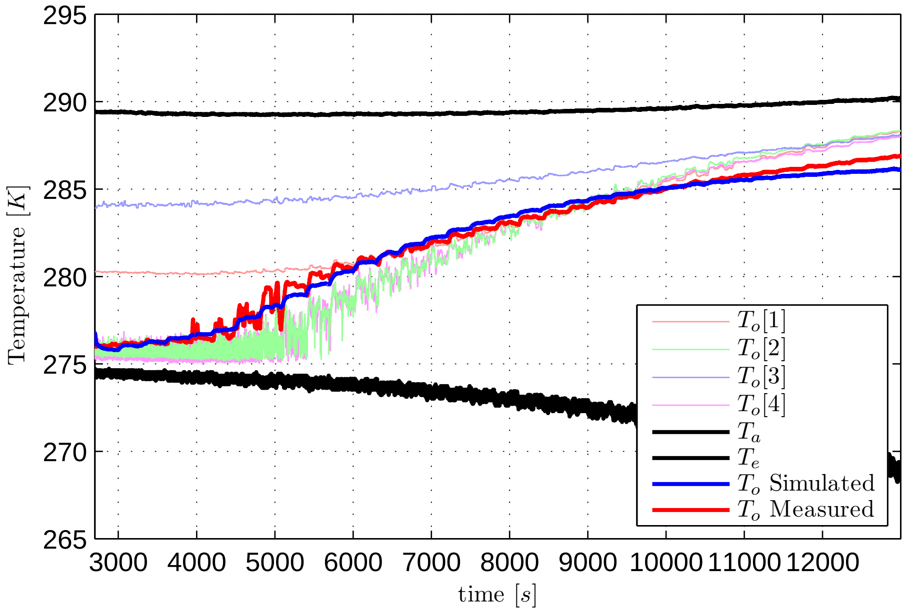

Figure 4.13: *Result from the estimated heat transfer coefficient for the two-phase zone and the superheated zone of the improved model. The system is simulated with the found parameters and compared to the measurements.*

It is seen that the fit is very good compared to the fit shown in Figure 4.12. There are several improvements.

First the improved model explains why the superheat temperature does not drop all the way to T_e as the evaporator overflows. Instead the transition is smooth because the pipes do not overflow at the same time because they are not evenly filled. This is a consequence of different air temperatures around different pipes, which gives different evaporation rates, which cause uneven filling.

Second, it explains why T_o never reaches T_a even at large superheat temperatures. This is again a consequence of different air temperatures around different pipes. The air around the pipes behind other pipes is cooled before hitting the pipe. Therefore the gas temperature of the particular pipe only reaches T_a', and when the gas is mixed with the gas from the other pipes, the result is a lower temperature.

To back this up we have included a Figure showing the simulated output temperature of each pipe compared to the measured. This is shown in Figure 4.14.

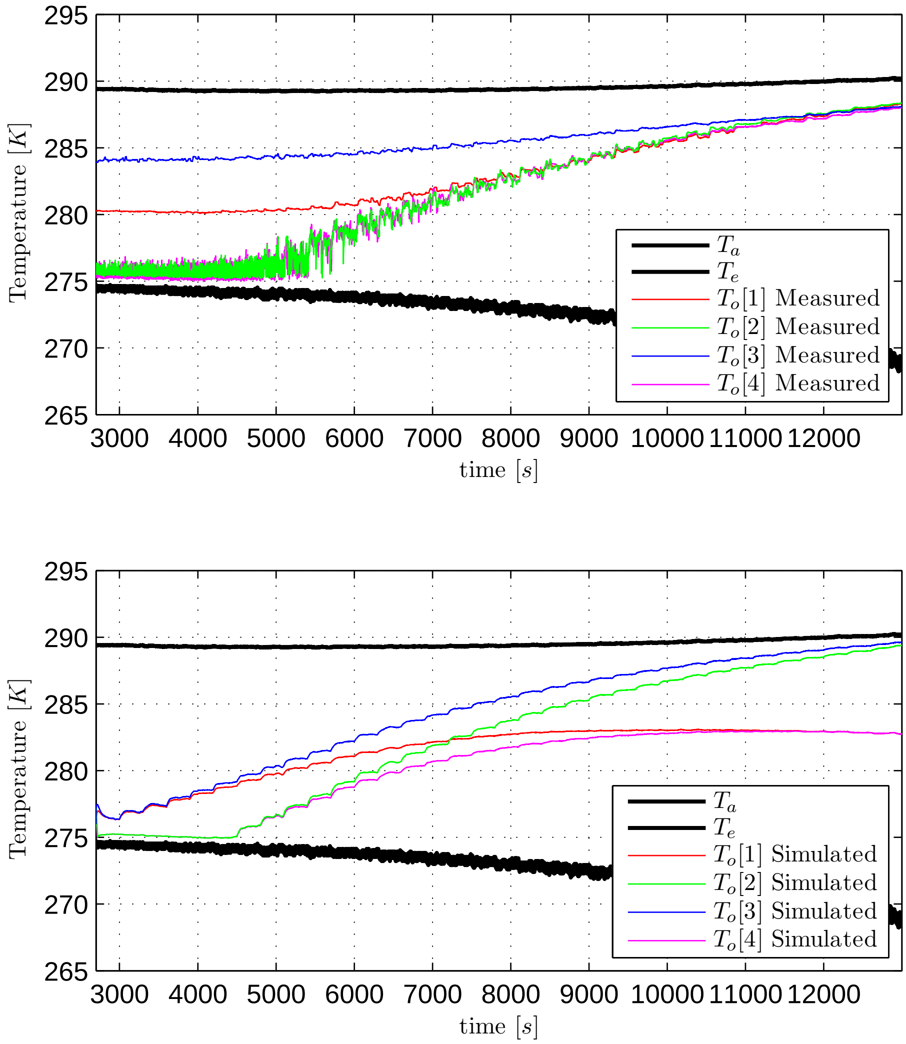

Figure 4.14: *The output temperatures of the different pipes compared to measurements. The improved model predicts that some pipes overflow well before others. When the superheat temperature is very large, the predicted output temperatures are no longer accurate. This is because the assumptions for the derivation of T_a' is no longer valid.*

It is seen in the figure, that the model captures the measurements to some extend, whereas the

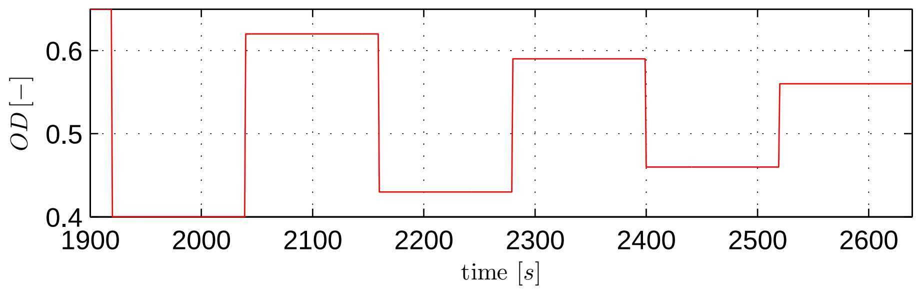

Figure 4.15: *Input signal in the experiment used to find the cross-section area of an evaporator pipe and the volume of the evaporator. f_{cp} is held at a constant $35.5\ Hz$.*

conventional model would predict the temperatures of each pipe to be the same, which is clearly not the case. Most importantly the improved model predicts each pipe to be overflowing at different times causing the smooth transition from a superheated state to an overflowed state. The improved model does not hold particularly well for very large superheat temperatures. This is because as T_o deviates more and more from T_e the estimate of η becomes less precise. In this situation, heat transfer from one superheat zone to another through the metal of the evaporator may account for the convergence of the output temperature of all the pipes when the superheat temperature is large. This is not included in the model. However, as the model is to be used for superheat control it is more important that it explains the behavior at low superheat temperatures. The model has now been estimated in steady state, but we have not yet covered the dynamics of the model. These are estimated in the next subsection.

4.2.4 Estimation of the Cross-section Area and the Volume

The cross-section area of an evaporator pipe is a part of the equation of the length of the two-phase zone in an evaporator pipe, Equation (4.8). It determines how fast the dynamics of ℓ_{2p} are. To estimate it, an experiment, which reveals the dynamics of the evaporator, is needed. The data is then fitted the parameter to the data.

The volume of the evaporator, manifold and evaporator outlet tube, V', determines how fast the dynamics in P_e are. See Equation (4.10). This parameter can also be estimated by conducting an experiment, which reveals the dynamics of P_e. Both parameters are estimated using the same experiment. The input signal of the experiment is shown in Figure 4.15. It has been necessary to include delays in the system to make the fitting, as they become significant in this type of experiment. If they are not included, the result would be hard to interpret. The parameters are fitted, so that the following error function is minimized.

$$error = \sum_{n=1}^{N} \left(0.5 \cdot 10^{10} \cdot \left(T_o[n] - \hat{T}_o[n - T_d]\right)^2 + \left(P_e[n] - \hat{P}_e[n]\right)^2\right) \qquad [-] \qquad (4.30)$$

T_d compensates for the time delay of T_o, which is not covered in the model, but included to make a better fit. T_d was found by inspection of the data. The weight on T_o compensates for the size difference on the steps on T_o and P_e.

The resulting parameters from the fit are

$$A_{pi} = 6.88 \cdot 10^{-6} \qquad [m^2] \tag{4.31}$$
$$V' = 43.1 \cdot 10^{-3} \qquad [m^3] \tag{4.32}$$

The result of the fit can be seen in Figure 4.16.

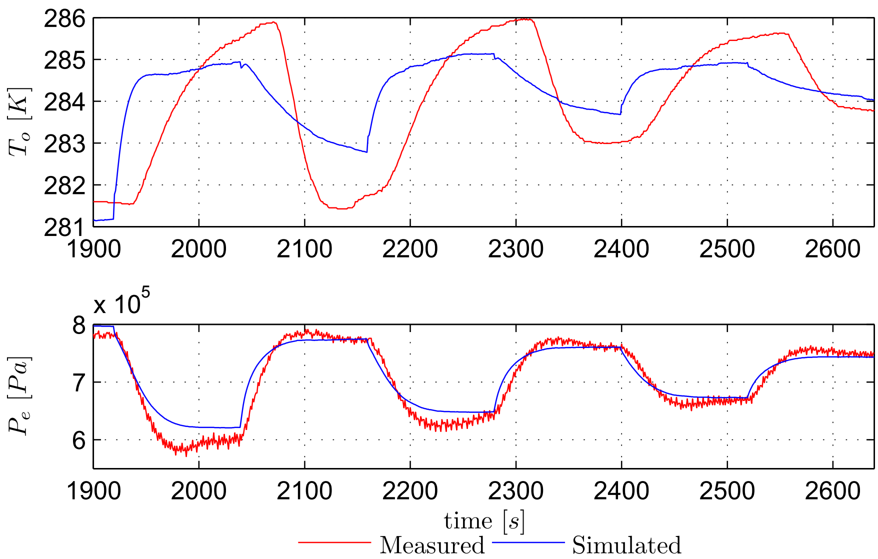

Figure 4.16: *Result of the estimation of A_{pi} and V_e. The figure shows the measured and the simulated T_o and P_e. The dynamics in T_o are not described that well. However, the dynamics in P_e fits reasonable well.*

As it is seen in the figure the dynamics in the simulation of the pressure is a good fit of the measured pressure, but the dynamics of the simulated output temperature does not fit accurately. The time delay of T_o is also not captured in the model. From the measurements it is seen that T_o rises slowly and falls fast. This is not captured by the model either. The implications of this are discussed further in the design of the controller.

The modifications of the conventional model has now been described, and evaluated by fitting the improved model to measurements. The split of the evaporator into pipes and the introduction of different ambient air temperatures around the parts in a pipe give a better fit of the steady state output temperature from the evaporator. The model no longer reaches T_a at large superheat temperatures, and it does not immediately reach T_e when the first pipe overflows. However the fit of the dynamics of T_o are not improved. The time delay is not covered in the model, and the varying rise and fall times are not covered properly. However, as we aim to save the pressure sensor of the system, but keep the temperature sensor, it may not be very critical that the dynamics do not fit accurately. Also the system may run in closed loop most of the time, in which case the dynamics is not very dominant. In closed loop the steady state estimates may be much more dominant, and they are predicted much better by the model.

The dynamics of the pressure does fit the data very well, both in the dynamics and the steady state. Since we want to save the pressure sensor, a model which is good at predicting P_e is desirable.

4.3 Temperature Oscillations at Low Superheat

In the experiments used to determine the heat transfer coefficients, some unexpected oscillations in T_o are observed. At low superheat temperatures the measured value of T_o began to oscillate around the expected value. The fluctuations began when the first evaporator pipes overflowed, and became smaller as T_o became closer to T_e. This was observed in the experiments used to estimate α_{2p} and α_{sh}, seen in Figure 4.13.

As the oscillations occur at low superheat temperatures consistently, it should be possible to detect it. One way to detect if something varies is to compute the sample variance of it. So if the sample variance of T_o is large it indicates the output is varying because this only occurs at low superheat, it also indicates that the evaporator is nearly overflowing. The sample variance, σ^2 is defined as

$$\sigma^2 = \frac{1}{N}\sum_{i=1}^{N}(x_i - \mu)^2 \qquad [-] \qquad (4.33)$$

where μ is the sample mean defined as

$$\mu = \frac{1}{N}\sum_{i=1}^{N} x_i \qquad [-] \qquad (4.34)$$

where x_i is element i of the vector x of which the variance is computed, and N is the sample size. From here on the population variance is simply referred to as the variance.

To test the method of overflow detection the variance of the last 5 minutes of T_o is computed at every time step for the dataset used to fit α_{2p} and α_{sh}. A plot of this is shown in Figure 4.13. In the experiment *OD* is decremented slowly. As a result the evaporator goes from being overflown to being more and more superheated. The variance of the last 5 minutes is computed for T_o at each time step. This is shown in Figure 4.17.

To verify that the oscillations is indeed an effect of low superheat, and not an effect of sweeping *OD*, another experiment was conducted. *OD* was set so the first pipe in the system was close to overflowing. Every 20 minutes a small increase to *OD* was performed. By increasing the time between the steps, the system was in steady state longer, and the steady state behavior of the system could be observed. The resulting data shows that T_o does indeed oscillate, even though it should be in steady state. The steps in *OD* affect the variance, but the variance does disappear after the steps. The result of the experiment is shown in Figure 4.18.

This is interesting as it can be used to detect when the superheat is low without the use of a pressure sensor. This may imply that the pressure sensor of many cooling systems is unnecessary, and may be saved. The superheat may not be accurately estimated at high superheat. However, this may be sufficient in many applications, because the systems mostly operate at low superheat. Another problem is that the variance also rises when the system is given an input or is subject to disturbances. In order to estimate the superheat, the expected fluctuations in T_o should be compensated.

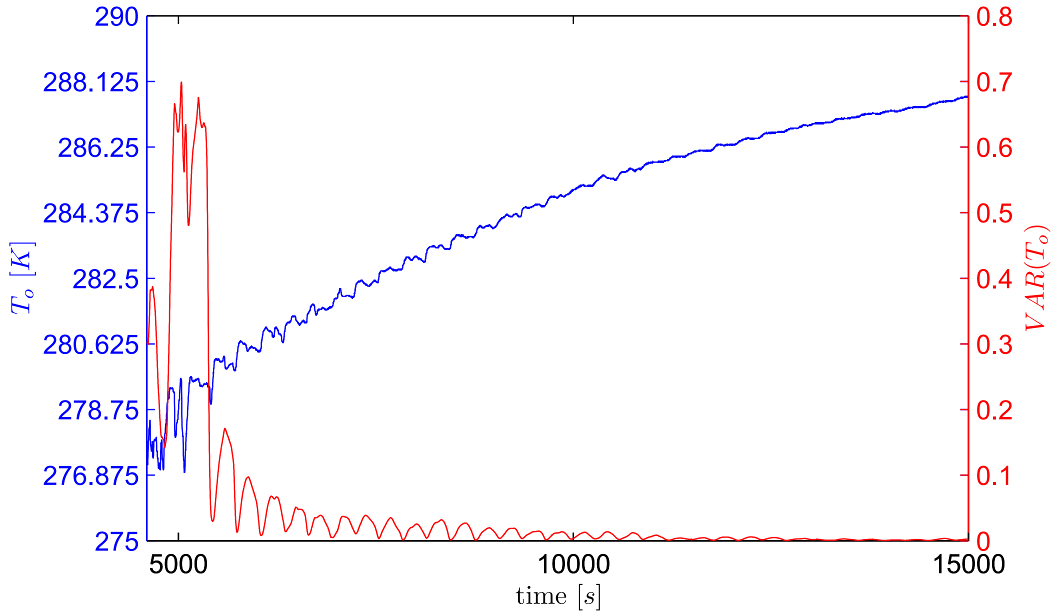

Figure 4.17: *Variance of T_o calculated for the experiment used to estimate α_{2p} and α_{sh}. Note that the time line is several hours, and therefore the T_o should be in steady state most of the time. But it clearly varies at low superheat temperatures.*

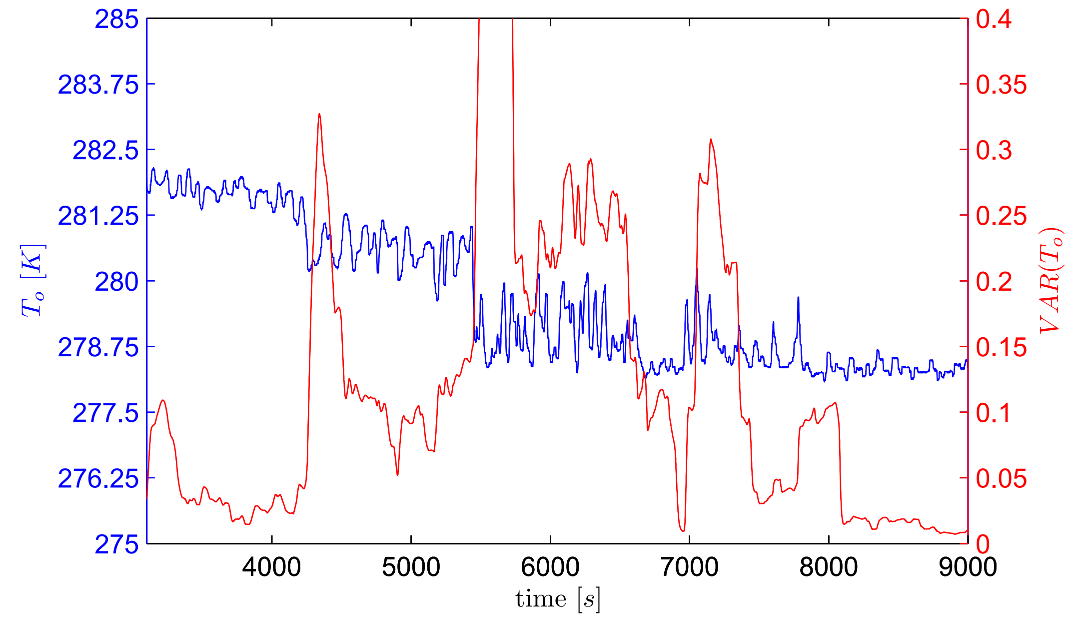

Figure 4.18: *Variance of T_o where OD is increased one step every 20 minutes. This shows the steady state with low superheat. Obviously the steps in OD influence the variance, but even when the system should be in steady state, the variance is present. Towards the end the variance decreases again. This is a sign that the evaporator is slowly starting to become overflowed.*

Chapter 5

Controller Design

The purpose of the controller is to control the superheat temperature of the system at a fixed low reference temperature, as this makes the system more efficient. However, it is important that the controller prevents the evaporator from overflowing, as this can cause damage to the compressor.

The non-linear controller designed in (Rasmussen and Larsen, 2011) results in a cascade structure, where P_e is controlled in the inner loop and the superheat is controlled in the outer loop. According to (Rasmussen and Larsen, 2011), this design improves the performance of the controller, and it works for large deviations in the length of the two-phase zone. The non-linear blocks can be seen as PI controllers without loss of concept. This interpretation is shown in Figure 5.1. However, the structure relies on an accurate pressure measurement, as it is used in the inner, fast, feedback loop of a cascade structure. This may not work without a pressure sensor.

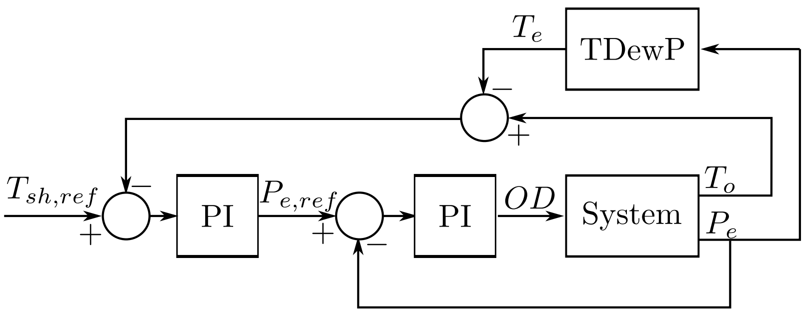

Figure 5.1: Illustration of the controller design used in (Rasmussen and Larsen, 2011). The controller utilizes an inner loop where the pressure is controlled.

The desired system is one that only utilize the T_o sensor, and not the pressure sensor, which measures P_e. It is desirable to save the pressure sensor because it lowers the overall cost of the system. However, without the pressure sensor, it is not possible to build the cascade structure. Furthermore the superheat temperature cannot be immediately calculated. Therefore we develop a controller for the system, which solely uses the T_o measurement. The structure of the controller is discussed next.

5.1 Superheat Controller with Estimated Pressure

We propose a controller structure, which does not control P_e in an inner loop. P_e is merely used to calculate T_e in order to obtain a $T_{o,ref}$ when $T_{sh,ref}$ is known. This structure is shown in Figure 5.2.

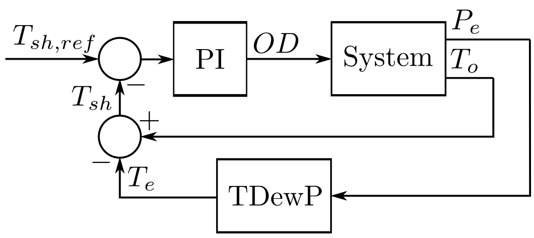

Figure 5.2: *Feedback loop of the proposed controller when T_e is assumed available.*

The PI controller, which is tuned in the worst case operating point, is tuned using Ziegler-Nichols tuning principle (Franklin et al., 2006, p. 198). This is used to control T_{sh}.

This structure is chosen because a P_e measurement is not readily available for control in an inner loop, but has to be estimated. The estimate is assessed not to be good enough for the cascade structure, which uses P_e in the inner loop. However, it may be good enough to estimate the superheat temperature, and use it to set a superheat reference. The proposed estimator is comprised of a linear small signal observer in conjunction with a steady state estimator. This is shown in Figure 5.3

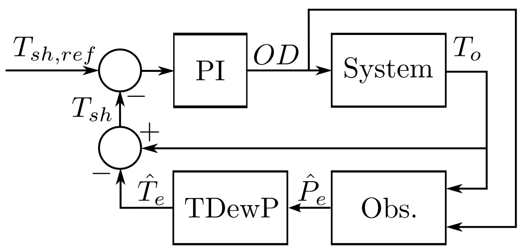

Figure 5.3: *Proposed controller structure where P_e and thus T_e is now estimated using an observer.*

A special reference logic continuously lowers $T_{sh,ref}$ until low superheat is detected using the method described in Section 4.3. That is when the variance in T_o rises, it indicates low superheat. A diagram of the control structure is shown in Figure 5.4.

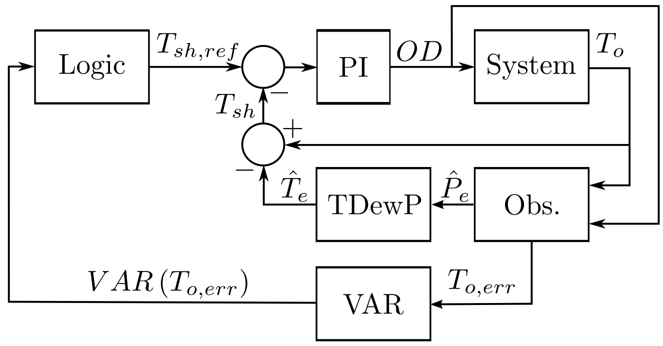

Figure 5.4: *Proposed controller structure where P_e and thus T_e is now estimated using an observer, and a special reference logic is used to continously lower $T_{sh,ref}$.*

However, the controller uses a filtered version of T_o for the calculations called $T_{o,err}$. This is the estimation error of T_o the observer predicts. In this way expected dynamics due to changes in *OD* are filtered out, preventing false detections of low superheat. When the low superheat is detected, $T_{sh,ref}$ is stepped back a small amount, and then lowered slowly. This is to keep the evaporator from overflowing, while still having near optimal filling.

A sufficiently good estimate of P_e is key to the success of the controller, as this provides information about the superheat level, even when low superheat is not detected. The next sections describe the development of the different parts of the controller structure. A prerequisite for both the development of the PI controller and the small signal observer is a linear model. The linear model is derived in the next Section of this chapter. The section after that is about the development of the PI controller used in the system. Then the reference logic is described. An observer is needed for filtering out the dynamics of the system from the oscillations of T_o at low superheat. The observer is described after the reference logic.

5.2 Linearized Model

A linear model of the evaporator, for the design of the observer, is derived. The linear model is based on the model of the evaporator described in Chapter 4. The linearization is done by approximating the behavior of the evaporator around an operating point with a small signal model. The linear model can the be parameterized in any operating point, to represent the system in that operating point. The scope of the linear model is to fit the non-linear model of the evaporator when calculated in an arbitrary operating point.

The linearization is done by simplifying the equation for the length of the two-phase zone in the evaporator, the equation for the pressure in the evaporator and the equation for the output temperature. The simplified equations are then collected in a small signal state space representation. The small signal model is represented so it can be calculated in all operating points. To simplify the linear model, it is assumed that the lengths of the two-phase zones in the four pipes are the same. This is done to ensure observability.

A more detailed calculation of the linear model can be seen in Appendix B.

5.2.1 Length of the Two-phase Zone

The state equation for the length of the two-phase zone in a single pipe in the evaporator is described in Equation (4.8). Some of the terms in the equation are calculated as functions of other variables in the system. When these dependencies are included, Equation (4.8) becomes

$$\begin{aligned} &A_{pi} \cdot (1 - \gamma_{2p}(\ell_{2p}, P_e, \dot{m}_v, T_{c,o})[j]) \cdot \rho_l(P_e) \cdot (h_g(P_e) - h_l(P_e)) \cdot \frac{d\,(\ell_{2p}[j])}{dt} \\ &= \dot{m}_v[j] \cdot (h_g(P_e) - h_i(P_e)) - \alpha_{2p} \cdot O_{pi} \cdot \ell_{2p}[j] \cdot \Delta T'[j] \qquad [J/s] \qquad (5.1) \end{aligned}$$

With the assumption that the lengths of the two-phase zone in the four pipes are the same, Equation (5.1) can be rewritten to express the change in the total length of the evaporator. This is done by adding the equations for all the pipes together.

At the left-hand side of the equation, the addition of the four pipes result in a multiplication with N_{pi}. γ_{2p} is calculated as the mean of the four pipes. All the variables multiplied with the derived length are collected into a single function of the operating point, $f_1(\bar{\ell}_{2p}, \bar{P}_e, \bar{\dot{m}}_v, \bar{T}_{c,o})$.

The mass flow into the evaporator pipes are estimated with a first order Taylor approximation. The approximation is a function of OD. The enthalpy difference and the terms from the valve equation, Equation (2.20), are collected into a single function of the operating point, $f_2(\bar{P}_e, \bar{P}_c, \bar{T}_{c,o})$.

The last term on the right-hand side of the equation is the heat transfer. When the length of the two-phase zone in all four pipes are assumed to be identical, the temperature difference is reduced to $\eta' \cdot (T_a - T_{e,2p}(P_e))$. η' is the mean of the value of η in all pipes. This is equal to the constant $(1+\eta)/2$ for all lengths of the two-phase zone.

With these alterations, Equation (5.1) becomes

$$f_1(\bar{\ell}_{2p}, \bar{P}_e, \bar{\dot{m}}_v, \bar{T}_{c,o}) \cdot \frac{d\,(\ell_{2p})}{dt} = f_2(\bar{P}_e, \bar{P}_c, \bar{T}_{c,o}) \cdot \big(od_1(\bar{OD}) + od_2(\bar{OD}) \cdot OD\big)$$
$$- \alpha_{2p} \cdot O_{pi} \cdot N_{pi} \cdot \eta' \cdot \ell_{2p} \cdot (T_a - T_e(P_e)) \qquad [J/s] \qquad (5.2)$$

5.2.2 Evaporator Pressure

The state equation for the pressure in the evaporator is described in Equation (4.10). Some of the terms in the equation are functions of other variables in the system. When these dependencies are included Equation (4.10) becomes

$$V' \cdot \rho_g'(P_e) \frac{d(P_e)}{dt} = \dot{m}_{v,g} - \dot{m}_{cp} + \frac{\alpha_{2p} \cdot O_{pi}}{h_g(P_e) - h_l(P_e)} \sum_{j=1}^{N_{pi}} \ell_{2p}[j] \cdot \Delta T'[j] \qquad [kg/s] \qquad (5.3)$$

The term on the left-hand side that is multiplied with the derivative of the pressure is joined into a function of the operating point, $f_3(\bar{P}_e)$.

The first term on the right-hand side of the equation is the mass flow of gas through the valve. Like in the length of the two-phase zone, this is estimated with a first order Taylor Approximation. The terms from the equation of the mass flow through the valve, Equation (2.20), and the enthalpy modifier are joined into a function of the operating point, $f_5(\bar{P}_e, \bar{P}_c, \bar{T}_{c,o})$.

The second term on the right-hand side of the equation is the mass flow through the compressor. This is expressed in Equation (2.8), which is inserted in the equation.

The last term on the right-hand side is the mass flow from evaporation. The temperature difference is expressed in the same way as in the equation for the length of the two-phase zone. Some of the variables in the term are joined into a function of the operating point, $f_4(\bar{P}_e)$. With these alterations, Equation 5.3 becomes

$$f_3(\bar{P}_e) \frac{d(P_e)}{dt} = f_5(\bar{P}_e, \bar{P}_c, \bar{T}_{c,o}) \cdot \big(od_1(\bar{OD}) + od_2(\bar{OD}) \cdot OD\big)$$
$$- V_{cp,i} \cdot f_{cp} \cdot \rho_g(P_e) + f_4(\bar{P}_e) \cdot (T_a - T_e(P_e)) \cdot \ell_{2p} \qquad [kg/s] \qquad (5.4)$$

5.2.3 Output Temperature

The output temperature is calculated based on Equation (4.14). By adding the evaporation temperature the equation expresses the output temperature. With the assumption that the lengths of the two-phase zone in all pipes are the same, the equation describes the output temperature from the evaporator. The equation becomes

$$T_o = T_a'(\bar{P}_e) - \big(T_a'(\bar{P}_e) - T_e(P_e)\big)\, e^{-\frac{\ell_{sh}}{\beta_e}} \qquad [K] \qquad (5.5)$$

where $T_a'(\bar{P}_e)$ is the average ambient temperature around the superheated zones.

The exponential function is estimated with a first order Taylor Approximation. The length of the superheated zone is expressed as the total length of the evaporator minus the length of the two-phase zone.

With these alterations, Equation 5.5 becomes

$$T_o = T_a'(\bar{P}_e) - \left(T_a'(\bar{P}_e) - T_e(P_e)\right) \cdot \left(c_1(\bar{\ell}_{e,sh}) - c_2(\bar{\ell}_{sh}) \cdot (\bar{\ell}_{2p} - \ell_{2p})\right) \qquad [K] \tag{5.6}$$

5.2.4 Combined Linearized Model

Based on Equation (5.2), (5.4) and (5.6) a linear small signal model of the evaporator is derived. The linear model of the evaporator has the form

$$\begin{aligned} \dot{\mathbf{x}} &= \mathbf{A}\mathbf{x} + \mathbf{B}u + \mathbf{E}\mathbf{v} \\ \mathbf{y} &= \mathbf{C}\mathbf{x} + \mathbf{D}u \end{aligned} \tag{5.7}$$

where the state, input, output and disturbance vectors are equal to

$$\mathbf{x} = \begin{bmatrix} \ell_{2p} \\ P_e \end{bmatrix}, \ u = OD, \ \mathbf{y} = \begin{bmatrix} T_o \\ P_e \end{bmatrix}, \ \mathbf{v} = \begin{bmatrix} f_{cp} \\ T_a \end{bmatrix} \tag{5.8}$$

The matrices in the model are:

$$\mathbf{A} = \begin{bmatrix} -\frac{\alpha_{2p} \cdot O_{pi} \cdot N_{pi} \cdot \eta' \cdot (\bar{T}_{e,a} - T_e(\bar{P}_e))}{f_1(\bar{\ell}_{2p}, \bar{P}_e, \bar{\dot{m}}_v, \bar{T}_{c,o})} & \frac{\alpha_{2p} \cdot O_{pi} \cdot N_{pi} \cdot \eta' \cdot \bar{\ell}_{2p} \cdot T_e'(\bar{P}_e)}{f_1(\bar{\ell}_{2p}, \bar{P}_e, \bar{\dot{m}}_v, \bar{T}_{c,o})} \\ \frac{f_4(\bar{P}_e) \cdot (\bar{T}_{e,a} - T_e(\bar{P}_e))}{f_3(\bar{P}_e)} & -\frac{\rho_g'(\bar{P}_e) \cdot V_{cp,i} \cdot \bar{f}_{cp} + f_4(\bar{P}_e) \cdot \bar{\ell}_{2p} \cdot T_e'(\bar{P}_e)}{f_3(\bar{P}_e)} \end{bmatrix} \tag{5.9}$$

$$\mathbf{B} = \begin{bmatrix} \frac{f_2(\bar{P}_e, \bar{P}_c, \bar{T}_{c,o}) \cdot od_2(\bar{OD})}{f_1(\bar{\ell}_{2p}, \bar{P}_e, \bar{\dot{m}}_v, \bar{T}_{c,o})} \\ \frac{f_5(\bar{P}_e, \bar{P}_c, \bar{T}_{c,o}) \cdot od_2(\bar{OD})}{f_3(\bar{P}_e)} \end{bmatrix} \tag{5.10}$$

$$\mathbf{C} = \begin{bmatrix} c_2(\bar{\ell}_{sh}) \cdot (T_e(\bar{P}_e) - T_a'(\bar{P}_e)) & c_1(\bar{\ell}_{sh}) \cdot T_e'(\bar{P}_e) \\ 0 & 1 \end{bmatrix} \tag{5.11}$$

$$\mathbf{D} = \begin{bmatrix} 0 \\ 0 \end{bmatrix} \tag{5.12}$$

$$\mathbf{E} = \begin{bmatrix} 0 & -\frac{\alpha_{2p} \cdot O_{pi} \cdot N_{pi} \cdot \eta' \cdot \bar{\ell}_{2p}}{f_1(\bar{\ell}_{2p}, \bar{P}_e, \bar{\dot{m}}_v, \bar{T}_{c,o})} \\ -\frac{\rho_g(\bar{P}_e) \cdot V_{cp,i}}{f_3(\bar{P}_e)} & \frac{f_4(\bar{P}_e) \cdot \bar{\ell}_{2p}}{f_3(\bar{P}_e)} \end{bmatrix} \tag{5.13}$$

The linear model is both used in the design of the PI controller, which is described in the next section. It is also used to construct the observer, which is derived in the section after the next.

5.3 PI Controller Design

The purpose of the PI controller is to control T_{sh}. The PI controller should be designed so the system tracks the reference in the best possible way. At the same time the PI controller has to be designed so the system is stable.

The PI controller is designed based on Ziegler-Nichols tuning principle (Franklin et al., 2006, p. 198). The parameters of the PI controller are found based on the lag and the slope of the step response of the system. From the result of the experiment shown in Figure 4.16 on page 65, it is known, that step up in OD gives the steepest slope of T_{sh}. Therefore only step up in OD is used to find the parameters of the PI controller.

The lag of the system is not covered in the model, therefore it is obtained from an experiment on the system. The experiment is a series of four step responses, and the lag of the system is found as the mean of the lag of the four step responses. The result of the experiment can be seen in Figure 5.5.

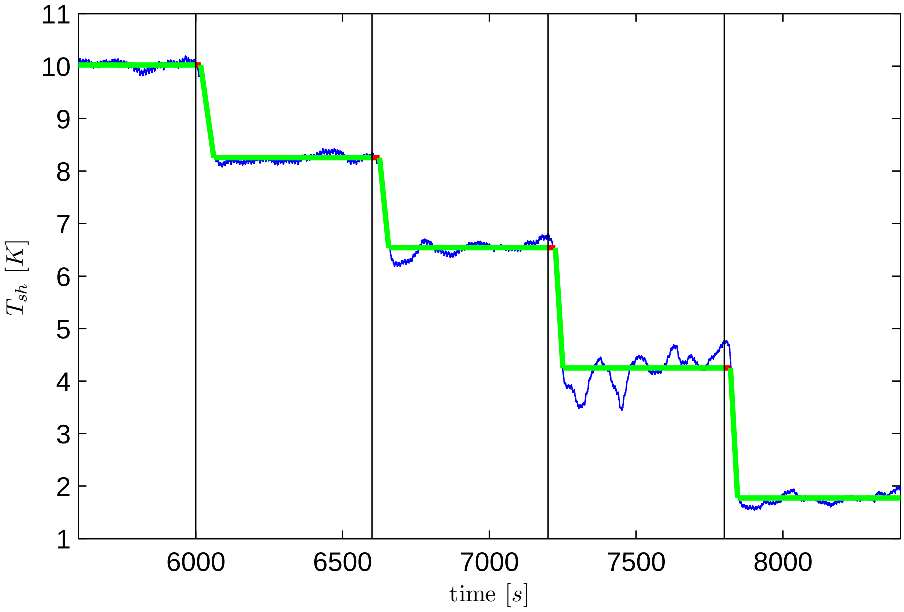

Figure 5.5: *Measured T_{sh} from four steps in OD. The measured T_{sh} is estimated with slopes, and the delay at each step is measured. The measurement is filtered to reduce measurement noise.*

Based on the experiment, the lag from a change in OD to the response of T_{sh} is

$$L = 23.6 \qquad [s] \tag{5.14}$$

To ensure that the system is stable, the PI controller is designed at the worst case operating point. To test stability, the linear model of the system is used. The linear model is calculated at the worst case operating point, and the controller is designed so the system is stable. Therefore the system is stable at all operating points. The worst case operating point is the operating point where the slope of the response is highest and where the steady state gain is highest. This operating point gives the highest amplification where the delay causes the first 180 deg phase shift.

The largest slope of T_{sh} occurs when the evaporator is close to overflowing. This can be seen in Figure 5.5. The difference in time constants comes from the nonlinearity of the output temperature as a function of the length of the superheated zone. The PI controller is therefore designed in the operating point where $\ell_{2p} = L_e$ and where the steady state gain is largest.

The linear model, described in Section 5.2, is used to find the operating point with the largest steady state gain. The operating point is found as the result of a constrained optimization problem. For the use in the optimization the operating point values of the system are limited to the values shown in Table 5.1.

	min	max	unit
ℓ_{2p}	13	13	m
P_e	4	10	bar
OD	0.01	1	-
f_{cp}	25	60	Hz
T_a	15	40	$^\circ C$
$T_{c,o}$	15	40	$^\circ C$
P_c	16	22	bar

Table 5.1: *Upper and lower limits on the values used to calculate the worst case operating point.*

By finding the operating point with the largest steady state gain, the worst case operating point is found to be

$$\begin{aligned}
\ell_{2p} &= 13 && [m] \\
P_e &= 8.98 \cdot 10^5 && [Pa] \\
OD &= 0.553 && [-] \\
f_{cp} &= 25 && [Hz] \\
T_a &= 15 && [^oC] \\
T_{c,o} &= 35.45 && [^oC] \\
P_c &= 21.46 \cdot 10^5 && [Pa] \qquad (5.15)
\end{aligned}$$

It is clear that the worst case operating point is where T_a is close to T_e, which means at low flow. This is supported by (Lim et al., 2009). The step response of the system at the worst case operating point is shown in Figure 5.6.

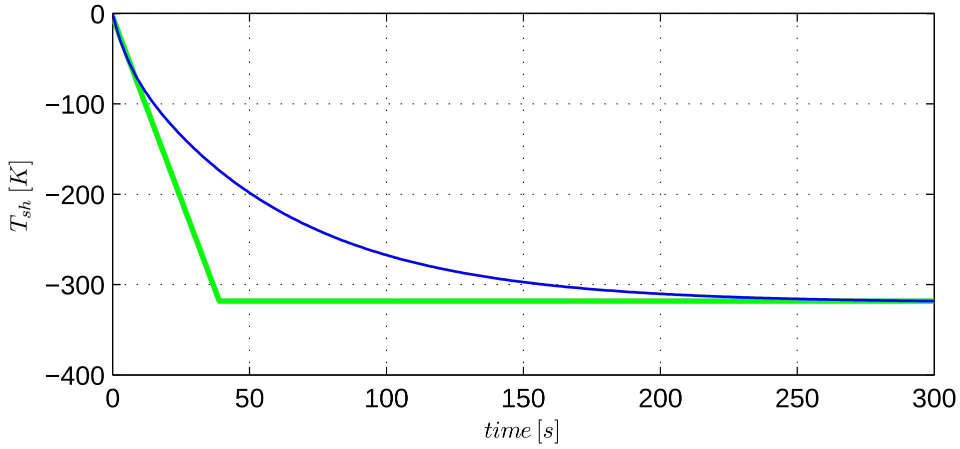

Figure 5.6: *Step response of T_{sh} at the worst case operating point. Note that the lag is not present as this is not a part of the linear model.*

From the step response of T_{sh} at the worst case operating point, the slope is found to

$$R = -8.0776 \qquad [K/s] \tag{5.16}$$

From the lag and the slope, the parameters of the PI controller are found to be

$$\begin{aligned} k_p &= -4.7 \cdot 10^{-3} && [-] \\ k_i &= -60 \cdot 10^{-6} && [-] \\ K(s) &= k_p + \frac{k_i}{s} && [-] \end{aligned} \tag{5.17}$$

Figure 5.7 shows a Nyquist plot of the open loop system. As it can be seen in the plot, the gain of the system never reaches an amplitude of 1 at 180 deg phase shift. The system is therefore stable at the worst case operating point, and it is therefore stable at all operating points.

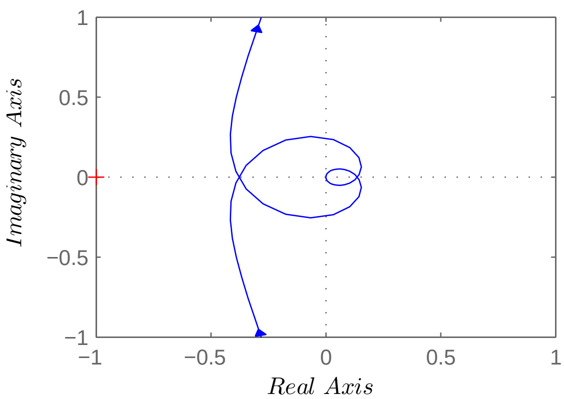

Figure 5.7: *Nyquist plot of the open loop system with the designed PI controller.*

Now the PI controller has been designed, but since P_e may not be known exactly nor is T_{sh}. This makes it inappropriate to run the system with a fixed reference. Instead a dynamic reference adjustment is needed. This is described in the next section.

5.4 Design of Reference Logic

With the controller in place, we are left with choosing the reference $T_{sh,ref}$. Normally this would be chosen to be around 6 degrees superheat to exploit as much of the evaporator as possible, while not risking overflow. However, as we have shown in Figure 4.13, when some pipes begin to overflow T_{sh} is not necessarily zero, unless all pipes overflow at the same time. Furthermore, we have shown that the estimated pressure may not be very accurate if the parameters of the plant changes. This also makes the estimated T_{sh} inaccurate. These two problems makes a fixed $T_{sh,ref}$ inappropriate. A dynamic reference adjustment is therefore called for.

In Section 4.3 it is shown, how the variance of T_o and therefore the estimation error of T_o begins to vary at low superheat. This comes to our aid in choosing an appropriate reference for the controller.

The idea is to use the increase in $VAR(T_{o,err})$ to indicate when a pipe is overflowing. When it reaches a given threshold $T_{sh,ref}$ is increased a bit, and then lowered gradually until the threshold is reached again. This ensures a superheat close to the optimal. The logic is presented as an algorithm in Algorithm 5.1. Note the initialization is omitted.

Line 4-6 locks the algorithm until the measured output is close to the reference, and the system is calm. Line 9-12 detects if the variance is below the lower threshold. If it is, the system is regarded as calm. Line 13-19 decides the new output. If the variance is above the high threshold, and the system has been calm since the last step, the reference is stepped up. Otherwise the reference is lowered along the slope. If the system has not calmed and the reference has reached the value where it was last stepped up, the reference is stepped further up as a safety measure. This is done in Line 20-23.

The reference logic is tested on the plant with the PI controller and the observer for estimation of P_e and thus T_{sh}. In the experiment the initial $T_{sh,ref}$ is chosen to be 8 degrees. When this is reached, the system begins to decrease the reference and step it up again according to Algorithm 5.1. The experiment is shown in Figure 5.8

Algorithm 5.1 Algorithm for dynamical reference adjustment. Loops only make one pass per time step.

$isCalm = true$
$T_{sh,ref} = 8$
$nSteps = 1$

{Do nothing until system calms down. σ^2_{low} and σ^2_{high} are hysteresis bounds to avoid effects from noise.}

while $|T_{sh,ref} - T_{sh}| > tol$ **or** $\sigma^2 > \sigma^2_{low}$ **do**
    $\sigma^2 = VAR(T_{o,err}, \tau_w)$
end while

loop
    $\sigma^2 = VAR(T_{o,err}, \tau_w)$

    {Do not reset if system is calm.}
    if $\sigma^2 < \sigma^2_{low}$ **then**
        $isCalm = true$
        $nSteps = 1$
    end if

    {Step back if system has become excited.}
    if $\sigma^2 > \sigma^2_{high}$ **and** $isCalm = true$ **then**
        $isCalm = false$
        $ref_{low} = T_{sh,ref}$
        $T_{sh,ref} = T_{sh,ref} + ref_{\Delta}$
    else {Otherwise decrease reference}
        $T_{sh,ref} = T_{sh,ref} - ref_{\alpha}$
    end if

    {System did not calm down since last reset. Step even further back.}
    if $isCalm = false$ **and** $T_{sh,ref} < ref_{low}$ **or** $T_{sh,ref} < 1$ **then**
        $nSteps = nSteps + 1$
        $T_{sh,ref} = T_{sh,ref} + ref_{\Delta} \cdot nSteps$
    end if
end loop

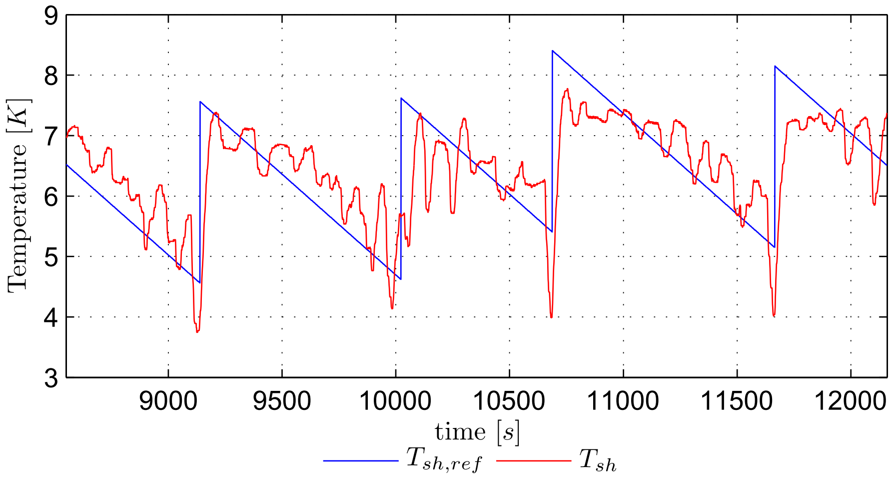

Figure 5.8: *The experiment shows how the reference is lowered until the variance of $T_{o,err}$ rises, and then it is stepped back.*

Another perspective on the experiment is presented in Figure 5.9. Here $VAR(T_{o,err})$ is shown. The red line indicates the threshold which causes the reference to step back, and the green line indicates the threshold which needs to be reached before the reference can be stepped back again. In other words the variance threshold has a hysteresis.

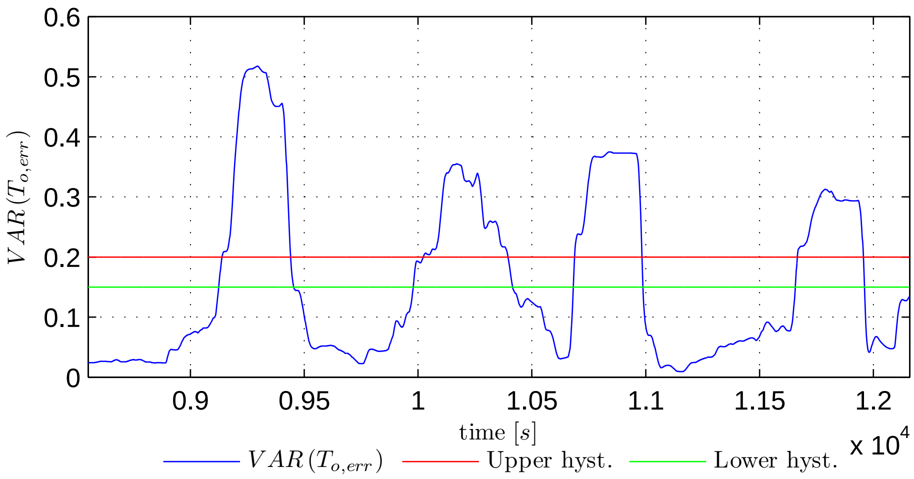

Figure 5.9: *The variance of the experiment rises and falls as the reference is changed. The red and green line shows the hysteresis of the variance.*

5.5 Observer Design

A linear model, which is parameterized with the operating point, has been derived. This allows the design of an observer as required to realize the controller structures described in Section 5.1. Recall the purposes of the observer:

1. To substitute the measurement of P_e.
2. To filter out the dynamics due to varying OD from the estimation error.

The reader should keep this in mind while reading the rest of this section.

5.5.1 Observer Structure

The system is very non-linear, and therefore a linear model based on only one operating point does not suffice to make a good observer, and a good estimate of P_e. Instead the linear small signal model, which is a function of the operating point is recalculated at every time step, as in (Larsen, 2005). The found **A**, **B**, and **C** matrices are then used in a linear small signal observer.

The small signal observer does not account for the steady state values. These are found by solving the equations of the non-linear model in steady state with the given OD. The structure can be seen in Figure 5.10.

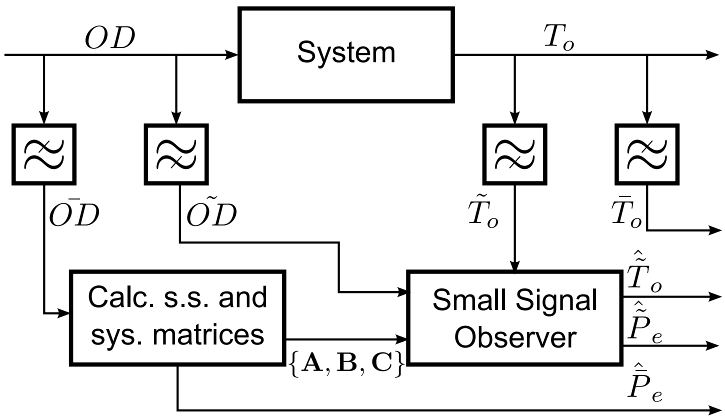

Figure 5.10: *The input signal is split into a low frequency and a high frequency part, and fed into the steady state solver and the small signal observer respectively. The output from the system is also converted to small signals, before being fed back to the small signal observer.*

The final state estimates are the steady state estimates plus the small signal estimates. Next the details of how the steady state and the system matrices for the linear observer are calculated, is shown.

5.5.2 Steady State Estimation and System Matrices

Two equations describe the steady state of the system. One describes the steady state of P_e and the other the steady state of ℓ_{2p}. The equation for P_e, Equation (5.18), does not dependent on ℓ_{2p}

and is therefore solved first.

$$0 = \dot{m}_v\left(P_c, P_e, OD\right) - \dot{m}_{cp}\left(P_e, f_{cp}\right) \tag{5.18}$$
$$0 = \dot{m}_v\left(P_c, P_e, OD\right) \cdot \left(h_g - h_i\right) - \alpha_{2p} \cdot O_e \cdot \ell_{2p} \cdot \left(T_a - T_e\right) \tag{5.19}$$

However Equation (5.18) cannot be solved explicitly, and is therefore solved numerically using a line search algorithm. Equation (5.19) can be solved explicitly once P_e is found. Equation (5.18) and (5.19) has dependencies on other inputs than OD, namely T_a, $T_{c,o}$, f_{cp}, and P_c. However, all these are considered constant, as their measurements are only available in the test setup, and not in real applications. Their values are chosen to fit the operating conditions of the particular system.

The recalculation of the steady state from one time step to another is only meaningful if it varies much slower than the states of the system. However, in this case OD may vary quickly, thus resulting in rapid changes in the calculation of the steady state point. To overcome this problem OD is low pass filtered before feeding it to the steady state solver, which is also shown in Figure 5.10.

When the steady state is found, and thus the operating point, the model can be linearized again and the new matrices describing the dynamics of the system can be calculated based on the parameterized linear model described in Subsection 5.2.4. The matrices are used in a small signal observer, which is described next.

5.5.3 Small Signal Observer

The small signal observer is designed as a linear observer. Therefore all inputs and outputs also has to be small signal values. This is ensured by high pass filtering the input OD to yield $\tilde{OD}$. The feedback from the system output T_o is filtered to yield $\tilde{T}_o$. Naturally the outputs from the observer is then also small signal values, which are then added to the estimated steady state values to yield the final state estimate.

It is the small signal observer that filters out the changes in OD from its estimation error, to reveal the oscillating T_o at low superheat, without the influence of system dynamics. This is an important point, since this is used to detect when the superheat is low, even when the pressure estimate is inaccurate, as it is later shown to be.

The structural context of the small signal observer is shown in Figure 5.10. For the observer to be useful, the linear model needs to be observable, even without the pressure sensor available. See (Franklin et al., 2006, p. 502). The observability matrix $\mathcal{O}$ must be non-singular. That is

$$\mathcal{O} = \begin{bmatrix} \mathbf{C} \\ \mathbf{CA} \end{bmatrix}$$
$$rank\left(\mathcal{O}\right) = 2 \tag{5.20}$$

This is true indeed. This means that the states of the system are connected to the output of the system and can thus be estimated by the observer. The system is also controllable, which can be shown in a similar way. If the controllability matrix is nonsingular, the system is controllable. See (Franklin et al., 2006, p. 457). That is

$$\mathcal{C} = \begin{bmatrix}\mathbf{B} & \mathbf{BA}\end{bmatrix}$$
$$rank\,(\mathcal{C}) = 2 \tag{5.21}$$

This is also the case. Controllability is not necessary to make an observer. However, because the observer provides access to all states, the system can be controlled.

The internal structure of the small signal observer is shown in Figure 5.11.

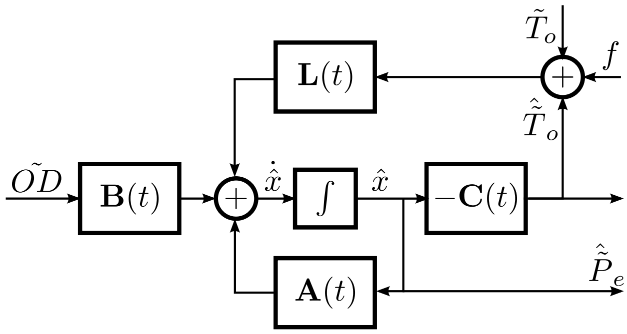

Figure 5.11: *The structure of the small signal observer block of Figure 5.10. Note: f is the disturbances in T_o due to low superheat.*

The small signal observer equations combined with the system equations are found to be

$$\dot{x} = \mathbf{A}x + \mathbf{B}u$$
$$\dot{\hat{x}} = \mathbf{A}\hat{x} + \mathbf{B}u - \mathbf{LC}\hat{x} + \mathbf{LC}x + \mathbf{L}f \tag{5.22}$$

Where the term f is a disturbance of the outputs of the system and represents the oscillations of T_o at low superheat. The state vector $\mathbf{x}$ is defined as $\mathbf{x} = [\ell_{2p} \;\; P_e]^T$. The estimation error dynamics are defined as

$$e = x - \hat{x}$$
$$\dot{e} = \mathbf{A}x + \mathbf{B}u - \mathbf{A}\hat{x} - \mathbf{B}u + \mathbf{LC}\hat{x} - \mathbf{LC}x - \mathbf{L}f$$
$$\dot{e} = (\mathbf{A} - \mathbf{LC})\,e - \mathbf{L}f \tag{5.23}$$

However, we are interested in the estimation error of T_o. This can be calculated by multiplying with the output gain, which gives the scalar value defined as

$$T_{o,err} = \mathbf{C}e \tag{5.24}$$

It is seen from Equations (5.23) that the oscillating variations in T_o, f, does indeed influence the estimation error, $T_{o,err}$. But the estimation error is attenuated by the observer gain.

However, we want f to be represented in the estimation error in order to detect the low superheat. The observer gain $\mathbf{L}$ is therefore designed to be as fast as possible, to ensure fast convergence with the system, but slow enough that it does not track the disturbances.

Design of Observer Feedback

To design the proper observer gain which satisfies the demands, the frequency spectrum of $T_o - mean(T_o)$ when the superheat is low is used. This is equivalent to the frequency spectrum of the disturbance f. To do this an experiment is conducted where the system is kept at a constant low superheat by a PI controller for more than one hour. The time series, and the frequency spectrum of $T_o - mean(T_o)$ during the experiment is shown in Figure 5.12.

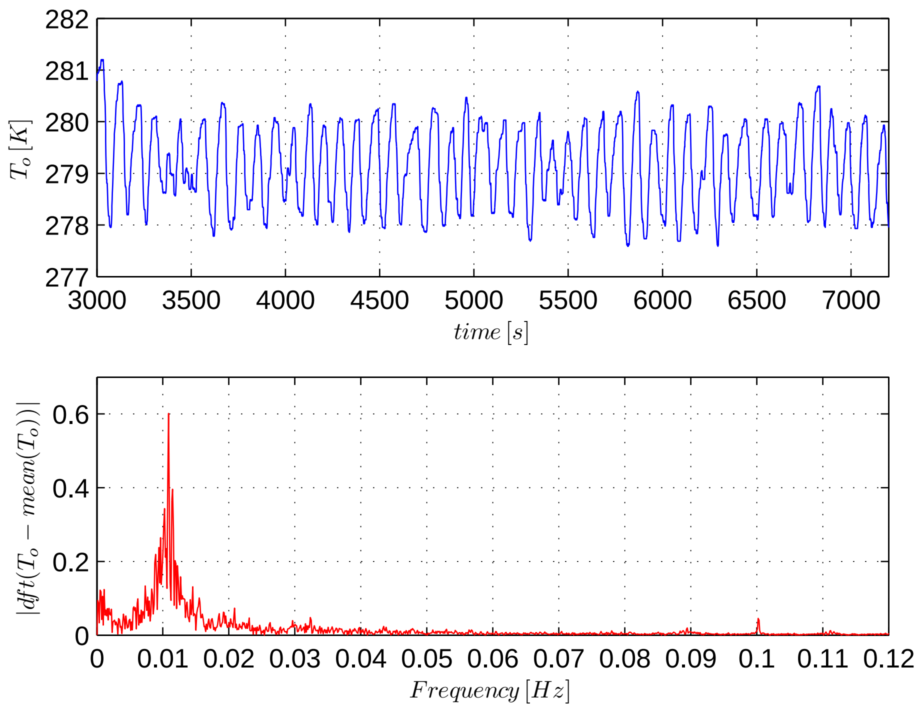

Figure 5.12: *The frequency spectrum of the oscillations of T_o. Notice the very strong periodicity in the signal, which also shows in the frequency spectrum at just over $0.01\ Hz$.*

It can be seen from the figure that there is a strong oscillation with a period of about 90 seconds or a frequency just over $0.01\ Hz$. The observer gain $\mathbf{L}$ is therefore designed to have a 3db attenuation at $0.01\ Hz$, and tuned hereafter.

5.5.4 Combined Estimator

Both the small signal observer and steady state estimator has now been designed. A complete estimate by combining the two can therefore be obtained. This is shown in Figure 5.13.

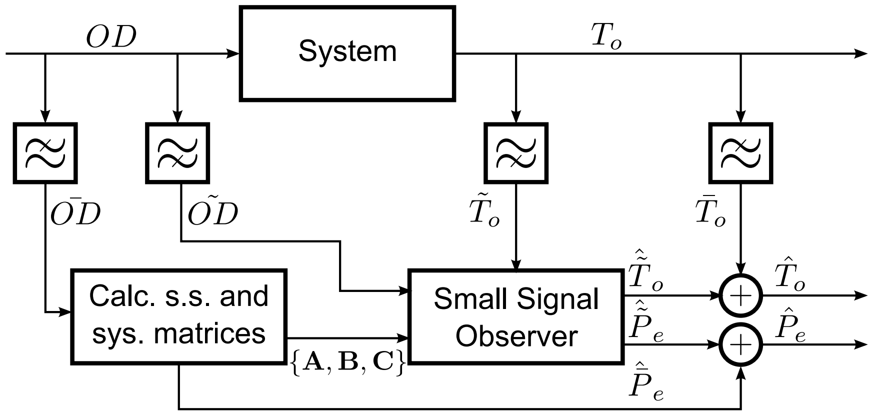

Figure 5.13: *The small signals from the small signal observer are combined with the steady state estimates to yield a final estimate. Note the lack of feedback in the steady state solver P_e leading to steady state errors.*

The equations for the estimates can be derived by inspection of Figure 5.13.

$$\hat{T}_o = \hat{\tilde{T}}_o + \bar{T}_o \tag{5.25}$$

The estimate of T_o is not strictly needed as we have the direct measurement of it, which is very reliable. However, we do need an estimate of P_e, as the system is designed to not use a pressure sensor. The estimate is defined as

$$\hat{P}_e = \hat{\tilde{P}}_e + \hat{\bar{P}}_e \tag{5.26}$$

Since P_e is not measured, it is not fed back into the small signal observer nor to the steady state estimator. However, information of P_e is present in T_o hence the observability, and convergence with respect to dynamics. But the estimation of the low frequency part of P_e is based on the solution to the steady state equation (5.18), denoted $\hat{\bar{P}}_e$ in Figure 5.10, which is purely feed forward.

This is a problem, since $\hat{\bar{P}}_e$ is pure feed forward, and may only be accurate with extensive knowledge of the model parameters. However, the oscillations of T_o at low superheat can be used, as they provide a fix point for the steady state of P_e. Model parameters that influence the prediction of $\bar{P}_e$, $\hat{\bar{P}}_e$ can then be adjusted to make $\hat{\bar{P}}_e$ coincide the known fix point a low superheat predicted by the oscillations in T_o. The adjustment is based on elements from adaptive control and is described next.

5.5.5 Adaptive Steady State Estimation

It was shown in Subsection 5.5.1 that the steady state estimate, $\hat{\bar{P}}_e$ may not be accurate if the model parameters are not accurate, or the disturbances are unknown. This is because there is no feedback to correct the estimate $\hat{\bar{P}}_e$. Also the steady state estimate of ℓ_{2p} may not be accurate. This causes two problems. The first problem is when estimating P_e a steady state error is present because of the lack of feedback. The second problem is that since the steady state values are incorrect, the calculated system matrices for the small signal observer may have the wrong dynamics, since they depend on the calculated operating point.

It is here the phenomenon of the varying T_o comes to our aid. Because we know the superheat is low when $VAR(T_{o,err})$ is high, we can calculate an estimate of the pressure as $\hat{\hat{P}}_e^* = PDewT\left(\hat{T}_o - T_{off}\right)$. Where T_{off} is a system specific offset from T_e to T_o when the oscillations begin and low superheat is detected. This gives a fix point to correct the steady state estimates.

The estimated pressure $\hat{\hat{P}}_e$ is corrected by adjusting the model parameter R_v to make $\hat{\hat{P}}_e = \hat{\hat{P}}_e^*$. The adjustments are performed using the MIT rule described in (Åström and Wittenmark, 2008, p. 186) to correct R_v. The error for R_v is defined as.

$$e_R = R_v^* - R_v \tag{5.27}$$

Where R_v^* is the R_v which makes $\hat{\hat{P}}_e^*$ the solution to the steady state equation for the pressure, so we have

$$\frac{\sqrt{\rho_l}}{\sqrt{R_v}} \cdot \sqrt{P_c - \hat{\hat{P}}_e^*} \cdot \bar{OD}^{1+\varepsilon} = V_{cp,i} \cdot f_{cp} \cdot \rho_g \tag{5.28}$$

$$R_v^* = \rho_l \left(P_c - \hat{\hat{P}}_e^*\right) \frac{\left(\bar{OD}^{1+\varepsilon}\right)^2}{V_{cp}^2 \cdot f_{cp}^2 \cdot \rho_g^2\left(\hat{\hat{P}}_e^*\right)} \tag{5.29}$$

In Equation (5.29) $\bar{OD}$ is a low pass filtered version of the real OD, in order for the steady state equations to be valid.

Now the error has been defined, we need a way to minimize the error online. Therefore we define performance functions as

$$J_R = \frac{1}{2} e_R^2 \tag{5.30}$$

Which is then minimized using MIT rule online. The MIT rule can be thought of as an online steepest descent optimization algorithm. It is defined as

$$\frac{d\theta}{dt} = -\gamma \cdot \frac{\partial J}{\partial \theta} = -\gamma \cdot e \cdot \frac{\partial e}{\partial \theta} \tag{5.31}$$

Where γ is the time constant of the adaption. When we correct the pressure estimate we have $\theta = R_v$. It is clear that $\frac{\partial e}{\partial R_v} = -1$ so Equation (5.31) becomes

$$\frac{dR_v}{dt} = \gamma \cdot e_R \tag{5.32}$$

The adaption corrects the steady states estimate of P_e and the system matrices. The procedure can be summarized in the following way.

1. Compute the variance of the estimation error from the small signal observer, $T_{o,err}$.
2. If the variance is over a given threshold, assume low superheat.
   (a) Calculate R_v^* using equation (5.29).
   (b) Update e_R.

3. Update e_R and apply the adaption law from equation (5.32).

A diagram showing the observer structure with the adaption block added is shown in Figure 5.14. It is seen that the adaption block acts as a feedback to the steady state solver through the small signal observer, thus correcting the steady state estimate of P_e.

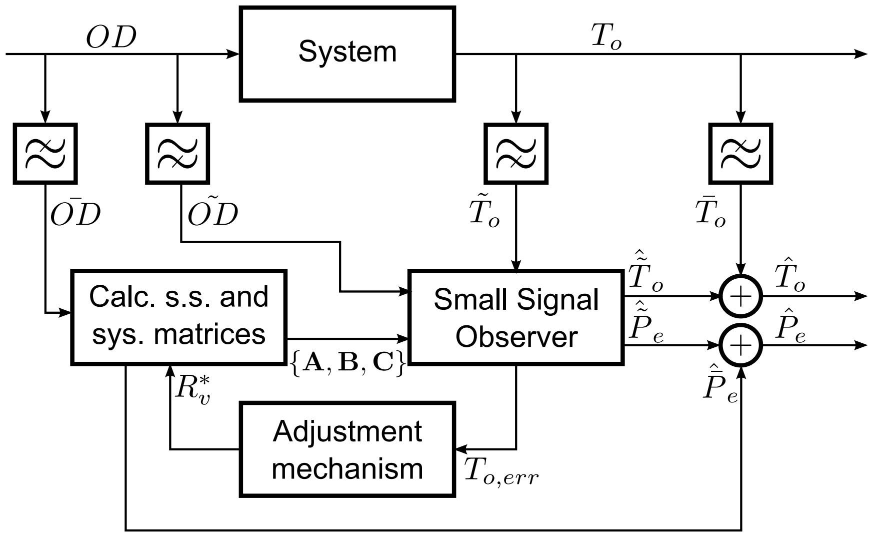

Figure 5.14: *The resistance of the valve, R_v, is continuously reestimated while the variance of $T_{o,err}$ is high indicating a specific superheat, and thus a specific $\hat{\bar{P}}_e^*$.*

5.5.6 Summary

An observer has been designed, which does not use a measurement of P_e, but does estimate it. This was achieved using a steady state estimator in conjunction with a small signal linear observer. The small signal observer was based on a linear model, parameterized by the operating point, which was recalculated in every time step. The feedback gain of the small signal observer was designed not to attenuate the frequencies of the oscillating T_o in the estimation error, $T_{o,err}$. Whenever $VAR(T_{o,err})$ reaches a given threshold, an estimate $\hat{\bar{P}}_e^*$ is obtained and the evaporator is assumed filled. Then R_v is adjusted using the MIT rule to make $\hat{\bar{P}}_e = \hat{\bar{P}}_e^*$. In this way both the steady state solver and the small signal observer has feedback, which ensures that $\hat{T}_{sh}$ and $\hat{P}_e$ is close to the actual values, despite uncertain model parameters and unmeasured disturbances. The adaption also makes the calculated small signal observer more accurate.

The controller and the observer for the system have now been designed. The next Section shows the results of the design.

5.6 Results

In this section the results of the designed controller, including the observer, is presented. First, the results of the observer are presented, but with the adaption disabled, as good model knowledge is assumed. Then the results of the PI controller are presented. Then the reference logic is presented, which is dependent on the detection of low superheat from the observer. The reference logic ensures that low superheat is detected periodically. This is used by the adaption scheme of the observer, which correct steady state estimates when some of the model parameters are uncertain. The results of the adaption are presented and finally the results are summarized and discussed.

5.6.1 Observer

The results of the observer designed in Section 5.5, with the adaption disabled are presented here. The purpose of the observer is

1. To substitute the measurement of P_e.
2. To filter out the dynamics due to varying *OD* out from the estimation error.

Pressure Estimation

An experiment in a broad range of operating points is conducted. The experiment shows how well the pressure is estimated when the model i well known. The experiment is shown in Figure 5.15.

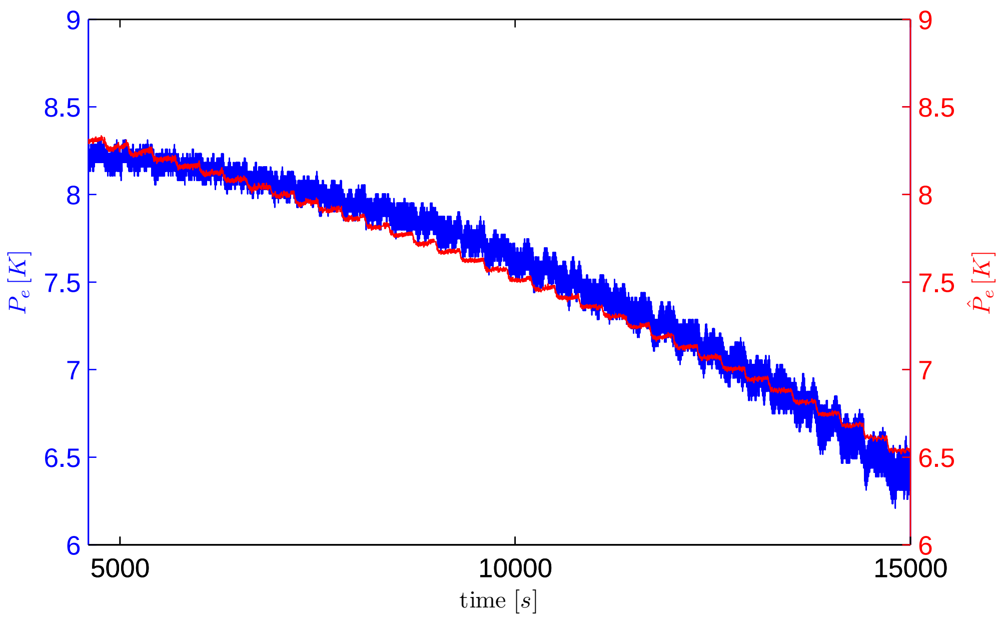

Figure 5.15: *Estimation error of P_e, in a broad range of operating points. Note the estimate is accurate to approximately ± 0.2 bar.*

The figure shows that the estimation of P_e is very accurate. The apparent noise in the P_e measurement is actually rapid pressure fluctuations due to the opening and closing of valve inlets. The effect is not covered by the linear model, and therefore nor by the observer. The experiment shows a good fit in a broad range of operating points.

Filtering of Dynamics from Estimation Error

It is important that the estimation error signal of T_o only contains the signal from variations of T_o due to low superheat, as it is used to obtain a fix point for P_e in the adaption. Figure 5.16 shows the variance of T_o without the observer compensating for the dynamics of the system.

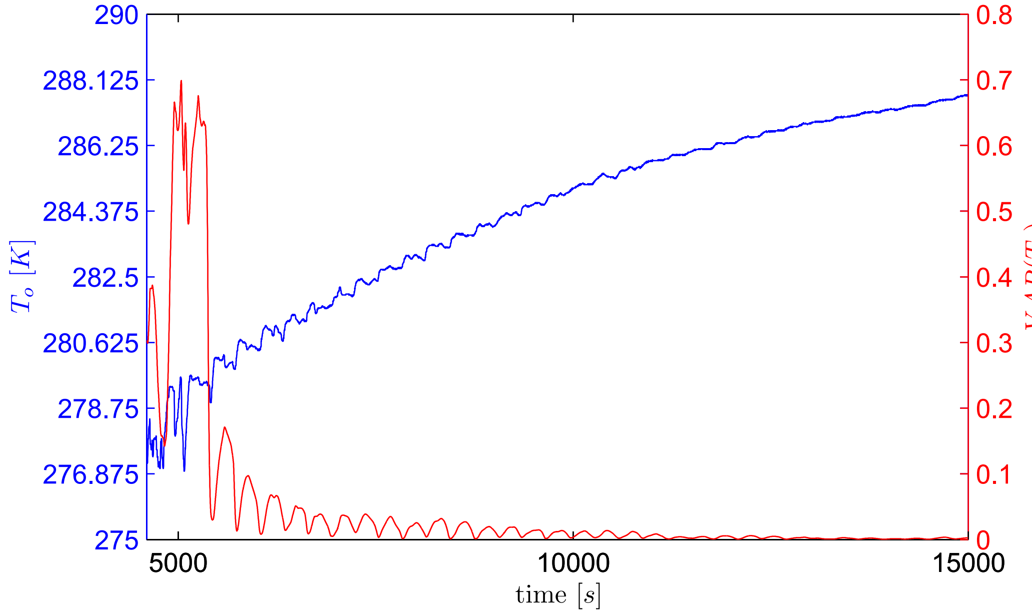

Figure 5.16: Variance of T_o without the observer compensating for varying OD. Note that each time OD is varied, the variance increases.

It is clear that the system dynamics influence the variance of T_o. At each step in *OD* the variance of the signal rises. The rise in variance increases as the length of the superheated zone decreases. This should be filtered out when taking the variance of the estimation error $VAR(T_{o,err})$. The variance of the residual from the observer is shown in Figure 5.17.

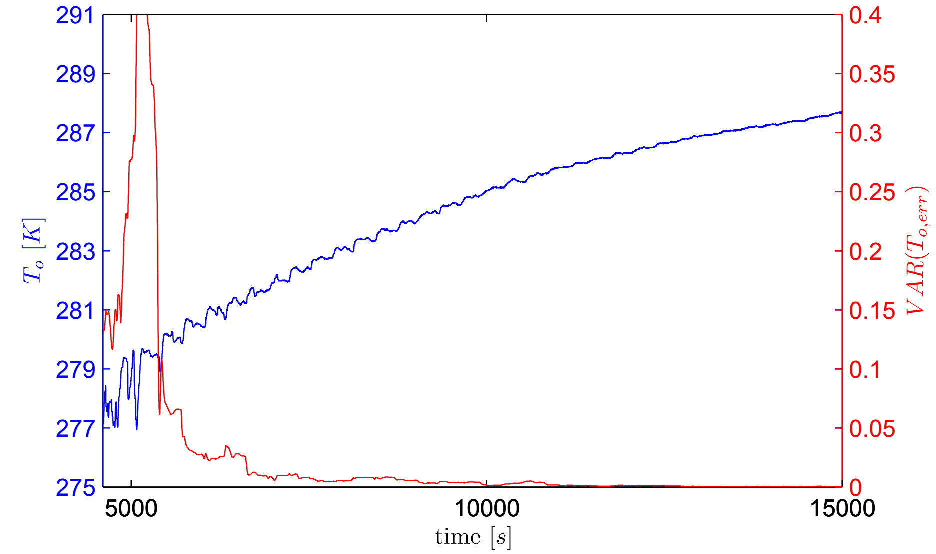

Figure 5.17: *Variance of the estimations error $VAR(T_{o,err})$ with the observer compensating for varying OD. Note that the changing OD is no longer visible in the variance*

The use of the observer filtered out most of the dynamics of the system. The effects of the system dynamics on the estimation error of T_o is therefore negligible when OD is not changed too much. The estimation error $T_{o,err}$ can thus be used to determine a fix point for P_e required to correct the steady state estimate of P_e with adaption.

It is also interesting to see the performance when there are large variations in OD. An experiment similar to the one shown in Figure 5.17 is conducted. However in this experiment the steps in OD is larger, and therefore requires better tracking from the observer to keep the system dynamics out of the estimation error. The experiment is shown in Figure 5.18.

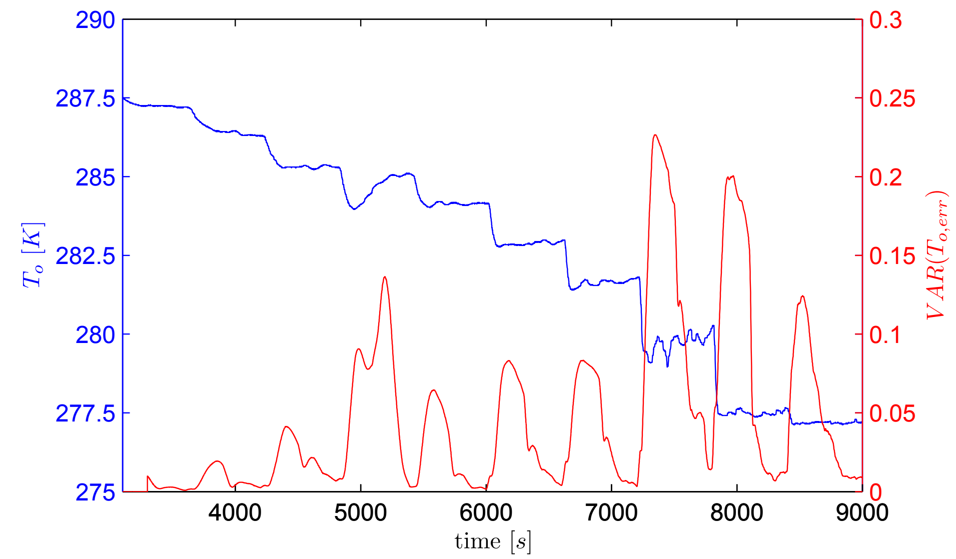

Figure 5.18: *Variance of the estimations error $VAR(T_{o,err})$ with the observer compensating for varying OD, but with larger steps in OD. Note the system dynamics now significantly influence the estimation error and cause a rise in the variance.*

It can be seen in Figure 5.18 that changes in OD now influences the estimation error significantly. This is in agreement with the result of the fitting of the model of the evaporator, see Section 4.2. As a consequence the estimate of the fix point of P_e cannot be trusted if there has been a large change in OD. This is not necessary as the system operates close to steady state most of the time, and this the variations in T_o are small, and can therefore be filtered by the observer.

5.6.2 PI Controller

The main purpose of the PI controller is to reject disturbances and track the reference. To test the performance of the PI controller, it is implemented on the test setup, and a series of experiments are conducted.

In the first experiment a series of three reference steps is performed, and the resulting tracking from the PI controller is seen. The result of the experiment is shown in Figure 5.19.

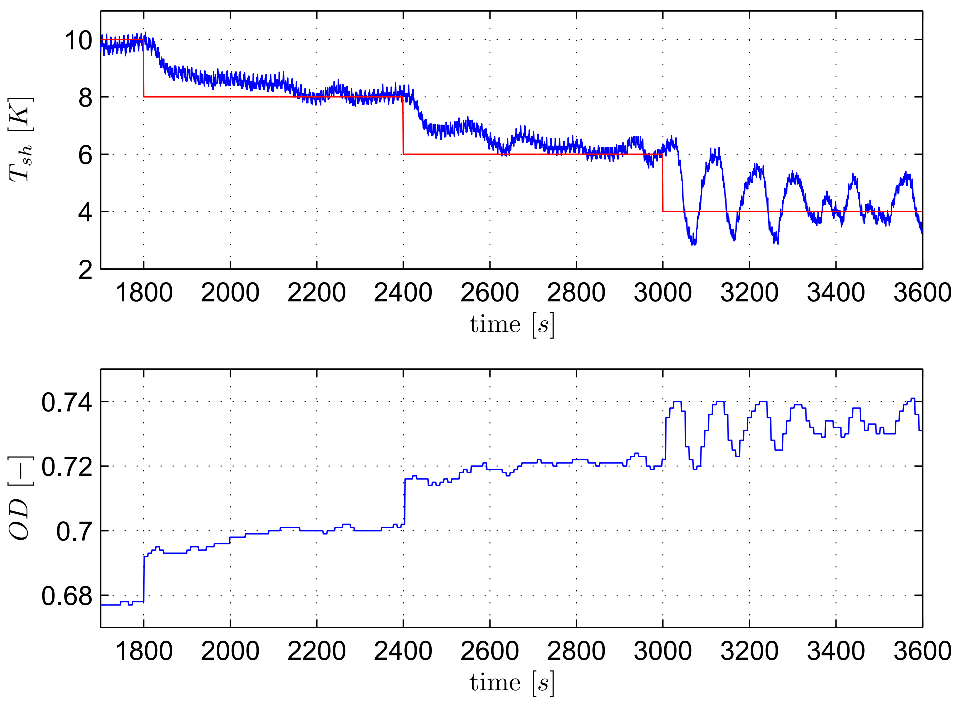

Figure 5.19: *Result of a test of the designed PI controller. The oscillations at the last step is the same frequency and amplitude as the variations described in Section 4.3. The proportional gain of the controller reacts to the changing measurement, but this does not affect the oscillations significantly.*

The controller tracks the reference, and is not destabilized by the oscillations at low superheat. The controller is too slow to have a significant effect on the oscillations.

To test the disturbance rejection, an experiment is conducted where the speed of the fan between the evaporator and the condenser room was changed thus changing the load on the system, see Figure 1.3 on page 12.

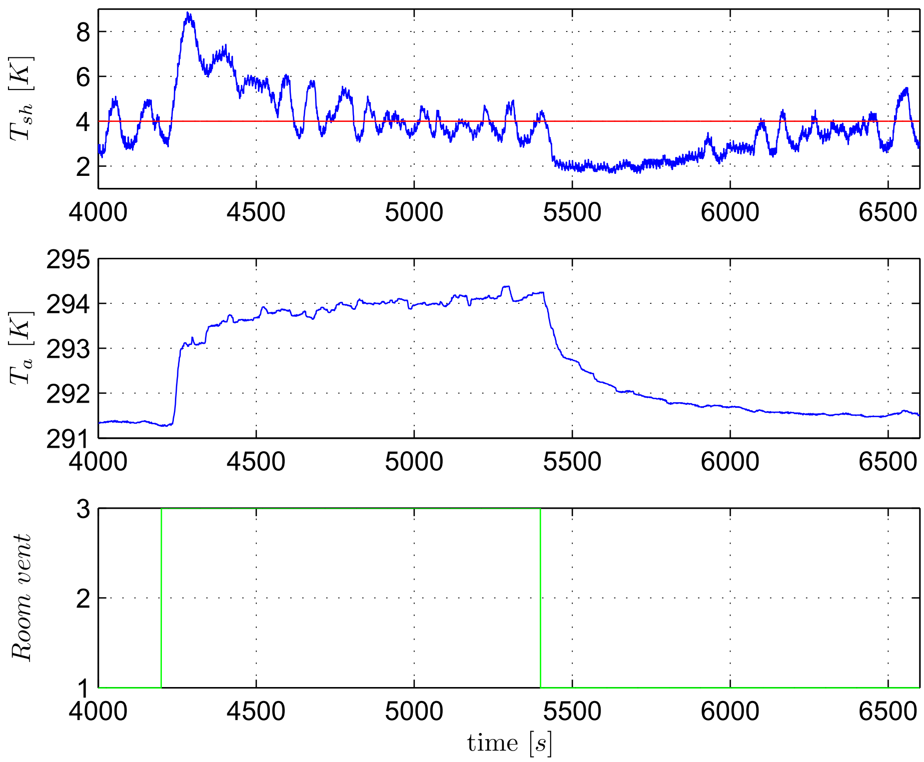

Figure 5.20: *Result of a test to see the disturbance rejection of the PI controller. The speed of the fan between the evaporator room and the condenser room was changed, which corresponds to a sudden load change. This leads to a quick change in the ambient temperature in the evaporator room, which gives a disturbance on the evaporator.*

The experiments show, that the designed PI controller is slow to reach the reference value, but it can not be faster without becoming unstable at the worst case operating point. The disturbance gives a fluctuation on T_{sh}, but the integrator counteracts the disturbance, and rejects it.

5.6.3 Reference Logic

The result of the reference logic algorithm is shown in Section 5.4 as a part of the explanation of how the algorithm works. The result of the experiment is shown in Figure 5.21 and 5.22. The result shows that the algorithm functions as intended. The reference is slowly lowered until the variance rises above the upper threshold. At this point the reference is increased, and slowly lowered again. This pattern continues.

Figure 5.22 shows the variance of the residual from the observer. The oscillations are clearly present in the variance, and the variance lowers after the step has been performed.

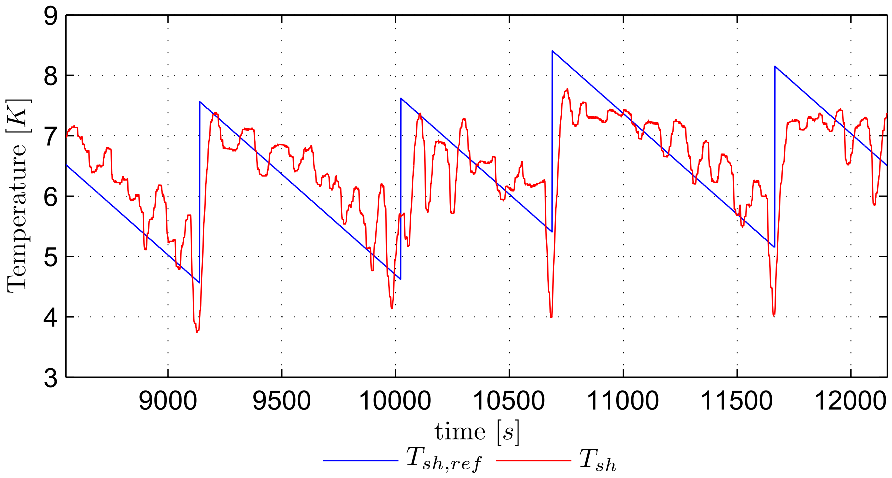

Figure 5.21: *The experiment shows how the reference is lowered until the variance of $T_{o,err}$ rises, and then it is stepped back.*

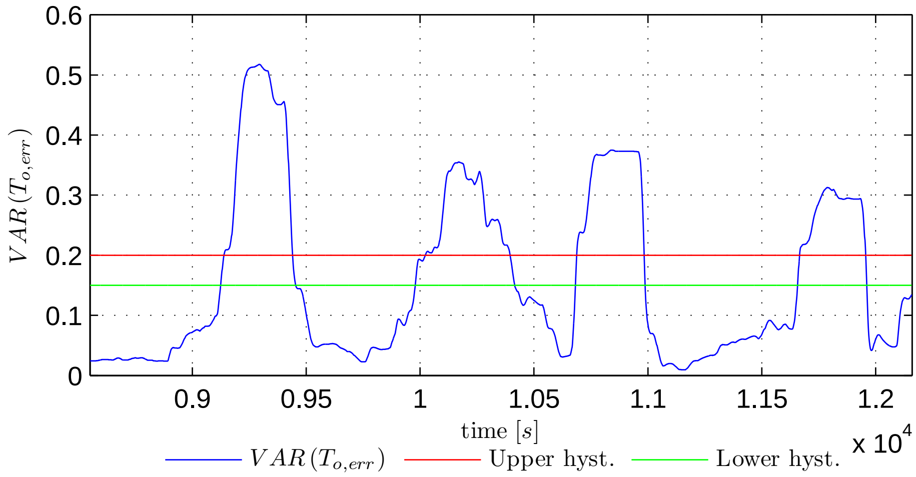

Figure 5.22: *The variance of the experiment rises and falls as the reference is changed. The red and green line shows the hysteresis of the variance.*

5.6.4 Adaption

Since the estimate of the steady state value $\hat{\bar{P}}_e$ is calculated entirely in open loop, we suspect the good estimate is due to the fact that the parameters of the system has been estimated using a similar experiment, and the fact that the model is very good. The estimate may therefore be inaccurate, if the model parameters are inaccurate. To compensate for model parameter inaccuracies we use adaption, and the results are described here.

To see how the observer performs when some of the parameters is inaccurate, we perturbate the parameter $\sqrt{R_v}$, which is the flow resistance of the valve, also described in Section 2.2. It is altered so that $\sqrt{R_{v,pert}} = \sqrt{R_v} \cdot 0.85$. This alters the predicted flow of the valve by 15%, and should produce a wrong steady state estimation of P_e. The experiment is conducted in closed loop. The controller used is described in Section 5.3. The experiment was conducted in closed loop to ensure low superheat while preventing overflow. The result is shown in Figure 5.23.

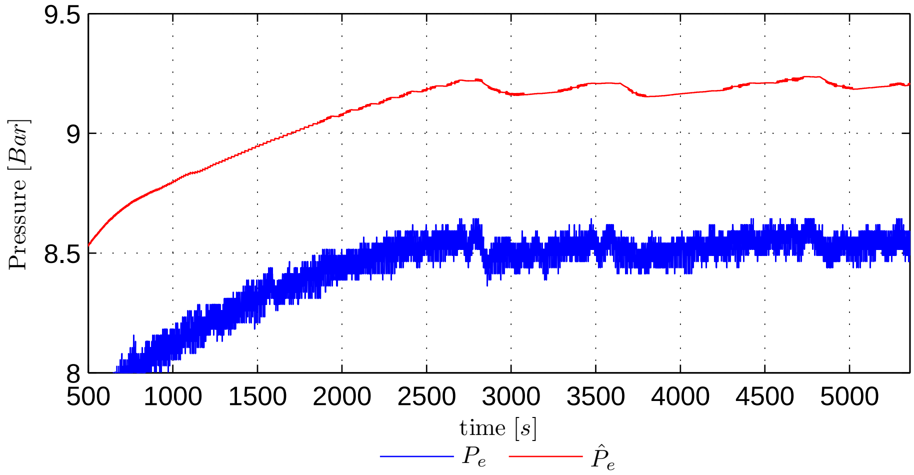

Figure 5.23: *Estimation of the pressure $\hat{P}_e$ with $\sqrt{R_v}$ perturbed with 15%. The result is a steady state error. The estimated dynamics are not accurate either. This is due to the wrong system matrices being calculated when the linearized model is parameterized with a wrong operating point.*

It is clearly seen from the figure that the predicted effect is present. Indeed any perturbation in a variable related to the flow or pressure in the evaporator may produce similar effects. That is P_c, $T_{c,o}$, $V_{cp,i}$, or T_a. This problem was predicted and a solution was designed using adaption of $\sqrt{R_v}$ based on the fix point of P_e obtained from the variance of the estimation error from the small signal observer when the superheat is low. Figure 5.24 and 5.25 shows a similar experiment to Figure 5.23, but with adaption enabled.

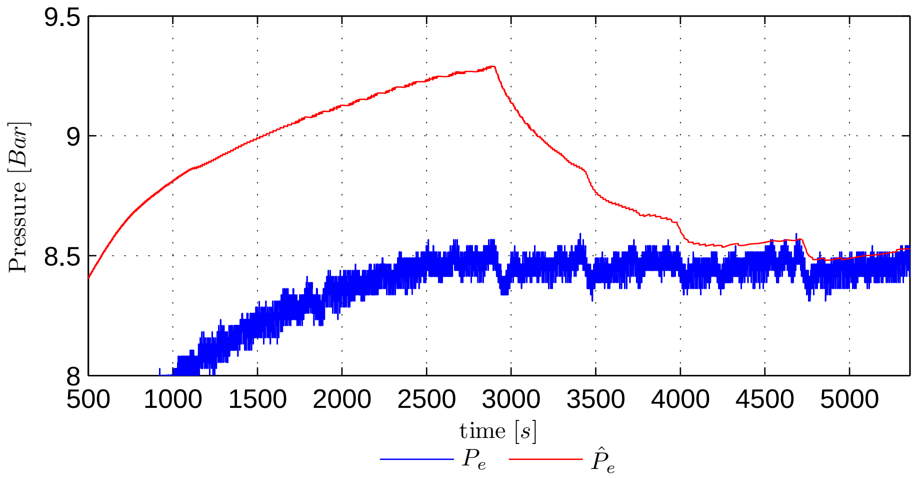

Figure 5.24: *Estimation of the pressure $\hat{P}_e$ with $\sqrt{R_v}$ perturbed with 15%, with adaption enabled. The steady state estimate is now corrected. The estimate of the dynamics is also improved because the linearized model is now calculated using an operating point closer to the actual one.*

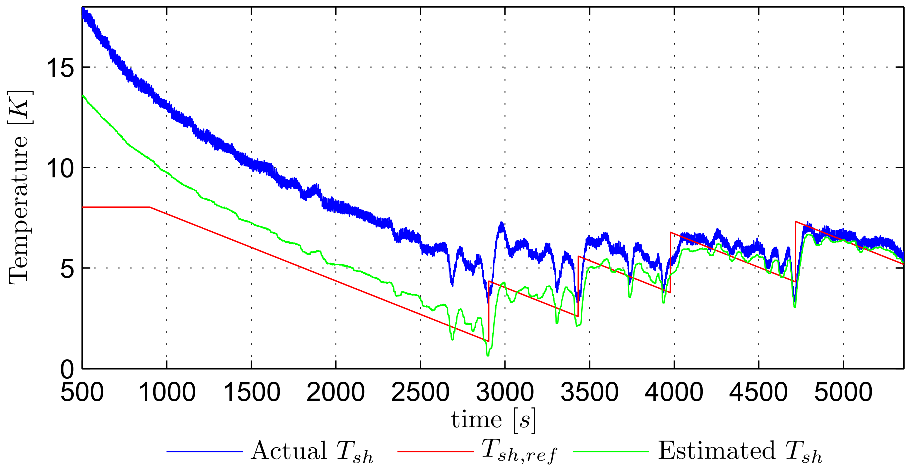

Figure 5.25: *The superheat reference, the estimated superheat, and the actual superheat. The parameter $\sqrt{R_v}$ is perturbed with 15%, and adaption is enabled. Note how the estimated superheat tracks the reference, and how they converge with the actual superheat as the adaption kicks in.*

The effects of the adaption algorithm are clearly visible. The controller decreases its reference until the superheat becomes low, and the first fix point is obtained. After this the estimated pressure and superheat begins to converge towards their true values, and the offset is removed.

The adaption also improves the estimate of the dynamics. This is because the system matrices used in the small signal model is calculated using an operating point ever closer to the actual operating point, as the adaption makes the steady state estimate converge. This can be seen by looking at the estimation of the dynamics in Figure 5.23 and comparing them to the ones in Figure 5.24 after steady state convergence.

5.6.5 Summary

The control structure has been realized, and its parts have been designed. The observer is able to estimate both the dynamics and the steady state of the system. This was achieved while only using one sensor for measuring the output temperature, T_o, of the evaporator. This means that one of the main goals of this research has been reached with success.

The observer was constructed as a steady state estimator, in conjunction with a small signal observer for estimation of dynamics. The variance of the estimation error of the output temperature, $VAR(T_{o,err})$ was used to indicate low superheat. This was exploited to obtain an estimate of the pressure, called $\hat{\hat{P}}_e^*$. If the estimates differ from the estimate predicted by the steady state estimator. The parameter R_v is adjusted using the MIT rule to make the steady state estimator converge towards the actual steady state.

The parameters of the system have been estimated using the pressure sensor. This is not possible on a system with only a temperature sensor. However, the insight gained helps us develop a more general method for superheat control using only one sensor. This is described in Chapter 6.

Chapter 6

Simplifications and Generalizations

It has been shown how the pressure can be estimated by using a steady state estimator, a small signal observer and an adaption mechanism, where the adaption mechanism relies on the phenomenon of oscillations in T_o at low superheat.

The approach requires extensive knowledge about most of the model parameters. The linearization used to calculate the small signal observer is particular demanding in this respect as shown in Section 5.2. The original structure is shown in Figure 6.1 without adaption.

The main purpose of the observer is to estimate P_e. Another purpose of the small signal observer in Figure 6.1 is to filter the dynamics due to changes in OD from the estimation error of T_o so only the oscillation due to low superheat is represented in the estimation error $T_{o,err}$. The variance of the estimation error is then used to detect the low superheat.

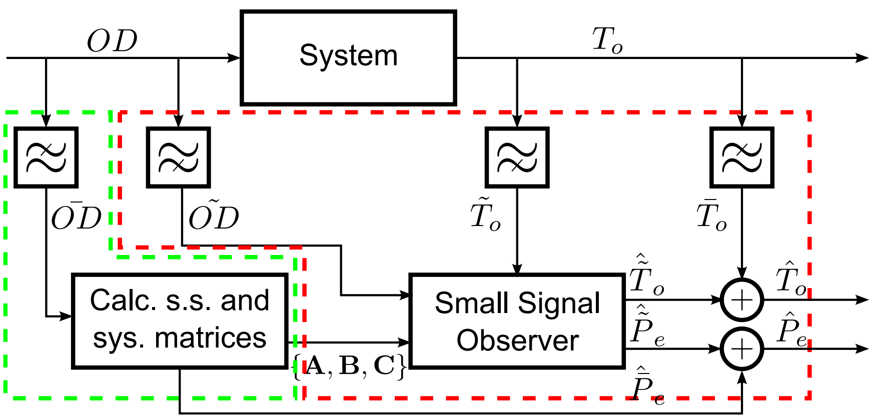

Figure 6.1: *Original model based structure. Everything in the red box is discarded in the simplification, whereas the the components in the green box are used with modifications.*

However, it is desirable to simplify the design, as the parameters of the model must be known in order to realize the small signal observer. This gives rise to the idea of estimating P_e as a function of OD, and nothing else. It can be seen in Figure 6.1 that the steady state estimator only takes a filtered version of OD as its input. The steady state estimator is marked with a green box. A steady state estimate of P_e may be good enough to estimate a sufficient T_e, as the system operates in steady state most of the time. If the system is in steady state most of the time, there is no need to filter out the increased variance in T_o. Then the small signal observer is not needed, and therefore we discard the small signal observer in the simplified structure. The small signal observer and related blocks are marked with a red box in Figure 6.1. Now that we do not need a small signal observer, we do not need the linear model, and therefore nor do we need the parameters regarding the dynamics of the system. We only need the steady state equation for estimation of P_e. As the system operates mostly in steady state, the contribution from the system dynamics to the variance of T_o may be insignificant. Therefore the simplified structure merely uses the raw measurement of T_o to calculate the variance. The simplified structure is shown in closed loop in Figure 6.2 where $\hat{P}_e$ is converted to $\hat{T}_e$ so $T_o - \hat{T}_e = \hat{T}_{sh}$.

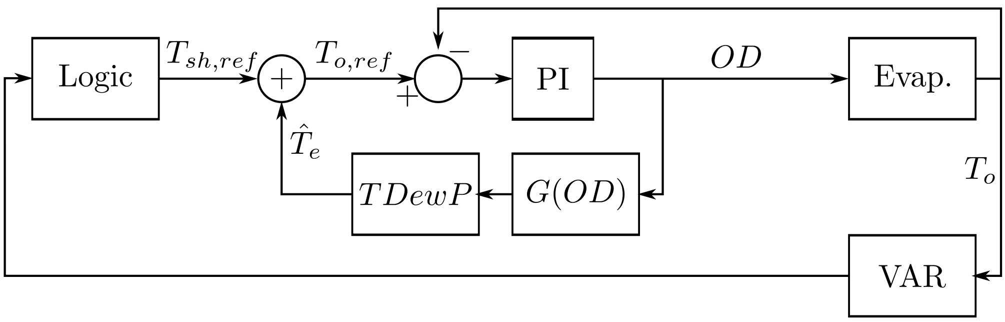

Figure 6.2: *Desired structure where T_e is approximated from OD by the function G.*

Because $\hat{T}_e$ is a slow varying steady state estimate, it is not used in the design of the control loop. It is merely used to slowly vary $T_{o,ref}$. This is opposed to the previous controller where the faster dynamics of T_e were also included in the control loop, thus requiring it to be included in the controller design, where T_{sh} was controlled. In the simplified version the PI controller is only used to control T_o. The only equation needed for the estimation of T_e is the steady state equation for P_e which is

$$\frac{\sqrt{\rho_l}}{\sqrt{R_v}} \cdot \sqrt{P_c - P_e} \cdot \bar{OD}^{1+\varepsilon} = V_{cp,i} \cdot f_{cp} \cdot \rho_g \tag{6.1}$$

Equation (6.1) is even independent of the steady state equation of the two-phase zone. This makes the estimator independent of even more parameters. Equation (6.1) can be simplified further in the following way. The liquid refrigerant is assumed to be incompressible, so ρ_l can be considered constant. The frequency of the compressor f_{cp} and the inlet volume $V_{cp,i}$ are considered constant. If we consider the refrigerant an ideal gas we have that ρ_g is proportional to P_e. We also assume the term $\sqrt{P_c - P_e}$ to be constant as any changes in P_e or P_c has to be relatively large to be significant because of the square root. With the simplifications Equation (6.1) reduces to

$$c \cdot OD^{1+\varepsilon} = P_e \tag{6.2}$$

This makes the estimator independent of all the original model parameters but ε, and a new aggregation of parameters c have been introduced. The developed relation between OD and $\hat{\hat{P}}_e$ is static. However, in order to tune the PI controller to T_o alone, we have to satisfy the condition that the outer loop must have slower dynamics than the inner loop. Therefore a first order filter is introduced to the relation so the estimated pressure does not change instantly when OD is changed. This gives

$$G(OD,s) = \frac{c}{1+s\cdot\tau}\cdot OD^{1+\varepsilon} \tag{6.3}$$

where τ is chosen sufficiently slow, to prevent controller hunting. The estimation of P_e is dependent on one parameter, as it depends on $OD^{1+\varepsilon}$ and not OD. The value of ε determines how good the estimation of the pressure is over large variations in OD. When the system operates at low superheat, P_e is nearly constant, and therefore the value of ε is not critical as long as c is fairly accurate. In practice we expect reasonable performance with $0.5 < 1+\varepsilon \leq 1$. However, the controller parameters and c may vary between systems. Therefore we develop methods to determine them online. This is discussed in the next section.

6.1 Determination of Parameters

The steady state gain $c = \frac{P_e}{OD^{1+\varepsilon}}$ needs to be known for the estimator to work. Also the reference logic and the PI controller has several parameters which need to be known. Until now the parameters has been set to yield good performance on the test setup. However, if the controller is to be used in a commercial product it is expensive to tune the parameters for every type of product. Therefore an automatic procedure for determination of the control parameters and the constant c is developed.

The control parameters that needs to be estimated are

- The variance windows size, τ_w
- The thresholds used to indicate when the superheat has become low, and when it has become high again. Called σ^2_{low} and σ^2_{high}.
- The temperature offset representing the temperature difference between T_e and the T_o where the first pipes overflow and the oscillations begin, called T_{off}.
- The gain from OD to P_e, called c
- The filter time constant which is significantly slower than that of P_e.
- The size of the step back in the reference when low superheat is detected ref_Δ.
- The reference decrease rate, ref_α, used by the reference logic to reach a new fix point with low superheat, after the reference has been stepped back.
- The lag and the reaction rate of OD to T_o. These are used for Ziegler-Nichols tuning of the PI controller.

6.1.1 Reference Logic Related Parameters

The parameters used in the reference logic are determined using a single experiment. The experiment is an OD sweep where OD is gradually turned up, and T_o is measured. The window size τ_w is not a very sensitive parameter, and is chosen to be 5 minutes, which has proved to be reasonable. When τ_w is known, the upper and lower variance hysteresis limits, σ^2_{low} and σ^2_{high}, can be found as

$$\sigma^2_{high} = \frac{1}{2} \cdot max\left(\sigma^2\right) \tag{6.4}$$

$$\sigma^2_{low} = \frac{3}{4} \cdot \sigma^2_{high} \tag{6.5}$$

Where $max\left(\sigma^2\right)$ is the highest measured variance during the *OD* sweep. The experiment is shown in Figure 6.3.

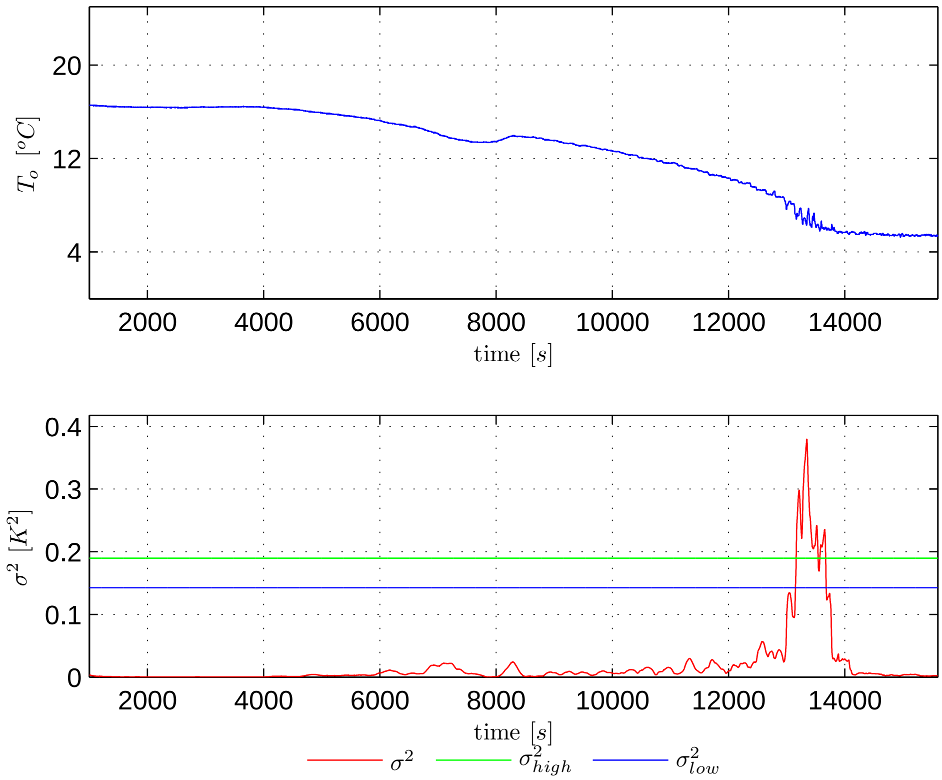

Figure 6.3: *The variance during an OD sweep. The variance thresholds are marked.*

The temperature offset T_{off} between T_e and T_o when the oscillations begin is defined as

$$T_{off} = T^*_o - min\left(T_o\right) \tag{6.6}$$

Where $min\left(T_o\right)$ is the lowest T_o during the *OD* sweep. This is reasonable since P_e at T^*_o and $min\left(T_o\right)$ is nearly the same. Now the parameters related to the reference logic have been found. Now the steady state gain of the estimator needs to be found.

6.1.2 Estimator Steady State Gain

The steady state gain of the pressure estimator, c is not known if one of the parameters it is an aggregate of is not known. Therefore c needs to be determined for the specific system for the estimator to work. This is done by reusing the *OD* sweep experiment shown in Figure 6.3 used for determining the reference logic related parameters.

When the variance reaches σ^2_{high}, it indicates low superheat. This can be used to estimate P_e at this point. When a fix point for P_e is obtained c can be calculated as

$$c = \frac{\hat{\hat{P}}_e^*}{OD^{1+\varepsilon}} \tag{6.7}$$

Where $\hat{\hat{P}}_e^* = PDewT\left(T_o^* - T_{off}\right)$ is the estimated steady state of P_e at the fix point. When c is obtained, it allows P_e to be estimated even if the system is not at the fix point.

6.1.3 PI Controller Related Parameters

The PI controller of the system is auto tuned using Ziegler-Nichols quarter decay ratio (Franklin et al., 2006, p. 198 - 199). Here we benefit from the fact that the controller is a controller of T_o as we do not need T_e for tuning the regulator. A downward step is performed at low superheat. The lag, and reaction rate is measured and the PI controller parameters are found. The PI controller is defined as

$$D(s) = k_p\left(1 + \frac{1}{T_I \cdot s}\right) \tag{6.8}$$

Where the proportional gain k_p and the integration constant T_I are found as

$$k_p = \frac{0.9}{R \cdot L} \tag{6.9}$$

$$T_I = \frac{L}{0.3} \tag{6.10}$$

Where R and L are the reaction rate and the slope respectively. The step is performed at low superheat and downward, as this is where the system gain is highest. Figure 6.4 shows an experiment where the step used for tuning is performed. The step is done in open loop.

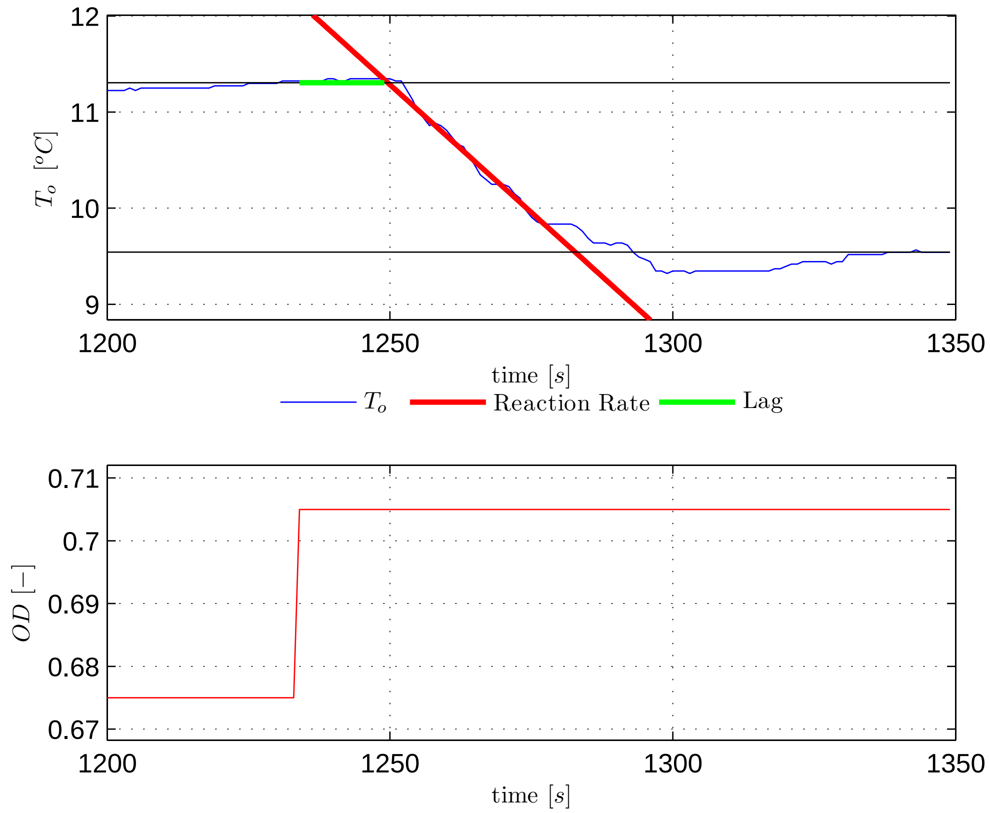

Figure 6.4: *Step performed at low superheat to determine the reaction rate ant the lag of the air conditioning system.*

We have now shown that only two open loop experiments are needed to determine all the parameters of the simplified system. Furthermore, only measurements of T_o are needed. It should be noted, however that T_a should be as low as allowable when performing the experiments in order to have the highest system gain (Lim et al., 2009). This allows the controller to be implemented on any system without knowing the specific model parameters. However, if the system changes characteristics during operation, the estimated c may become inaccurate. Therefore c is adapted continuously using the MIT rule. This is described in the next section.

6.2 Adaption

The steady state gain of the P_e estimator, c can be found in the same way as R_v was found in Section 5.3, namely by estimating c at a fix point where P_e is known. The designed reference logic ensures that a fix point of P_e is obtained periodically. This allows updates of the constant c every time a fix point is obtained. To avoid sudden changes in the estimated P_e when OD is changed, c is adapted slowly using the MIT rule. The constant c is found in a fix point in the same way as in the open loop experiments as

$$c^* = \frac{\hat{\hat{P}}_e^*}{OD^{1+\varepsilon}} \tag{6.11}$$

$\hat{\hat{P}}_e^* = PDewT\,(T_o^* - T_{off})$ is the estimated steady state of P_e when the variance of T_o indicates low superheat, and c^* is then calculated c in this point. When c is found P_e can be estimated using Equation (6.2). The resulting structure is shown in Figure 6.5

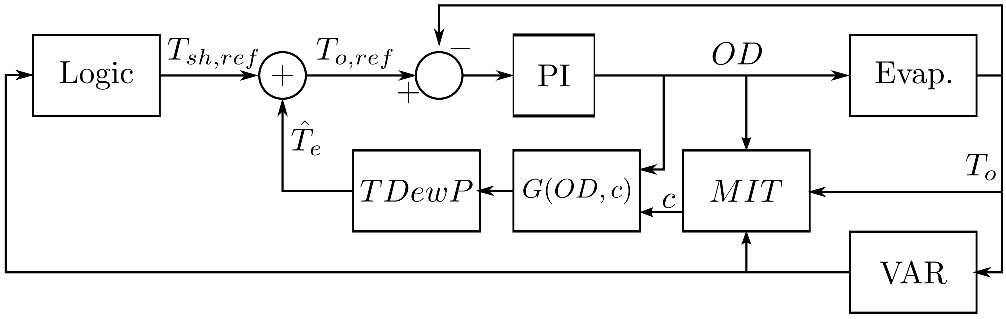

Figure 6.5: *Desired structure where T_e is approximated from OD alone, and c is adapted online.*

The MIT adaption law for c can easily be calculated as the final value c^* can be calculated explicitly. The error of c is defined as

$$e_c = c^* - c \tag{6.12}$$

where c^* is the c calculated the last obtained fix point, and c is the current c. A performance function to be minimized is then defined as

$$J_c = \frac{1}{2}e_c^2 \tag{6.13}$$

The performance function is then minimized using the MIT rule (Åström and Wittenmark, 2008, p. 186 - 194), which is defined to be

$$\frac{d\theta}{dt} = -\gamma\frac{\partial J}{\partial\theta} = -\gamma \cdot e\frac{\partial e}{\partial\theta} \tag{6.14}$$

where $\theta = c$, $J = J_c$, and $e = e_c$. Also $\frac{\partial e_c}{\partial c} = -1$, so the adaption law of the system becomes

$$\frac{dc}{dt} = \gamma \cdot e_c \tag{6.15}$$

where γ is the time constant of the adaption law.

A simplified controller structure has now been designed, which is independent of almost all model parameters. Procedures for the determination of the controller parameters have been developed, which allow the controller to be implemented on any system without prior knowledge of the system parameters. Finally the pressure estimator has been made robust to system changes by applying the MIT adaption algorithm. In the next section the performance of the developed controller is verified, and the results presented.

6.3 Results

The estimator is tested using the data from an *OD* sweep, where c is calculated in a single fix point, with no adaption. This is to verify that the estimator has not been overly simplified, and is still generally valid. The adaption is disabled as it would otherwise obscure the results. In the experiment c is calculated in a single point where the superheat is low, and then P_e is estimated in the full range of different pressures in the experiment. The estimate is shown along with the actual measurement, see Figure 6.6

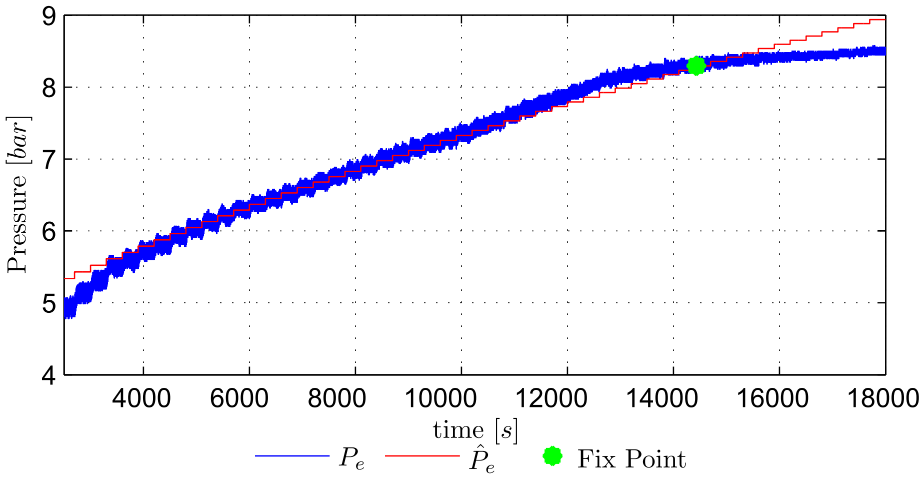

Figure 6.6: *OD sweep where one fix point, at low superheat, is used to calculate c and P_e is estimated for the rest of the range. Both done by using Equation* (6.2).

The figure shows a very good fit, despite no prior knowledge of the system parameters apart from ε. When the controller is active, the system operates at low superheat most of the time, and the reference logic ensures the adaption of c, as a fix point is obtained periodically. See Figure 6.7.

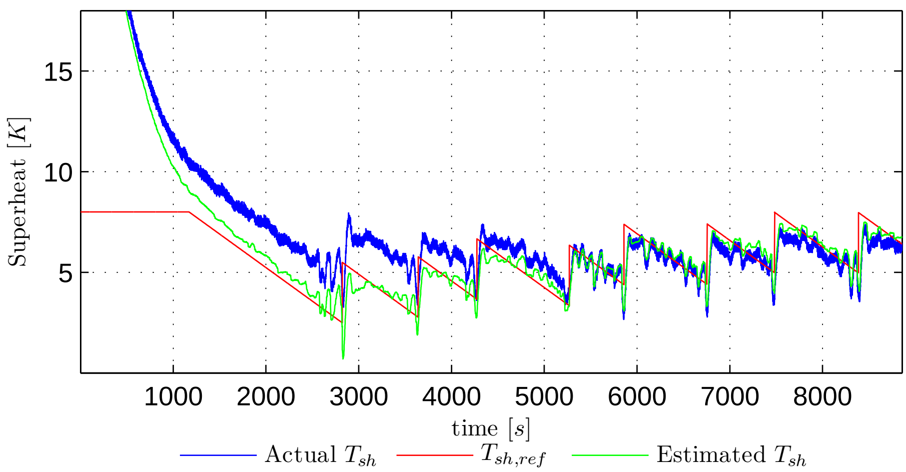

Figure 6.7: *The constant c is adjusted using the MIT rule, which causes the T_{sh}, $T_{sh,ref}$ and $\hat{T}_{sh}$ to coincide as they should.*

The initial value of the constant c is 10% wrong, but is corrected as fixpoints of the pressure are obtained. This results in the convergence of T_{sh} and $\hat{T}_{sh}$ shown in Figure 6.7.

Figure 6.8 shows the response to a disturbance to the ambient temperature. It is seen that that the controller handles the disturbance, but that it takes some time before the controller detects that the evaporator overflows.

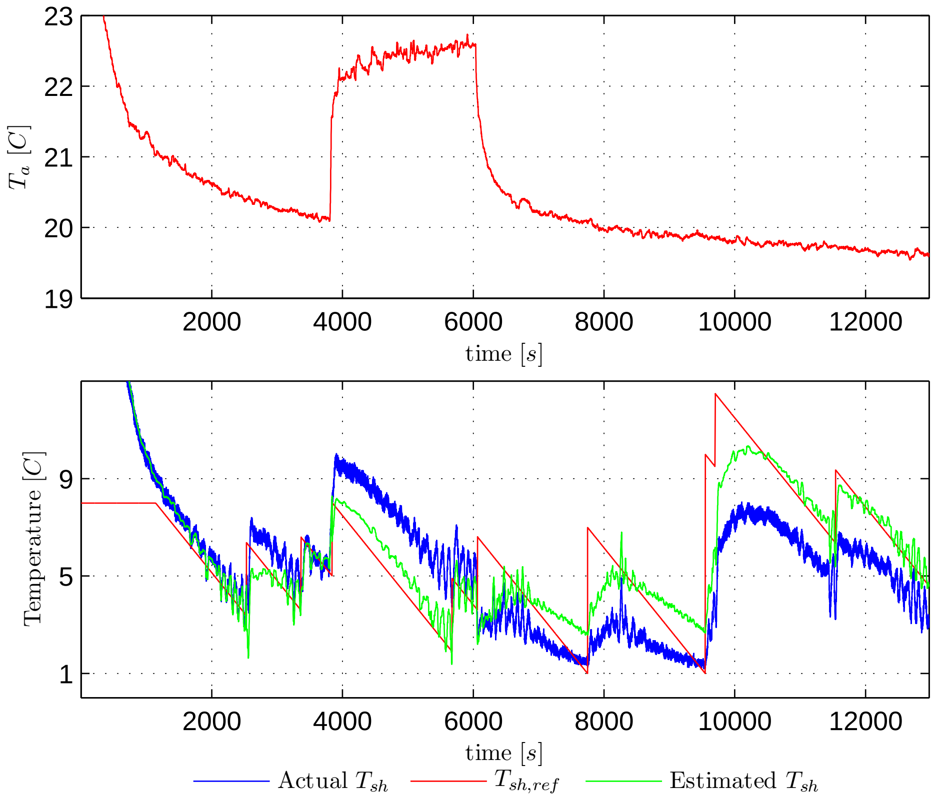

Figure 6.8: *System response to a disturbance to T_a. When T_a decreases, T_e does as well, causing $\hat{T}_{sh}$ to be too high. It takes some time for the controller to recover from this, during which the evaporator overflows.*

The results show that it is indeed possible to control the plant without knowledge of the model parameters apart from ε. However, the adaption compensates for inaccuracies in ε so the estimate is accurate at low superheat. But the estimate may become increasingly inaccurate with larger superheat. This may be tolerable in most cases. Therefore the result is a breakthrough, as we have shown that is possible to control the superheat in an air conditioning system with only one temperature sensor and qualitative knowledge about the system behavior.

A simplified controller structure has now been designed, which is independent of almost all parameters. To test if the control strategy is generic, it is tested on another test setup in the next chapter. The controllers ability to handle disturbances is improved with feed forward, described in Chapter 8.

Chapter 7

Implementation on Alternative Test Setup

The simplified controller has been shown to work on the test setup. However, the goal of the simplified controller is to make it general enough to work on other systems without further development. To verify that the simplified controller is indeed general it is implemented on a different test setup than the one used until now. The initial experiments described in Section 6.1 are performed and all the necessary parameters for the simplified structure are found. The system is then run in closed loop and its performance is evaluated.

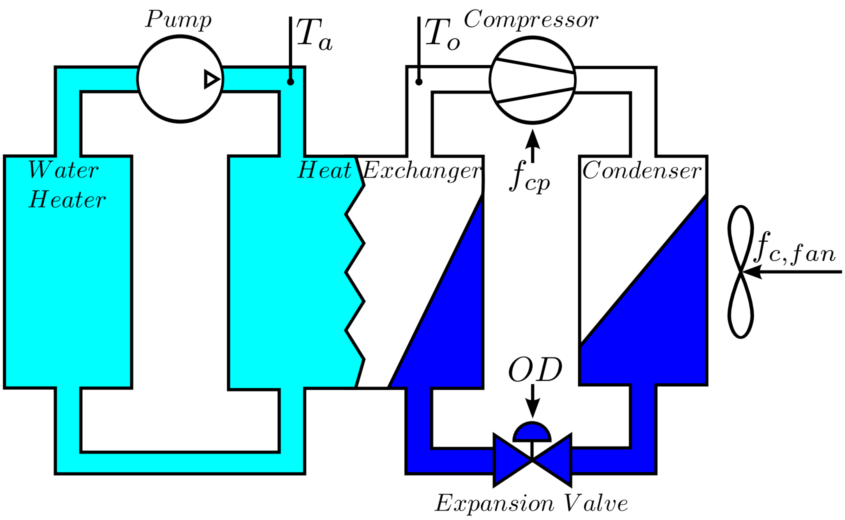

Figure 7.1: Overview of the alternative test setup. Instead of an air ventilator, the evaporator in the alternative system is heated using hot water and a heat exchanger. The water is electrically heated to simulate load on the system.

The alternative system is also a vapor-compression cycle system as the one used until now. However, the alternative system uses a heat exchanger between the refrigerant and water instead of a fin and tube evaporator. The system is equipped with multiple sensors as the one used until now, but only the T_o sensor is used in the experiments. The valve in the alternative system is an expansion valve. An overview of the system can be seen in Figure 7.1. Despite the differences the plant should have some of the same characteristics as original test plant. First the parameters of the controller are found.

7.1 Initial Experiments

Two initial experiments are conducted to determine the controller parameters. The first is an *OD* sweep to determine the Reference logic related parameters. Next, the system is operating at low superheat, and a step is performed. This experiment is used to determine the parameters of the PI controller of the system.

7.1.1 Reference Logic Related Parameters

To determine the variance parameters of the controller an *OD* sweep is performed using the alternative test setup. The experiment is similar to the one used for the original test setup shown in Figure 6.3 on page 98. The experiment is shown in Figure 7.2.

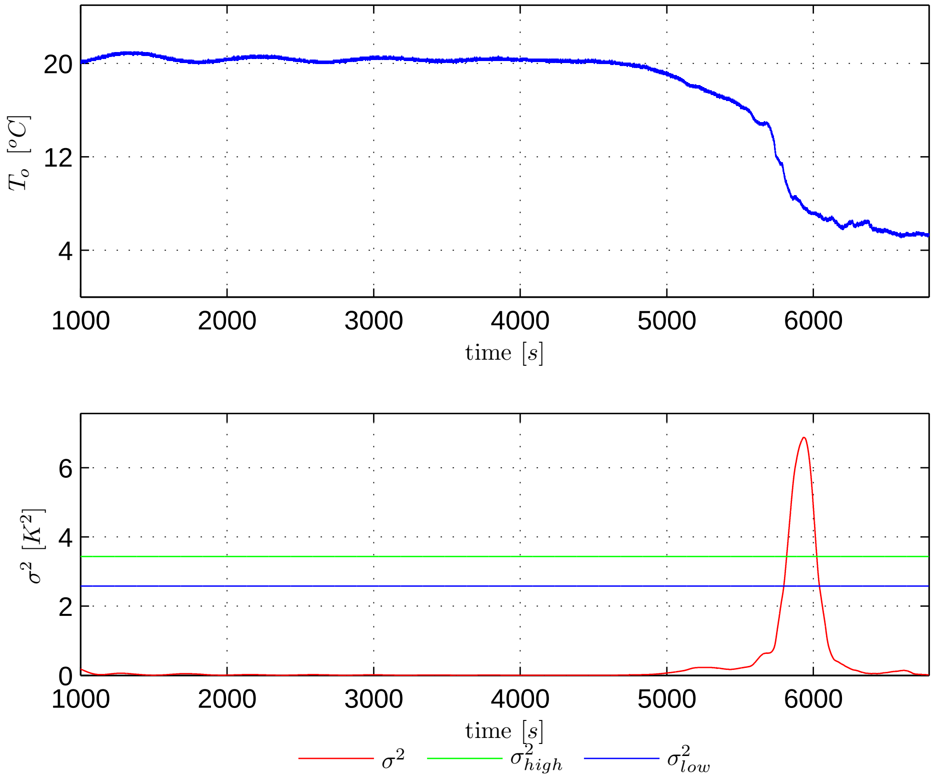

Figure 7.2: *Experiment for finding variance thresholds. The alternative system has more dramatic behavior than the original, which causes a high variance and easy detection of low superheat.*

The thresholds σ^2_{high}, σ^2_{low}, the offset T_{off}, and the variance window size τ_w are found according to the method described in Subsection 6.1.1, but using the experiment shown in Figure 7.2. The initial guess on the gain c is also found here. However, c is continuously adapted when the system is running in closed loop.

It is clear that the alternative test setup behaves significantly different from the original test setup. Figure 7.2 shows a sharp drop in T_o. The drop covers the temperature range where we expected to see variance due to low superheat as we did in the original setup. Here we see the strength of the method for detection of low superheat we have developed. Even though the alternative system has a sharp drop instead of oscillations, the variance detection method is still very effective. The increase in variance is even much more pronounced in the alternative system, than in the original system, which it was designed to run on.

7.1.2 Auto Tuning the PI Controller

The PI controller is auto tuned using Ziegler-Nichols as described in Subsection 6.1.3. For this the reaction rate and the lag of the system is needed. To find this an experiment is conducted where *OD* is stepped up, causing T_o to decrease. The gain of in the system is highest when T_a is close to T_e and the superheat is small (Lim et al., 2009). Therefore the experiment should be performed where the load of the system is as small as it gets during normal operation. The experiment is shown in Figure 7.3 and the lag and reaction rate are marked.

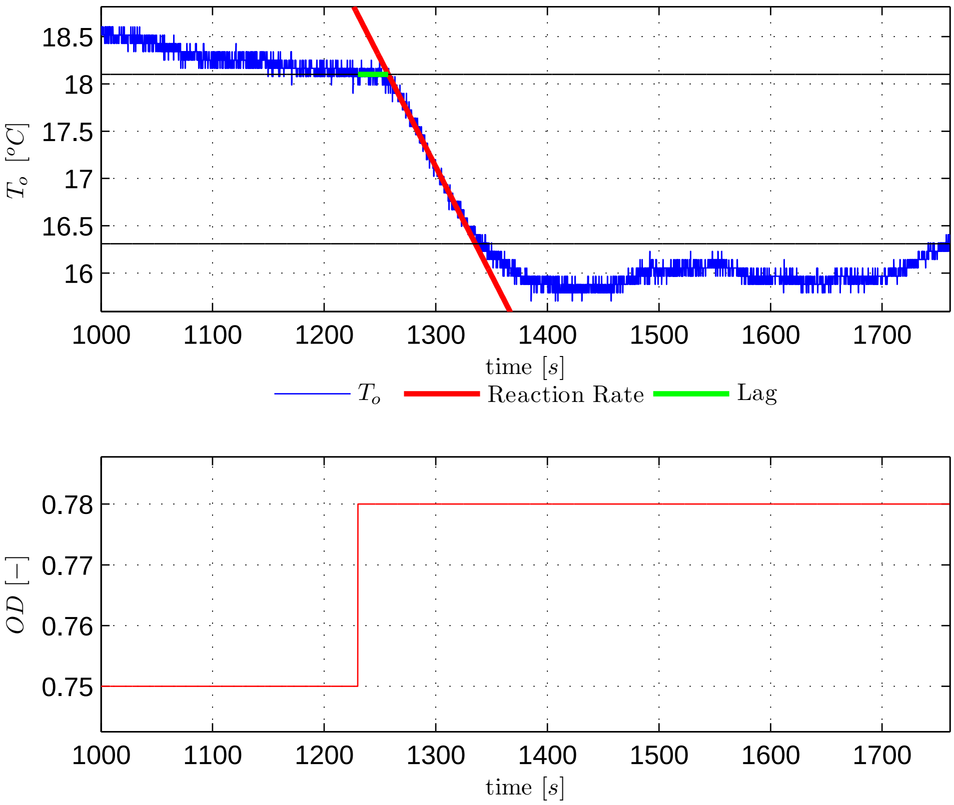

Figure 7.3: *A step in OD is performed at low superheat. The lag and reaction rate of the system is found, which is used to tune the PI controller.*

All the needed parameters has been obtained from the two experiments and only by using the T_o sensor. Now the controller is ready to control the system.

7.2 Results

To test the alternative system, it is run in closed loop. An experiment is conducted, where the reference logic and the PI controller is activated. The system should then periodically find the point where the sharp drop in T_o occurs, by continuously reducing $T_{o,ref}$, and then step it back when the variance becomes too high. The result from the experiment is shown in Figure 7.4

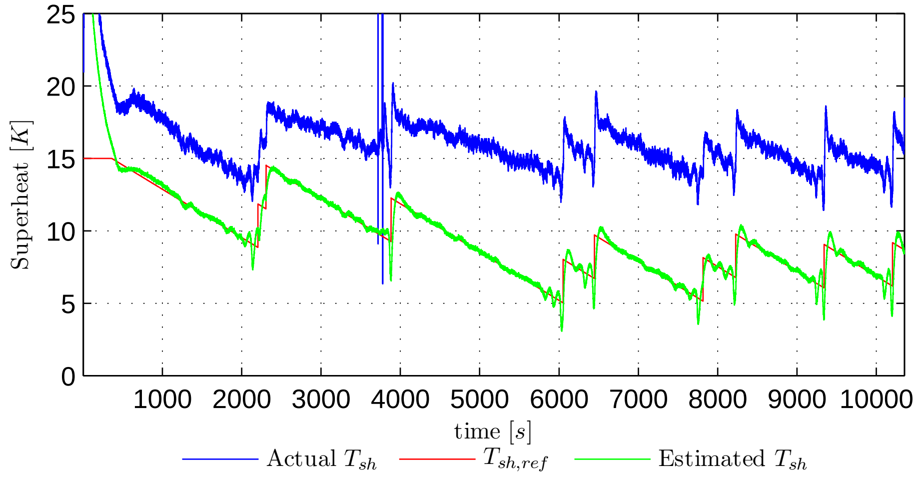

Figure 7.4: *Closed loop experiment with the alternative test setup. The estimated T_{sh} is lower than the actual because T_{off} is not accurate. The spikes in the actual T_{sh} are due to measurement noise in P_e.*

The experiment shows $\hat{T}_{sh}$ to be different from T_{sh}. This is because the T_{off} is poorly estimated in the parameter estimation procedures. We suspect this poor estimate is due to the characteristics of the alternative system. The drop in T_o on the alternative system occurs already around 12 degrees superheat, which is significantly higher than where the oscillations occurred in the original system. This behavior is very different from the original test setup.

However, the self tuned controller and reference logic are able to control the system, even though the characteristics of the alternative system are quite different from the original, and even though $\hat{T}_{sh}$ has an offset error, $T_{sh,ref}$ is still lowered until the system detects overflow. Therefore the system still operates at the desired superheat.

The result from an experiment to test the controllers ability to handle a disturbance is shown in Figure 7.5. The controller handles the disturbance. The disturbance affects the pressure estimate, but does not hinder the effort of the controller to keep the output temperature at the reference.

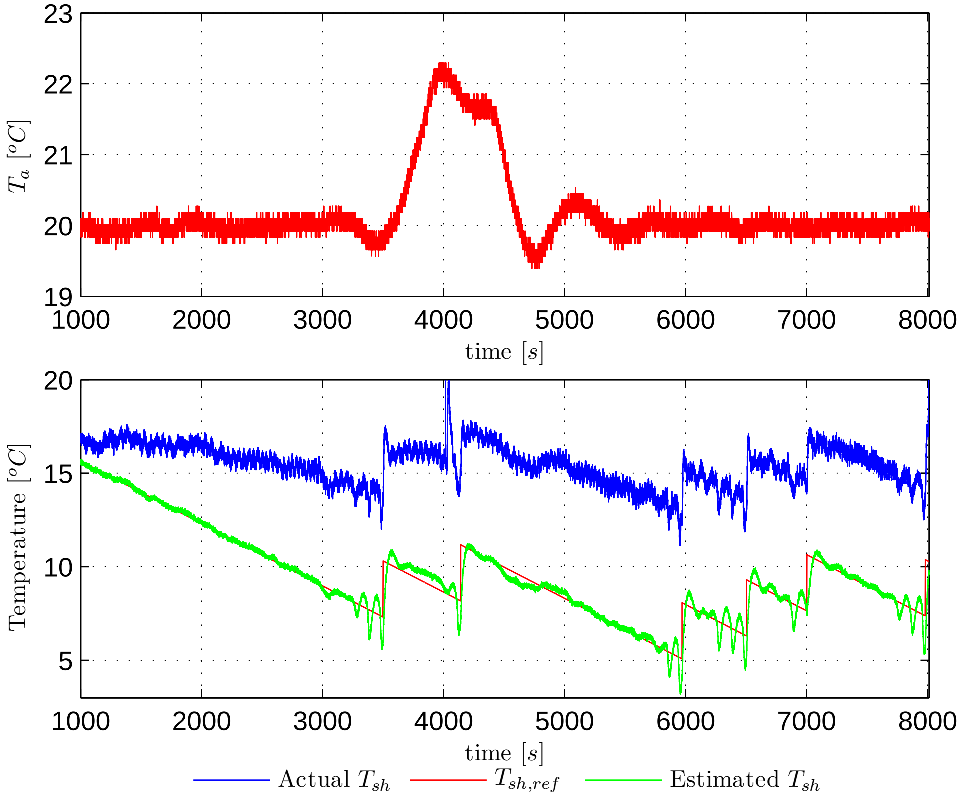

Figure 7.5: *Result from the experiment to test the ability of the controller to handle a disturbance.*

The tests prove that the controller and the algorithms for auto tuning are robust enough to work on at least two very different systems, without interference from an engineer. This should work in any system that has dramatic behavior when it is close to overflowing. This is a very good result as it makes us more confident that the controller will work with most systems.

Chapter 8

Feed Forward

In this chapter we develop a feed forward method to help the controller be more robust to sudden disturbances. Normally we do not think of feed forward in relation to disturbance rejection. It is, however, relevant in this case because of the special reference logic. In the first section the idea of the feed forward, and its projected consequences are discussed. In the next section the performance when there is no feed forward are presented, and compared to the performance when there is feed forward. The experiments show how the system reacts to a disturbance. In the last section a method for finding the correct feed forward adaptively is developed and evaluated.

8.1 Idea and Projected Effect

The idea of using feed forward is to aid the controller in tracking the steps in the reference. This is done by artificially injecting extra accumulated error into the integrator of the PI controller when a step in the reference occurs. If the correct amount of extra accumulated error is injected, it should cause the rise time of the controller to be improved significantly when the reference is stepped back. The expected effect is shown in Figure 8.1.

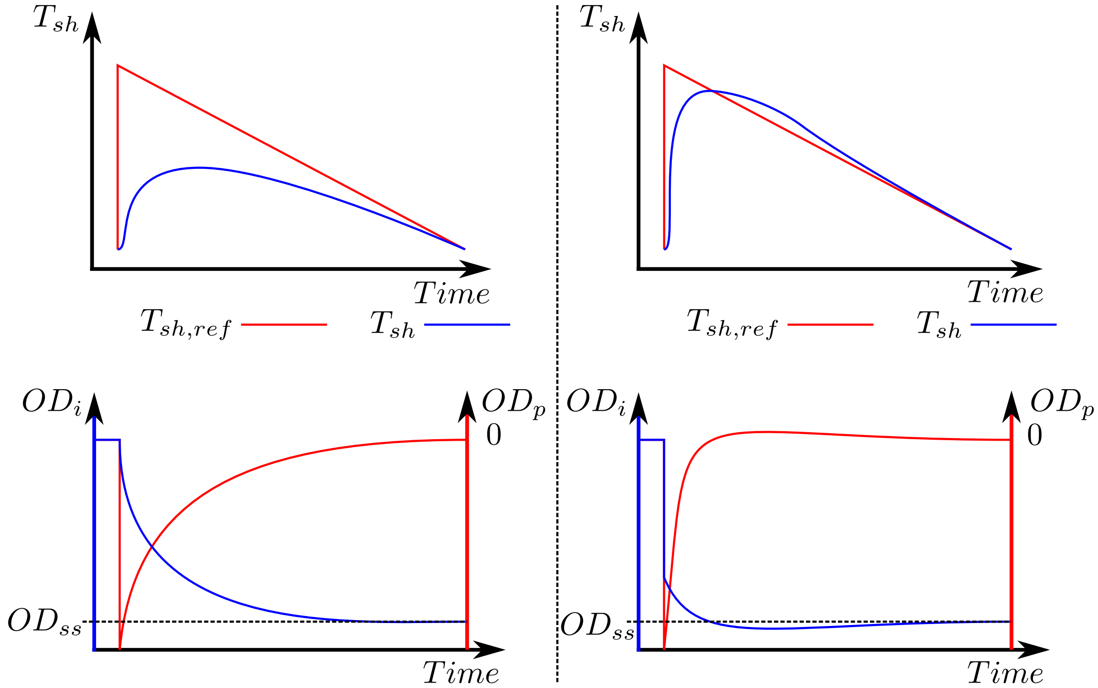

Figure 8.1: *The expected effect of feed forward in the system. Left: No feed forward. Right: With feed forward. OD_i and OD_p are the contributions to OD from the integral and proportional gains of the controller, respectively.*

In the next section we examine why this kind of feed forward may increase the performance of the controller with regard to disturbance rejection.

8.2 Actual Effect

In this section we examine the problem when there is no feed forward, and the effect of adding the correct amount of feed forward to the system. This is done by conducting two experiments.

In the experiments, the system is operating in closed loop. The ambient temperature of the evaporator T_a is then changed by venting hot air from the room with the condenser, into the room with the evaporator. Because of the very effective ventilators between the two rooms, the change in T_a, and thus the rate of evaporation, is very sudden. This causes T_o to rise. After a while the ventilators are stopped, which has the opposite effect, and makes T_o decrease. The experiment with no feed forward is shown in Figure 8.2.

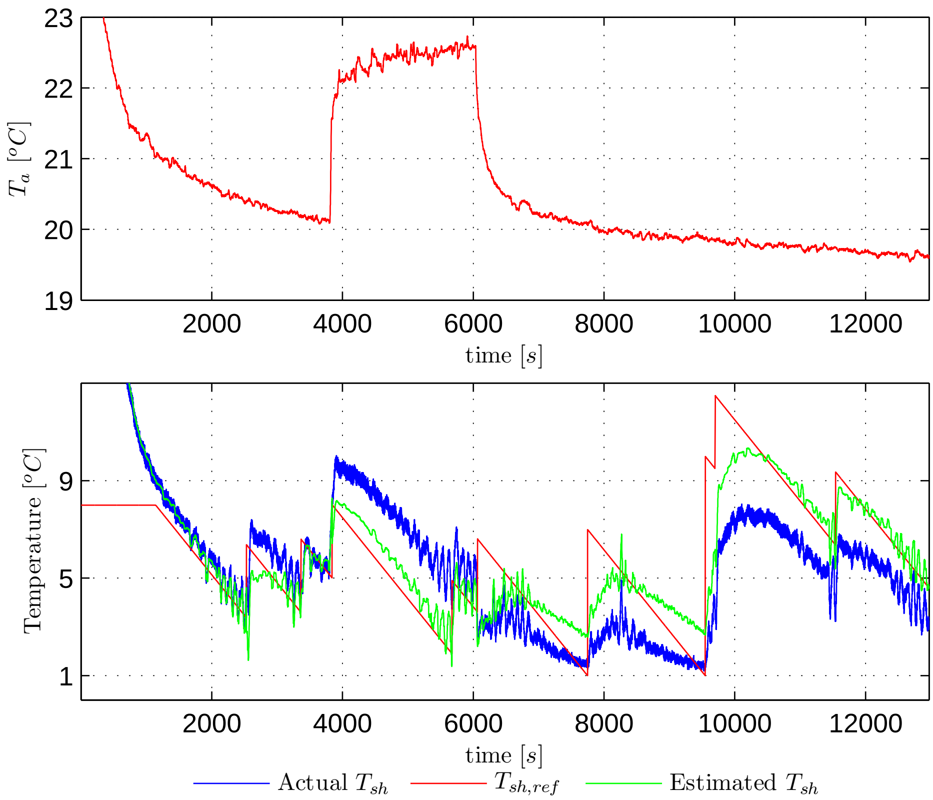

Figure 8.2: *The problem with no feed forward in the system. When T_a decreases, T_e does as well, causing $\hat{T}_{sh}$ to be too high. It takes some time for the controller to recover from this, during which the evaporator overflows.*

The disturbance where T_a is decreased causes the evaporator to fill up very quickly. The change in T_a causes $\hat{T}_{sh}$ to be too high since the gain c from OD to P_e is no longer accurate. The reference logic attempts to recover by stepping the reference back. However, the disturbance is so powerful that the PI controller does not recover before the reference has decreased again. Only when $\hat{T}_{sh}$ reaches $1K$ the reference logic detects the problem and attempts to step back the reference even further, but even this is not enough. Only the next time, the step back is sufficient for recovery. During the elapsed time since the disturbance the evaporator has been overflowing and thus wearing the compressor.

The next experiment is similar to the previous, but here a good value for the feed forward has been found beforehand. The experiment is shown in Figure 8.3

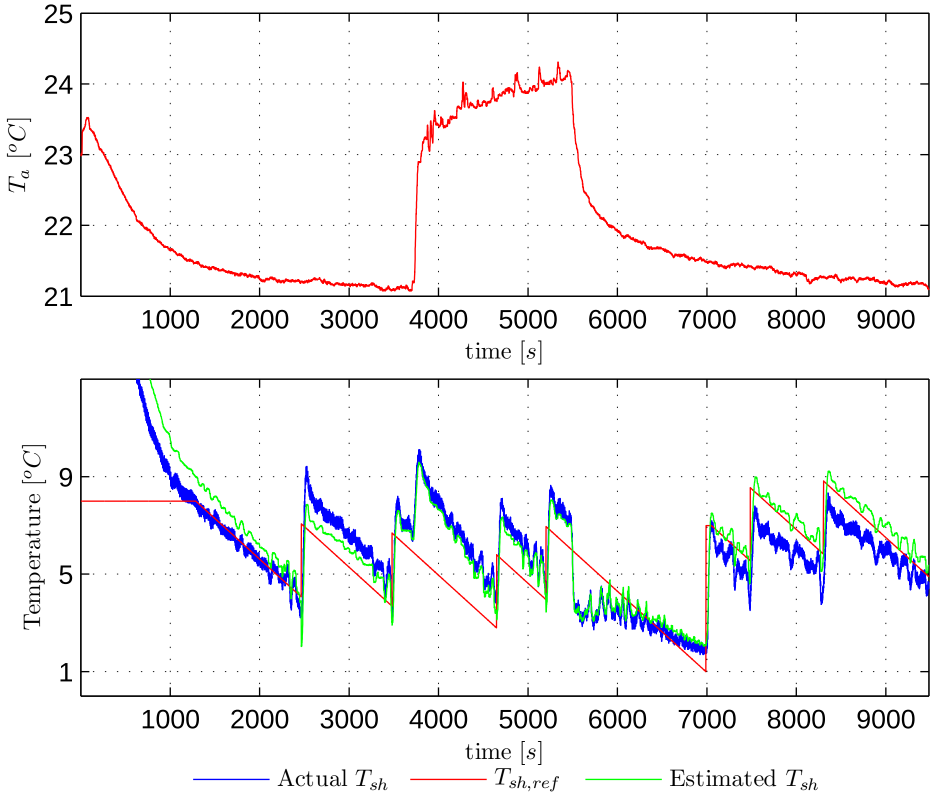

Figure 8.3: *Disturbance rejection in worst case when the feed forward gain is known. The controller only takes one period to recover, instead of two.*

In this experiment the system recovers much quicker after the disturbance. This is because the feed forward helps the PI controller reach the reference after the step before the reference has been decreased too much. However, the disturbance may be so powerful that even the system with feed forward enabled takes time to recover, but this should be much rarer than without feed forward.

It has been shown that feed forward improves the disturbance rejection of the controller if the correct amount of feed forward is known in advance. In the next section an adaptive algorithm for finding the correct feed forward is developed and the results are presented.

8.3 Adaptive Feed Forward Gain

We have shown that the correct amount of feed forward can improve the performance of the controller. However, as we aim for the controller to be generic in the sense that it should operate correctly on many different systems without human intervention, the amount of feed forward should be automatically adapted to each system.

To find the correct amount of feed forward, we need to define what the correct amount is. We define the correct amount of feed forward to be the amount, which makes

$$\Delta T = \Delta T_{ref} \qquad [K] \tag{8.1}$$

during one period. ΔT is the maximal change in T_{sh} between two steps. The reference ΔT_{ref} is the maximal change in $T_{sh,ref}$ during the step, which is the size of the step. Figure 8.4 shows the tracking and the controller output with and without feed forward. The feed forward is injected into the integrator when the step in $T_{sh,ref}$ occurs.

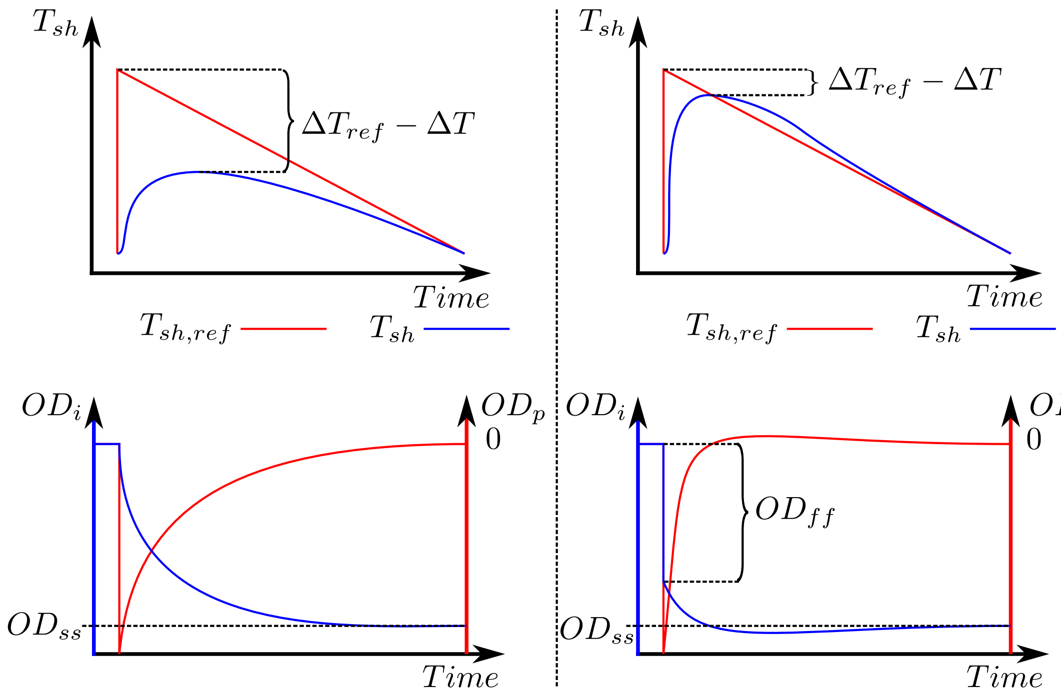

Figure 8.4: *To the left: The projected response when $OD_{ff} = 0$. To the right: The projected response after OD_{ff} has been updated.*

We use the MIT rule to obtain the amount of feed forward, which makes Equation (8.1) true. We therefore define the error to be

$$e_{ff} = \Delta T_{ref} - \Delta T \tag{8.2}$$

and the performance to be

$$J_{ff} = \frac{1}{2} e_{ff}^2 \tag{8.3}$$

We can then define the adaption law according to the MIT rule which states that

$$\frac{d\theta}{dt} = -\gamma \frac{\partial J}{\partial \theta} = -\gamma \cdot e \frac{\partial e}{\partial \theta} \tag{8.4}$$

where $\theta = OD_{ff}$, which is the amount injected into the integrator, $J = J_{ff}$, and $e = e_{ff}$. However, the gain $\frac{\partial e_{ff}}{\partial OD_{ff}}$ is unknown. But, we can approximate it by looking at the actual gain from the last step.

When a step in $T_{sh,ref}$ occurs, the proportional gain of the controller instantly reacts together with the feed forward, which together gives a certain ΔOD just when the step occurs. It is assumed that T_{sh} peaks and thereby gives ΔT, before the integrator of the PI controller have had time to gather significant momentum. Therefore we assume ΔT as being proportional to ΔOD, where $\Delta OD = max(OD_p) + OD_{ff}$, that is the OD contribution from the proportional controller just when the step occurred last time plus OD_{ff}. We can therefore approximate $\frac{\partial e_{ff}}{\partial OD_{ff}}$ by inspecting the actual gain last time the step occurred.

$$\frac{\partial e_{ff}}{\partial OD_{ff}} = -\frac{\Delta T}{\Delta OD} \tag{8.5}$$

We now have the adaption law in continuous time.

$$\frac{dOD_{ff}}{dt} = \gamma \cdot (\Delta T_{ref} - \Delta T)\,\frac{\Delta T}{\Delta OD} \tag{8.6}$$

However, OD_{ff} is not updated continuously. It is merely updated between steps in the reference, as it represents the extra kick used to help the controller track the step. Therefore we reformulate it in a discrete manner, which only updates once per step in the reference.

$$OD_{ff}[n+1] = \gamma \cdot (\Delta T_{ref}[n] - \Delta T[n])\,\frac{\Delta T[n]}{\Delta OD[n]} + OD_{ff}[n] \tag{8.7}$$

Where n denotes the last time the feed forward was active. The system may produce false positives on the detection of low superheat. Therefore the calculated feed forward gain may be sometimes be incorrect. To avoid problems with this, γ is chosen sufficiently small, which makes the calculation of feed forward gain more robust to false positive detections of low superheat. The price paid for this is slower convergence. Also OD_{ff} is capped so it is always negative, as there is no situation where it should be positive.

The method was implemented and tested by conducting an experiment similar to the one shown in Figure 8.3, where the feed forward was known in advance. We expect to see similar results in the new experiment, which is shown in Figure 8.5.

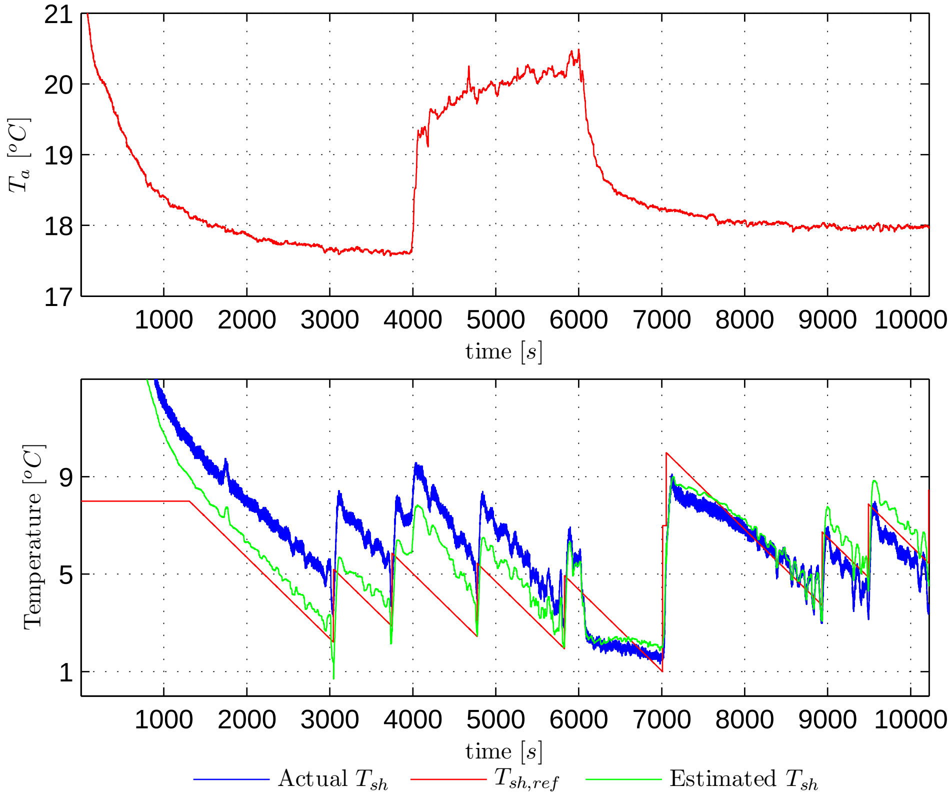

Figure 8.5: *Disturbance rejection in worst case when the feed forward gain is adjusted adaptively. The performance is similar to the case where the feed forward is known beforehand.*

It is seen that the performance of the adaptive feed forward algorithm and the fixed, known feed forward, does indeed produced similar results. However, the adaptive version has the benefit of being generic and able to adjust itself to other systems. In this way the generic nature of the simplified controller is maintained, even with feed forward enabled.

Chapter 9

Conclusion

The goal of this thesis is to develop a digital algorithmic generic controller for the evaporator in a vapor-compression cycle cooling system, which does not use a pressure sensor. The designed controller only uses one sensor; a temperature measurement of the refrigerant as it leaves the evaporator. Conventionally the pressure of the refrigerant in the evaporator is measured as well. By eliminating this sensor, a cheaper and more generic control structure is achieved.

The model of the vapor-compression cycle cooling system was derived to obtain knowledge about superheat related phenomenon. The knowledge gained from the model was used to develop a model specific control strategy. This control strategy requires extensive knowledge of the parameters of the system. Even though the controller is not generic, it was developed to see if control with only one sensor is possible. The results were positive, as the controller was indeed able to control the superheat temperature of the evaporator. The controller was then simplified to a point where knowledge of the parameter values in the system was no longer needed to control the evaporator superheat temperature. This was achieved by developing a procedure for online estimation of a few necessary parameters. The controller was tested using two different systems, with very positive results. Therefore it is concluded that the goal of developing a simple generic evaporator controller, which only uses one sensor was achieved.

The improved model of the evaporator features the inclusion of the different ambient temperature around different pipes. This helps to describe the uneven filling of the individual pipes in the evaporator and in turn the superheat behavior. A key discovery is that the temperature difference around the pipes depends on the intensity of the air flow in the evaporator. This can be seen in Equation (4.6). This means that the length of the two-phase zone in the individual pipes depends on the air flow around the evaporator. As a consequence it can be concluded that there is no fixed optimal distribution of refrigerant to the pipes, because if the airflow changes, the optimal distribution changes. The model of the evaporator also shows, that the more uneven the filling in the pipes are, the smaller the changes in T_o are when OD is changed. Therefore the nonlinearity of T_o is most significant when the pipes in the evaporator is filled evenly. In a very unevenly filled evaporator T_o may not be close to T_e when the first pipe, and even the second pipe, overflows.

The model of the evaporator was made with the assumption, among others, that there are no delays in the system. However when the test results, seen in Figure 4.15 and Figure 4.16 are compared, we do see delay from changes in OD to T_o. To improve the fit of the model, this delay should be included in the model. Furthermore Figure 4.16 shows that the derived model does not fit the dynamics of T_o very precisely. In part this is because of the delay and in part it is because of the difference in rise and fall time due to transient phenomena not considered here. However, the model does capture the dynamics of the pressure, as the delay is small compared to T_o. The model is very good at predicting the superheat phenomenon in steady state compared to the conventional model.

During the modeling of the compressor a new method for estimating the mass flow of refrigerant was used, as the test setup does not have a sensor to measure the mass flow. The mass flow was instead estimated by dividing the power consumed by the compressor with the enthalpy difference of the refrigerant as in exists and enters the compressor, as shown in Equation 2.10. The result yields a plausible result and predicts COPs in the expected region. However, the method has yet to be verified using a flow meter.

The results from the developed model specific controller shows that a controller using only the measurement of the output temperature from the evaporator can indeed be realized. The controller was able to keep a low superheat temperature without overflowing. The results from the controller shows that a better estimation of the output temperature would help filter the dynamics of the temperature from the oscillations at low superheat, but the current model is sufficient for this task. The control structure demands knowledge of the system parameters for the observer to work. However, some robustness are added by adapting some of the parameters in the valve. This makes the estimation of the evaporator pressure more accurate when the parameters are not precise. This also improves the estimated amount of superheat when there is no direct pressure measurement.

The simplified controller does not attempt to filter out the dynamics of the system, as the model based version. Therefore it does not need an observer, and thus not a linearized model. It is based purely on the steady state equations, where the gains are estimated in a single online experiment. The controller parameters are found in another online experiment. This has proven sufficient for superheat control using two different systems. The generalized method therefore works without knowledge of the parameters of the system, and is therefore generic. The pressure estimation is improved by continously adapting the gain from the valve opening degree to the pressure. The generalized version of the controller therefore succesfully solves the problem that we set out to solve, and it is the answer to the title of this thesis.

By adding feed forward to the control structure the system response of the steps in the reference signal is improved. This helps to ensure adequate controller response if a safety step in the reference is needed, for example if a disturbance of the system has occurred. By adapting the size of the feed forward, the varying gain of the system is handled, and the controller is still generic.

The control strategy was tested on two different test systems, with good results. It has thus been shown that the structure is feasible as a generic controller that can be used with no parameter knowledge. The two test systems has very different responses to increasing opening of the valve, as can be seen when Figure 4.13 and Figure 7.2 are compared. Common for the two systems are that there is a significant change in the response of the output temperature when the system is close to overflowing. This change in the response is needed by the control strategy, as this gives the increased variance of the output temperature.

We conclude that most of the goals we set out to achieve has been achieved with success. We think that the simplified version of the controller has the potential to be very valuable for to the industry as it has some of the merits from the TEV, while still allowing more sophisticated control modes.

Chapter 10

Perspective

The controllers developed all depends on dramatic behavior of T_o when the pipes begins to overflow. We have found behavior, which satisfies this criteria in both the test setups.

The controller can be disturbed and make overflow for a while, and then it recovers. Further development of the reference logic may lead to improvements in this respect. Specifically, the reference logic may be improved. If the reference is not merely stepped back every time low superheat is reached, but instead slowly increased until the variance disappears. Then the requirement for a setling time may be eleminated. The reference could be stepped back only when abnormal behavior is detected.

In most systems there are a T_a sensor used for feedback in an outer loop, which controls the amount of cooling, typically using the compressor speed, f_{cp}. If T_a and f_{cp} were made available to the superheat controller, they could be fed forward relatively easy. This would make the controller able to anticipate disturbances much better, and the disturbance problem may then be overcome. This remains to be studied.

There was a problem estimating the superheat temperature at which the dramatic behavior of T_o occurs, called T_{off} using the alternative test setup. This caused $\hat{T}_{sh}$ to be offset. This may be corrected if T_{off} was adapted online by giving a short burst with OD causing a very short period of overflow, during which T_o would equal T_e. From this T_{off} may be found.

The Danfoss EcoFlow^{TM} valve allows control of the distribution of flow among the pipes in the evaporator. The idea is to obtain even filling of the pipes with an algorithm. We have shown that the optimal distribution is not fixed, but it varies with varying load conditions and ventilation of the evaporator. Therefore an algorithm for finding the optimal distribution should be adaptive, and adjust the distribution online in closed loop.

Bibliography

Duprez, M.-E., Dumont, E., and Frère, M. (2007). Modelling of reciprocating and scroll compressors. *International Journal of Refrigeration*, 30(5):873–886.

Franklin, G. F., Powell, J. D., and Emami-Naeini, A. (2006). *Feedback Control of Dynamic Systems*. Pearson Education, Inc., 5th edition. ISBN: 0-13-149930-0.

He, X.-D., Liu, S., Asada, H. H., and Itoh, H. (1998). Multivariable control of vapor compression systems. *HVAC&R Research*, 4(3):205–230.

Larsen, L. F. S. (2005). *Model Based Control of Refrigeration Systems*. ISBN: 87-90664-29-9.

Lim, D., Rasmussen, B. P., and Swaroop, D. (2009). Selecting pid control gains for nonlinear hvac&r systems. *HVAC&R Research*, 15(6):991–1019.

Rasmussen, H. and Larsen, L. F. S. (2011). Nonlinear and adaptive control of a refrigeration system. *IET Control Theory & Applications*, 5(2):364–378.

Raymond A. Serway, J. W. J. J. (2004). *Physics for Scientists and Engineers with Modern Physics*. David Harris, 6th edition. ISBN: 0-534-40844-3.

Skovrup, M. J. (2000). Thermodynamic and thermophysical properties of refrigerants. Software guide 3, DTU.

Åström, K. J. and Wittenmark, B. (2008). *Adaptive Control*. Dover, 2nd edition. ISBN: 0-486-46278-1.

Wedekind, G., Bhatt, B., and Beck, B. (1978). A system mean void fraction model for predicting various transient phenomena associated with two-phase evaporating and condensing flows. *International Journal of Multiphase Flow*, 4(1):97–114.

Appendix A

Temperature Increase in the Compressor Based on Adiabatic Compression

During the compression of the refrigerant, the temperature of the gas increases as well as the pressure. To be able to estimate the increase in temperature, the connection between the increase in pressure and temperature needs to be calculated. The connection is based on the ideal gas law (Raymond A. Serway, 2004, p. 595)

$$P \cdot V = n \cdot R \cdot T \qquad [J] \qquad \text{(A.1)}$$

where P is the pressure, V is the volume, n is the quantity of gas, R is the universal gas constant and T is the temperature.
The model is also based on the first law of thermodynamics (Raymond A. Serway, 2004, p. 618)

$$\Delta U = Q + W \qquad [J] \qquad \text{(A.2)}$$

where ΔU is the change in internal energy, Q is the energy transfered to the gas by heat and W is the work done on the gas.

It is assumed that the compression process is an isoentropic process. This means, that no energy is transfered to the gas by heat. The work done on the system is equal to the pressure times the change in volume (Raymond A. Serway, 2004, p. 616). Therefore the change in internal energy can be expressed as

$$dU = -P \cdot dV \qquad [W] \qquad \text{(A.3)}$$

The change in internal energy can also be expressed by the molar specific heat of the gas at constant volume (Raymond A. Serway, 2004, p. 647)

$$dU = n \cdot C_v \cdot dT \qquad [W] \qquad \text{(A.4)}$$

where C_v is the molar specific heat at constant volume.

The ideal gas law, formula (A.1), is differentiated with respect to time. This equation together with formula (A.3) and (A.4) gives an equation where the internal energy, the temperature change and the amount of gas is eliminated

$$P \cdot dV + V \cdot dP = n \cdot R \cdot dT \qquad [W]$$
$$P \cdot dV + V \cdot dP = \frac{-R}{C_v} \cdot P \cdot dV \qquad [W] \qquad \text{(A.5)}$$

By rearranging formula (A.5) and integrating it across the pressure and the volume changes, an equation that describes the relationship between the pressure change and the volume change is derived.

$$\frac{-1}{P} \cdot dP = \frac{R + C_v}{C_v} \cdot \frac{1}{V} \cdot dV \qquad [1/s]$$
$$-\int_{P_e}^{P_c} \frac{1}{P} \cdot dP = \frac{R + C_v}{C_v} \cdot \int_{V_{cp,i}}^{V_{cp,o}} \frac{1}{V} \cdot dV \qquad [-]$$
$$-\,ln\left(\frac{P_c}{P_e}\right) = \frac{R + C_v}{C_v} \cdot ln\left(\frac{V_{cp,o}}{V_{cp,i}}\right) \qquad [-]$$
$$\frac{P_c}{P_e} = \left(\frac{V_{cp,o}}{V_{cp,i}}\right)^{-\frac{R+C_v}{C_v}} \qquad [W] \qquad \text{(A.6)}$$

The universal gas constant, R, can be expressed as the difference between the molar specific heat at constant pressure and constant volume, $R = C_p - C_v$ (Raymond A. Serway, 2004, p. 648). Formula (A.6) can with this together with the relationship $\xi = C_p/C_v$ be rewritten to formula (A.7).

$$\frac{P_c}{P_e} = \left(\frac{V_{cp,o}}{V_{cp,i}}\right)^{-\xi} \qquad [W] \qquad \text{(A.7)}$$

It is assumed that the amount of gas is unchanged during the compression, and therefore that the number of mol, *n*, of the gas is unchanged. By combining the ideal gas law before and after the compression and this assumption, a relation between the volume before and after the compression is found to be

$$\frac{P_e \cdot V_{cp,i}}{T_o} = \frac{P_c \cdot V_{cp,o}}{T_{c,i}} \qquad [J/K]$$
$$\frac{V_{cp,o}}{V_{cp,i}} = \frac{P_e \cdot T_{c,i}}{P_c \cdot T_o} \qquad [-] \qquad \text{(A.8)}$$

By inserting formula (A.8) into formula (A.7) the volumes are eliminated, and the connection between the pressure and the temperature can be derived. The result is shown in formula (A.9).

$$\frac{P_c}{P_e} = \left(\frac{P_e \cdot T_{c,i}}{P_c \cdot T_o}\right)^{-\xi} \qquad [-]$$
$$\left(\frac{P_c}{P_e}\right)^{1-\xi} = \left(\frac{T_{c,i}}{T_o}\right)^{-\xi} \qquad [-]$$
$$\frac{T_{c,i}}{T_o} = \left(\frac{P_c}{P_e}\right)^{\frac{\xi-1}{\xi}} = \left(\frac{P_c}{P_e}\right)^{\frac{C_p - C_v}{C_p}} \qquad [-] \qquad \text{(A.9)}$$

Appendix B

Linearization of the Evaporator

This appendix documents the linearization of the evaporator. The linearization is done by approximating the behavior of the evaporator around a operating point with a small signal model. The model is based on the model derived in Chapter 4. The scope of the linear model is to fit the non-linear model of the evaporator when calculated in an arbitrary operating point.
In the linear model it is assumed that the length of the two-phase zones in the four pipes are the same.
In this appendix the equation for the length of the two-phase zone in the evaporator, the equation for the pressure in the evaporator and the equation for the output temperature is linearized, and a combined linear model is formed.

B.1 Simplification of l2p

The state equation for the length of the two-phase zone in a single pipe in the evaporator is described in Equation (4.8), and reprinted here for convenience.

$$\begin{aligned} & A_{pi} \cdot (1-\gamma_{2p}[j]) \cdot \rho_l \cdot (h_g - h_l) \cdot \frac{d\left(\ell_{2p}[j]\right)}{dt} \\ & = \dot{m}_v[j]\,(h_g - h_l) - \alpha_{2p} \cdot O_{pi} \cdot \ell_{2p}[j] \cdot \Delta T'[j] \qquad [J/s] \end{aligned} \tag{4.8}$$

Some of the terms in the equation is calculated as functions of other variables in the system. When these dependencies are included, Equation (4.8) becomes

$$\begin{aligned} & A_{pi} \cdot (1-\gamma_{2p}(\ell_{2p}, P_e, \dot{m}_v, T_{c,o})[j]) \cdot \rho_l(P_e) \cdot (h_g(P_e) - h_l(P_e)) \cdot \frac{d\left(\ell_{2p}[j]\right)}{dt} \\ & = \dot{m}_v[j] \cdot (h_g(P_e) - h_i(P_e)) - \alpha_{2p} \cdot O_{pi} \cdot \ell_{2p}[j] \cdot \Delta T'[j] \qquad [J/s] \end{aligned} \tag{B.1}$$

With the assumption that the length of the two-phase zone in the four pipes are the same, Equation (B.1) can be rewritten to express the change in the total length of the evaporator. This is done by adding the equations for all the pipes together. The void fraction is calculated as the mean of the void fraction in the four pipes. The temperature difference is rewritten to cover all four pipes.

$$\gamma_{2p}(\ell_{2p}, P_e, \dot{m}_v, T_{c,o}) = \frac{1}{N_{pi}} \sum_{j=1}^{N_{pi}} \gamma_{2p}(\ell_{2p}, P_e, \dot{m}_v, T_{c,o})[j] \qquad [-] \qquad \text{(B.2)}$$

$$\Delta T' = (T_a - T_e(P_e)) \cdot \underbrace{\frac{1}{N_{pi} \cdot \ell_{2p}} \sum_{j=1}^{N_{pi}} \sum_{i=1}^{N_{pa}} \ell_i[j] \cdot \eta_i[j]}_{\eta' = (1+\eta)/2} \qquad [K] \qquad \text{(B.3)}$$

The mass flow into each pipe adds up to the mass flow in the valve. With these alterations, the length of the two-phase zone can be described as

$$\underbrace{N_{pi} \cdot A_{pi} \cdot (1 - \gamma_{2p}(\ell_{2p}, P_e, \dot{m}_v, T_{c,o})) \cdot \rho_l(P_e) \cdot (h_g(P_e) - h_l(P_e))}_{f_1(\ell_{2p}, P_e, \dot{m}_v, T_{c,o})} \cdot \frac{d(\ell_{2p})}{dt}$$
$$= \dot{m}_v \cdot (h_g(P_e) - h_i(P_e)) - \alpha_{2p} \cdot O_{pi} \cdot N_{pi} \cdot \eta' \cdot \ell_{2p} \cdot (T_a - T_e(P_e)) \qquad [J/s] \qquad \text{(B.4)}$$

It is assumed that the terms on the left-hand side of the equation can be joined into a single equation, calculated in the operating point.

$$f_1(\bar{\ell}_{2p}, \bar{P}_e, \bar{\dot{m}}_v, \bar{T}_{c,o}) \cdot \frac{d(\ell_{2p})}{dt} = \dot{m}_v \cdot (h_g(P_e) - h_i(P_e))$$
$$- \alpha_{2p} \cdot O_{pi} \cdot N_{pi} \cdot \eta' \cdot \ell_{2p} \cdot (T_a - T_e(P_e)) \qquad [J/s] \qquad \text{(B.5)}$$

The mass flow in the valve is expressed in Equation (2.20) as

$$\dot{m}_v = OD^{1+\varepsilon_v} \cdot \sqrt{P_c - P_e} \cdot \frac{\sqrt{\rho_l}}{\sqrt{R_v}} \qquad [kg/s] \qquad \text{(2.20)}$$

By inserting this equation in the first term on the right hand side of Equation (B.5), the first term becomes

$$\dot{m}_v \cdot (h_g(P_e) - h_i(P_e)) = \underbrace{(h_g(P_e) - h_i(P_e)) \cdot \sqrt{P_c - P_e} \cdot \frac{\sqrt{\rho_l(P_c)}}{\sqrt{R_v}}}_{f_2(P_e, P_c, T_{c,o})} \cdot OD^{1+\varepsilon_v} \qquad [J/s] \qquad \text{(B.6)}$$

It is assumed that the terms on the right hand side can be joined into a function of the operating point. The term $OD^{1+\varepsilon}$ is approximated with a first order Taylor Approximation.

$$OD^{1+\varepsilon} \approx \underbrace{-\varepsilon \cdot \bar{OD}^{1+\varepsilon}}_{od_1(\bar{OD})} + \underbrace{\frac{\bar{OD}^{1+\varepsilon} \cdot (1+\varepsilon)}{\bar{OD}}}_{od_2(\bar{OD})} \cdot OD \qquad [-] \qquad \text{(B.7)}$$

$$\dot{m}_v \cdot (h_g(P_e) - h_i(P_e)) = f_2(\bar{P}_e, \bar{P}_c, \bar{T}_{c,o}) \cdot \left(od_1(\bar{OD}) + od_2(\bar{OD}) \cdot OD\right) \qquad [J/s] \qquad \text{(B.8)}$$

Equation (B.8) and Equation (B.5) are combined.

$$f_1(\bar{\ell}_{2p}, \bar{P}_e, \bar{\dot{m}}_v, \bar{T}_{c,o}) \cdot \frac{d(\ell_{2p})}{dt} = f_2(\bar{P}_e, \bar{P}_c, \bar{T}_{c,o}) \cdot \left(od_1(\bar{OD}) + od_2(\bar{OD}) \cdot OD\right)$$
$$- \alpha_{2p} \cdot O_{pi} \cdot N_{pi} \cdot \eta' \cdot \ell_{2p} \cdot (T_a - T_e(P_e)) \qquad [J/s] \qquad \text{(B.9)}$$

B.2 Simplification of Pe

The pressure in the evaporator is described in Equation (4.10) and reprinted here for convenience.

$$V' \cdot \frac{d(\rho_g)}{dP_e} \frac{d(P_e)}{dt} = \dot{m}_{v,g} - \dot{m}_{cp} + \frac{\alpha_{2p} \cdot O_{pi}}{h_g - h_l} \sum_{j=1}^{N_{pi}} \ell_{2p}[j] \cdot \Delta T'[j] \qquad [kg/s] \qquad \text{(4.10)}$$

Some of the terms in the equation is functions of other variables in the system. It is assumed that the length of the two-phase zone is equal in all four pipes. The temperature difference is replaced with Equation (B.3) and multiplied with the number of pipes. When these alterations are included, the system becomes

$$\underbrace{V' \cdot \rho_g'(P_e)}_{f_3(P_e)} \frac{d(P_e)}{dt} = \dot{m}_{v,g} - \dot{m}_{cp} + \underbrace{\frac{\alpha_{2p} \cdot O_{pi} \cdot N_{pi} \cdot \eta'}{h_g(P_e) - h_l(P_e)}}_{f_4(P_e)} \cdot (T_a - T_e(P_e)) \cdot \ell_{2p} \quad [kg/s] \qquad \text{(B.10)}$$

It is assumed that the term on the left hand side of the equation can be expressed as a function of the operating point. Likewise it is assumed that the heat transfer divided by the enthalpy difference can be expressed as a function of the working point. With these assumptions, Equation (B.10) becomes

$$f_3(\bar{P}_e) \frac{d(P_e)}{dt} = \dot{m}_{v,g} - \dot{m}_{cp} + f_4(\bar{P}_e) \cdot (T_a - T_e(P_e)) \cdot \ell_{2p} \qquad [kg/s] \qquad \text{(B.11)}$$

The mass flow through the compressor is described in Equation (2.8). The density of the gas in the evaporator is a function of P_e. The mass flow can be described by

$$\dot{m}_{cp} = V_{cp,i} \cdot f_{cp} \cdot \rho_g(P_e) \qquad [kg/s] \qquad \text{(B.12)}$$

It is assumed that the mass flow of gas through the valve can be estimated by the same principle as in Equation (B.6).

$$\dot{m}_{v,g} = \underbrace{\frac{h_i(T_{c,o}) - h_l(P_e)}{h_g(P_e) - h_l(P_e)} \cdot \frac{\sqrt{P_c - P_e} \cdot \sqrt{\rho_l(P_c)}}{\sqrt{R_v}}}_{f_5(P_e, P_c, T_{c,o})} \cdot \left(od_1(\bar{OD}) + od_2(\bar{OD}) \cdot OD\right) \quad [kg/s] \qquad \text{(B.13)}$$

It is assumed that the function f_5 can be calculated from the operating point.
Equation (B.12) and Equation (B.13) are inserted into Equation (B.11)

$$f_3(\bar{P}_e)\frac{d(P_e)}{dt} = f_5(\bar{P}_e,\bar{P}_c,\bar{T}_{c,o}) \cdot \left(od_1(\bar{OD}) + od_2(\bar{OD}) \cdot OD\right)$$
$$-V_{cp,i} \cdot f_{cp} \cdot \rho_g(P_e) + f_4(\bar{P}_e) \cdot (T_a - T_e(P_e)) \cdot \ell_{2p} \qquad [kg/s] \qquad (B.14)$$

B.3 Simplification of To

The output temperature is calculated based on Equation (4.14), which is reprinted here for convenience.

$$T_{sh}[j] = \left(T_a'[j] - T_e\right)\left(1 - e^{-\frac{\ell_{sh}[j]}{\beta_e'[j]}}\right) \qquad [K] \qquad (4.14)$$

By adding the evaporation temperature the equation expresses the output temperature. The evaporation temperature is dependent on the pressure in the evaporator.

$$T_o[j] = T_a'[j] - \left(T_a'[j] - T_e(P_e)\right) e^{-\frac{\ell_{sh}[j]}{\beta_e'[j]}} \qquad [K] \qquad (B.15)$$

It is assumed that the length of the two-phase zone, and thereby the length of the superheated zone, in all four pipes are the same. The ambient temperature around a pipe is calculated in Equation (4.11). The total ambient temperature is calculated as the mean of the ambient temperatures around the four pipes. It is assumed that the ambient temperature can be calculated from the operating point of the pressure.

$$T_a'(P_e) = T_e(P_e) + (T_a - T_e(P_e)) \cdot \frac{1}{N_{pi}} \sum_{j=1}^{N_{pi}} \eta_{N_{pa}}[j] \qquad [K] \qquad (B.16)$$

$$T_o = T_a'(\bar{P}_e) - \left(T_a'(\bar{P}_e) - T_e(P_e)\right) e^{-\frac{\ell_{sh}}{\beta_e}} \qquad [K] \qquad (B.17)$$

The exponential part of the equation is approximated by a first order Taylor Approximation.

$$e^{-\frac{\ell_{sh}}{\beta_e}} \approx \underbrace{e^{-\frac{\bar{\ell}_{sh}}{\beta_e}}}_{c_1(\bar{\ell}_{sh})} - \underbrace{\frac{1}{\beta_e} \cdot e^{-\frac{\bar{\ell}_{sh}}{\beta_e}}}_{c_2(\bar{\ell}_{sh})} \cdot (\ell_{sh} - \bar{\ell}_{sh}) \qquad [-] \qquad (B.18)$$

Equation (B.18) is inserted into Equation (B.17)

$$T_o = T_a'(\bar{P}_e) - \left(T_a'(\bar{P}_e) - T_e(P_e)\right) \cdot \left(c_1(\bar{\ell}_{sh}) - c_2(\bar{\ell}_{sh}) \cdot (\ell_{sh} - \bar{\ell}_{sh})\right) \quad [K] \qquad (B.19)$$

The length of the superheated zone can be expressed as the total length of the evaporator minus the length of the two-phase zone

$$T_o = T_a'(\bar{P}_e) - \left(T_a'(\bar{P}_e) - T_e(P_e)\right) \cdot \left(c_1(\bar{\ell}_{sh}) - c_2(\bar{\ell}_{sh}) \cdot (\bar{\ell}_{2p} - \ell_{2p})\right) \qquad [K] \qquad (B.20)$$

B.4 Linearized model

A linear small signal model of the evaporator is derived by linearizing the simplified models. The linear model of the evaporator has the form

$$\begin{aligned} \dot{\mathbf{x}} &= \mathbf{A}\mathbf{x} + \mathbf{B}u + \mathbf{E}\mathbf{v} \\ \mathbf{y} &= \mathbf{C}\mathbf{x} + \mathbf{D}u \end{aligned} \tag{B.21}$$

where the state, input, output and disturbance vectors are equal to

$$\mathbf{x} = \begin{bmatrix} \ell_{2p} \\ P_e \end{bmatrix}, \; u = OD \; , \; \mathbf{y} = \begin{bmatrix} T_o \\ P_e \end{bmatrix}, \; \mathbf{v} = \begin{bmatrix} f_{cp} \\ T_a \end{bmatrix} \tag{B.22}$$

The state matrix is derived based on the simplified model of the length of the two-phase zone, described in Equation (B.9), and the simplified model of the pressure, described in Equation (B.14). The linear small signal model of the states is

$$\mathbf{A} = \begin{bmatrix} \frac{\partial \dot{\ell}_{2p}}{\partial \ell_{2p}} & \frac{\partial \dot{\ell}_{2p}}{\partial P_e} \\ \frac{\partial \dot{P}_e}{\partial \ell_{2p}} & \frac{\partial \dot{P}_e}{\partial P_e} \end{bmatrix} = \begin{bmatrix} -\frac{\alpha_{2p} \cdot O_{pi} \cdot N_{pi} \cdot \eta' \cdot (\bar{T}_a - T_e(\bar{P}_e))}{f_1(\bar{\ell}_{2p}, \bar{P}_e, \dot{\bar{m}}_v, \bar{T}_{c,o})} & \frac{\alpha_{2p} \cdot O_{pi} \cdot N_{pi} \cdot \eta' \cdot \bar{\ell}_{2p} \cdot T_e'(\bar{P}_e)}{f_1(\bar{\ell}_{2p}, \bar{P}_e, \dot{\bar{m}}_v, \bar{T}_{c,o})} \\ \frac{f_4(\bar{P}_e) \cdot (\bar{T}_a - T_e(\bar{P}_e))}{f_3(\bar{P}_e)} & -\frac{\rho_g'(\bar{P}_e) \cdot V_{cp,i} \cdot \bar{f}_{cp} + f_4(\bar{P}_e) \cdot \bar{\ell}_{2p} \cdot T_e'(\bar{P}_e)}{f_3(\bar{P}_e)} \end{bmatrix} \tag{B.23}$$

The input matrix is derived based on the simplified model of the length of the two-phase zone, described in Equation (B.9), and the simplified model of the pressure, described in Equation (B.14). The input model is

$$\mathbf{B} = \begin{bmatrix} \frac{\partial \dot{\ell}_{2p}}{\partial OD} \\ \frac{\partial \dot{P}_e}{\partial OD} \end{bmatrix} = \begin{bmatrix} \frac{f_2(\bar{P}_e, \bar{P}_c, \bar{T}_{c,o}) \cdot od_2(\bar{OD})}{f_1(\bar{\ell}_{2p}, \bar{P}_e, \dot{\bar{m}}_v, \bar{T}_{c,o})} \\ \frac{f_5(\bar{P}_e, \bar{P}_c, \bar{T}_{c,o}) \cdot od_2(\bar{OD})}{f_3(\bar{P}_e)} \end{bmatrix} \tag{B.24}$$

The output matrix is derived based on the simplified model of the output temperature, described in Equation (B.18). One of the outputs, P_e, is also a state in the model. The output model is

$$\mathbf{C} = \begin{bmatrix} \frac{\partial T_o}{\partial \ell_{2p}} & \frac{\partial T_o}{\partial P_e} \\ \frac{\partial P_e}{\partial \ell_{2p}} & \frac{\partial P_e}{\partial P_e} \end{bmatrix} = \begin{bmatrix} c_2(\bar{\ell}_{sh}) \cdot (T_e(\bar{P}_e) - T_a'(\bar{P}_e)) & c_1(\bar{\ell}_{sh}) \cdot T_e'(\bar{P}_e) \\ 0 & 1 \end{bmatrix} \tag{B.25}$$

The feed through matrix of the system is equal to zero.

$$\mathbf{D} = \begin{bmatrix} \frac{\partial T_o}{\partial OD} \\ \frac{\partial \, P_e}{\partial OD} \end{bmatrix} = \begin{bmatrix} 0 \\ 0 \end{bmatrix} \tag{B.26}$$

The disturbance matrix is derived based on the simplified model of the length of the two-phase zone, described in Equation (B.9), and the simplified model of the pressure, described in Equation (B.14). The disturbance model is

$$\mathbf{E} = \begin{bmatrix} \frac{\partial \dot{\ell}_{2p}}{\partial f_{cp}} & \frac{\partial \dot{\ell}_{2p}}{\partial T_a} \\ \frac{\partial \dot{P}_e}{\partial f_{cp}} & \frac{\partial \dot{P}_e}{\partial T_a} \end{bmatrix} = \begin{bmatrix} 0 & -\frac{\alpha_{2p} \cdot O_{pi} \cdot N_{pi} \cdot \eta'(\bar{\ell}_{2p}) \cdot \bar{\ell}_{2p}}{f_1(\bar{\ell}_{2p}, \bar{P}_e, \dot{\bar{m}}_v, \bar{T}_{c,o})} \\ -\frac{\rho_g(\bar{P}_e) \cdot V_{cp,i}}{f_3(\bar{P}_e)} & \frac{f_4(\bar{P}_e) \cdot \bar{\ell}_{2p}}{f_3(\bar{P}_e)} \end{bmatrix} \tag{B.27}$$

Appendix C

Nomenclature

A_{cp}	compressor surface area
A_e	evaporator cross-section area
A_{pi}	evaporator pipe cross-section area
$c_{cp,w}$	compressor wall heat capacity
C_p	molar specific heat at constant pressure
$c_{p,a}$	air heat capacity
$c_{p,sh}$	superheat zone heat capacity
C_v	molar specific heat at constant volume
D	valve pipe distribution
e_{cp}	compressor efficiency
e_R	valve resistance estimation error
f_{cp}	compressor speed
$h_{c,i}$	condenser input specific enthalpy
h_g	specific enthalpy at evaporator dew point
h_i	evaporator input specific enthalpy
h_l	specific enthalpy at evaporator boil point
h_o	evaporator output specific enthalpy
$\dot{H}_o$	evaporator enthalpy output flow
k_i	PI controller integral gain
k_p	PI controller proportional gain
ℓ_{2p}	length of two-phase zone
L	step response lag
L_e	length of evaporator
ℓ_i	length of i'th part
ℓ_{sh}	length of superheated zone
$\dot{m}_a$	mass flow of air
$\dot{m}_{cp}$	compressor mass flow
$\dot{m}_v$	valve mass flow
$\dot{m}_{v,g}$	valve gas mass flow
N_{pa}	number of parts in evaporator
N_{pi}	number of evaporator pipes
$M_{cp,w}$	compressor wall mass
OD	valve opening degree
O_e	evaporator circumference
O_{pi}	evaporator pipe circumference
P_c	condenser pressure
P_e	evaporator pressure
P_{loss}	compressor power loss
R	step response slope
R_v	valve flow resistance
S	entropy
T_a	evaporator ambient temperature
$T_{c,i}$	condenser input temperature
$T_{cp,o}$	compressor output temperature
$T_{cp,w}$	compressor wall temperature
T_e	evaporator boil temperature
T_o	evaporator output temperature
T_{off}	temp. offset for pressure estimation
$T_{pi,o}$	evaporator pipe output temperature
T_{sh}	evaporator superheat temperature
V'	evaporator gas volume
$V_{cp,i}$	compressor intake volume
v_g	specific volume of gas
v_l	specific volume of liquid
W_{pi}	evaporator pipe width
α_{2p}	two-phase zone heat transfer coefficient
α_{cp}	compressor heat transfer coefficient
α_{sh}	superheated zone heat transfer coefficient
β_a	ambient air temperature factor
β_e	superheated zone length factor
Δh_{cp}	compressor specific enthalpy increase
ΔP	condenser and evap. pressure difference
$\Delta T'$	mean ambient to evap. temp. difference
ε_v	valve opening factor
η	evaporator ambient air temperature factor
γ	adaption time constant
γ_{am}	area mean void fraction
γ_{2p}	two-phase zone void fraction
ρ_g	gas density
ρ_l	liquid density
σ^2	variance
σ^2_{max}	upper variance hysteresis value
σ^2_{min}	lower variance hysteresis value
τ_v	valve open time
τ_{cl}	valve closed time

Accents

$\hat{}$	estimated value
$\bar{}$	operating point value
$\tilde{}$	small signal value

Appendix D

Paper Draft: 'Evaporator Superheat Control with One Temperature Sensor using Qualitative System Knowledge'

Evaporator Superheat Control with One Temperature Sensor using Qualitative System Knowledge

Kasper Vinther, Casper Hillerup Lyhne, Erik Baasch Sørensen and Henrik Rasmussen
Department of Electronic Systems, Section of Automation and Control
Aalborg University, 9220, Denmark
{kv,chlyhne,baasch,hr}@es.aau.dk

***Abstract*—This paper proposes a novel method for superheat control using only a single temperature sensor at the outlet of the evaporator, while eliminating the need for a pressure sensor. An inner loop controls the outlet temperature and an outer control loop provides a reference set point, which is based on estimation of the evaporation pressure and suitable reference logic. The pressure is approximated as being linear and proportional to the opening degree of the expansion valve. This gain and the reference logic is based on calculation of the variance in the outlet temperature, which have shown to increase at low superheat. The parameters in the proposed controller structure can automatically be chosen based on two open loop tests. Results from tests on two different refrigeration systems indicate that the proposed controller can control the evaporator superheat to a low level giving close to optimal filling of the evaporator, with only one temperature sensor. No a priori model knowledge was used and it is anticipated that the method is applicable on a wide variety of refrigeration systems.**

***Index Terms*—Refrigeration system, Vapor compression, Evaporator, Superheat, Control, Estimation, variance.**

I. Introduction

Refrigeration systems normally operate by continuous vaporization and compression of refrigerant. This process is maintained by a valve, an evaporator, a compressor and a condenser, and this setup remains to a considerable extent the same in most refrigeration systems. The details of the vapor compression type refrigeration process are not given here, but can be found in e.g. [1]. Refrigeration systems are typically controlled by decentralized control loops and evaporator superheat is controlled in one of these loops.

Superheat control can be achieved by regulating the opening degree of the expansion valve. Superheating of the refrigerant beyond the evaporation temperature is important, since no superheat means that two-phase refrigerant will enter the compressor and consequently damage it. This means that the flow through the valve must be kept a level, where all the refrigerant is evaporated before it reaches the compressor. At the same time, it is important to have as much two-phase refrigerant in the evaporator as possible, to increase the heat transfer and thus optimize the refrigeration process. So a key variable, which greatly effects the efficiency of a refrigeration system, is the superheat, which again is an indirect measure of the filling of the evaporator.

The heating, ventilating and air conditioning (HVAC) industry commonly use some variant of proportional-integral (PI) feedback control [2]. These controllers have traditionally been tuned by refrigeration and control specialists, due to the complexity and nonlinearity of the refrigeration process and the huge amount of different refrigeration system designs available. The problem is that the human operator often copies parameter values from any previous system in the hope that the new refrigeration system will work with these settings. However, each system is associated with different optimal working point conditions, sensor/actuator configurations and cooling demands. Furthermore, the tuning process can be time consuming and there is a risk of system damage, if the operator is not cautious. It is therefore desirable to automate the tuning process of controllers for refrigeration systems and/or implement adaptive algorithms.

Automatic tuning of PI/PID controllers have been treated in many books, see e.g. [3] and [4]. The relay method is used in [5] to obtain the ultimate frequency and gain, which is used to find PID controller parameters based on model knowledge. These parameters are compared with Zeigler-Nichols tuned parameters and model based gain scheduling is additionally employed to cope with the operating point dependent system gain. In [6], auto-tuners for PI/PID control of HVAC systems are designed based on a combination of relay an step tests. The auto-tuners show better performance than manual tuning and standard relay auto-tuning.

The response from valve opening degree to superheat is in general very nonlinear, making controller tuning difficult. The need for gain scheduling in [5] is eliminated in [7], by transferring the superheat to a referred variable. In both papers a cascaded control setup is utilized, where a flow meter is used to control the refrigerant mass flow in an inner loop. However, most refrigeration systems does not have such a sensor and [8] instead proposes a cascaded control, where evaporator pressure measurements are used in an inner loop to reduce the nonlinearities. Backstepping can also be used to design a nonlinear controller, as done in [9]. This controller can be made almost independent of the cooling capacity and therefore does not require any gain scheduling. Another possibility is to control the superheat with the compressor and the cooling capacity with the valve. In [10], backstepping is again used to derive a nonlinear controller. However, extensive model knowledge is required in both cases and some model parameters are only partly known and varies with the operating conditions, thus requiring adaptive methods for finding these parameters, which has been pursued in [10].

All the controllers mentioned so far require at least a temperature sensor and a pressure and/or a flow meter to control the filling of the evaporator. In this paper, we will present a novel control method capable of controlling the filling with only one temperature sensor placed at the outlet of the evaporator. This will make it easier to install and buy superheat controllers based on electronic valves. The method utilize that the variance of the output temperature increases when the evaporator is close to overflowing and this gives a fix point, where the gain, in a simple linear model relating the valve opening degree to the pressure, can be identified. The estimated pressure can then be converted into evaporation temperature and thus a reference for a simple PI controller for the output temperature. Furthermore, the reference is slowly decreased until the fix point is reached and then stepped back. This makes it possible to adaptively correct the gain in the linear model each time the fix point is reached and ensures that the system is continuously operated close to where the evaporator is fully filled (low superheat). In other words, qualitative system knowledge is used to identify when the filling of the evaporator is suitable and the method is independent of the working point and it has been shown in tests that the method works on two completely different vapor compression type refrigeration systems. Additionally, only two open loop tests are required to set the control parameters and these tests can be performed in an automated fashion. Another benefit of the proposed controller is that no a priori model knowledge is required, which is often the case when e.g. gain scheduling and nonlinear control design methods are used.

The structure of this paper is as follows. The two test refrigeration systems are first presented in Section II. Then, calculation of variance of the output temperature is shown in Section III, followed by a presentation of the control strategy in Section IV. Then, an adaptive pressure estimator is derived in V and the startup procedure is shown in Section VI. Finally, test results are presented in Section VII and conclusions are drawn in Section VIII.

II. System Description

The proposed superheat control method in this paper are designed for unknown vapor compression type refrigeration systems, where no a priori model knowledge is assumed. The method should work on a wide variety of setups and two different types of refrigeration systems have therefore been used for test. The first system is an air conditioning system and the second is a refrigeration system with a water tank and heater as load on the evaporator. Simplified drawings of these systems are shown in Figure 1.

The air conditioning system in Figure 1(a) has a finned-tube evaporator with four channels and a Danfoss Ecoflow^{TM} valve. It is possible to control the opening degree (OD) of the valve and the distribution of flow into the individual pipes, however, the distribution is kept constant in this setup. Furthermore, it is possible to control the frequency of both the evaporator and condenser fans, and also the frequency of the fans between the cold room, the hot room and the outside. The scroll compressor frequency is also controllable and sensors measure temperature and pressure at the indicated places.

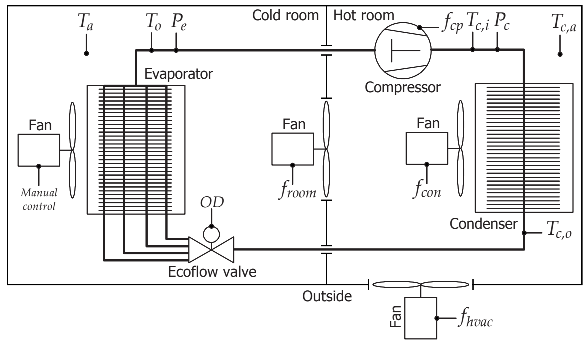

(a)

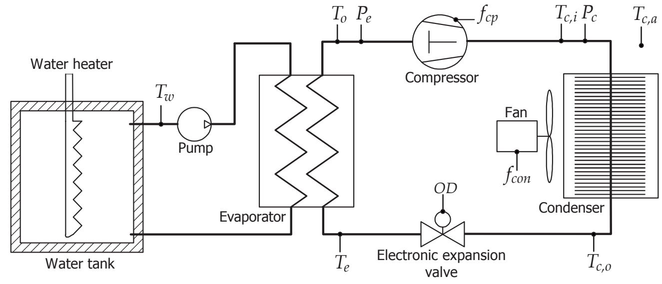

(b)

Fig. 1. Simplified drawings of the two available test systems. T, P and f are indicators for temperature sensors, pressure sensors and frequency control, respectively. Only T_o and OD are used for the superheat control and the other sensors are used for verification purposes. System (a) is an air conditioning system and system (b) is a refrigeration system with water on the secondary side of the evaporator.

The refrigeration system in Figure 1(b) has an evaporator with water on the secondary side, which is connected to a water tank with controllable heater and pump. It is possible to control the OD of the electronic expansion valve and the frequency of the condenser fan. The compressor frequency is again controllable and sensors measure temperature and pressure at the indicated places. Both systems are monitored and controlled using the XPC toolbox for Simulink.

Evaporator superheat T_{sh} is defined as the output temperature T_o minus the evaporation temperature T_e and the evaporation temperature is normally measured indirectly by measuring the evaporation pressure P_e. We propose a control method, which does not require an direct or indirect measurement of T_e, but only the T_o measurement. Instead, qualitative system knowledge is used to calculate the variance on T_o to estimate P_e, which is further discussed in Section III. This makes this controller easier to install and buy, compared to other superheat controllers using electronic expansion valves, since we save a pressure sensor.

In the following it is assumed that the condenser pressure is controlled separately and that the compressor is running at constant frequency, which means that any change is considered as a disturbance.

III. Variance Calculation

An open loop test has been performed on each of the test systems, where the OD signal was increased slowly while output temperature T_o measurements were saved. By calculating the sample variance as

$$\sigma^2 = \frac{1}{n}\sum_{i=1}^{n}(x_i - \bar{y})^2 \tag{1}$$

$$\bar{y} = \frac{1}{n}\sum_{i=1}^{n} x_i \tag{2}$$

where σ^2 is the sample variance using n samples, x_i is the i'th sample and $\bar{y}$ is the sample mean, then it is possible to get an estimate of the variance in the output temperature. Figure 4 and 5 shows the test results using a five minute sample window on the air conditioning system and the refrigeration system, respectively. The system response is clearly different between the two systems, however, the tests indicate, in both cases, that the variance increases considerably at low superheat and then decreases again when the evaporator is flooded. This increase in variance can be used to identify when the evaporator is nearly flooded and provides an alternative way of controlling the filling of the evaporator compared to conventional control.

IV. Control Strategy

The control strategy is illustrated in Figure 2. A simple PI feedback control is used in an inner loop to control the evaporator outlet temperature T_o and an outer loop provides the temperature controller with a suitable reference set point.

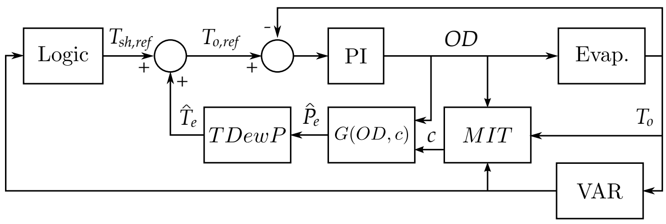

Fig. 2. Control structure for control of the evaporator outlet temperature. A suitable reference is found based on adaptive estimation of the evaporation temperature and superheat reference logic.

The Logic block in Figure 2 controls the superheat reference, which is implemented so that it continuously decreases in temperature until the variance has increased to a predetermined variance level σ^2_{high}. Then it is stepped back and the cycle is repeated, so that the superheat is constantly kept at a low level despite a change in system load. A waiting period is introduced during startup, which prevents the reference from decreasing until the system has calmed down and the variance is below the hysteresis bound σ^2_{low}, see Figure 4 for a definition of the variance levels. Furthermore, a step back in reference can only be made if the system has calmed down since last step, since a step will cause a temporary increase in variance. A larger step back in reference is taken if the system did not calm down since last step and the reference decreased to the level where it was at the last step. For further safety, the reference is also stepped back if the superheat reference goes below 1 degree.

The reference to the inner loop $T_{o,ref}$ is made by adding the superheat reference $T_{sh,ref}$ with an estimated evaporation temperature $\hat{T}_e$. The estimated evaporation temperature is based on an estimate of the evaporator pressure, which in steady state can be approximated as being proportional to the OD signal. The gain c from OD to $\hat{P}_e$ is adapted using the MIT rule and updated each time the reference logic brings the evaporator to a state where it is nearly flooded, which can be identified by an increase in variance. It is important to note that no pressure sensor is used in this setup. Design of a pressure estimator and adaption is treated in Section V.

The startup procedure should be made so that the control can start automatically and work on a wide variety of refrigeration systems. This is the subject of Section VI, where it is shown how the controller can be tuned based on two open loop tests.

V. Pressure Estimator Design and Adaption

The fundamental concept of conservation of mass in physics (refrigerant is neither added nor removed from the system), implies that the mass flow rate $\dot{m}$ through a tube is constant and equal to the product of the density ρ, velocity v and cross-sectional area A:

$$\dot{m} = \rho v A \tag{3}$$

If assuming laminar, inviscid and incompressible refrigerant mass flow rate through the expansion valve, then Bernoulli's equation furthermore states that

$$\frac{1}{2}v^2 + gz + \frac{P}{\rho} = c \tag{4}$$

where g is the gravitational constant, z is the elevation, P is the pressure and c is a constant, which does not change across the valve. Combining Equation 3 and 4, while isolating for the mass flow, gives

$$\dot{m}_v = \sqrt{P_c - P_e}\sqrt{\rho_l}C_v \tag{5}$$

where P_c and P_e are the pressures in the condenser and the evaporator, ρ_l is the density of the liquid refrigerant and C_v is a collection of constants. Equation 5 is consistent with the result in e.g. [11] for a fully open expansion valve and C_v is also called the orifice coefficient.

A variable opening degree (OD) term for the valve is added to Equation 5. The OD is in most systems a linear function going from zero (closed) to one (fully open), however, it might also be nonlinear and therefore a constant ϵ_v, which in most cases is very small, is added as the power of OD, as shown in Equation 6.

$$\dot{m}_v = OD^{1+\epsilon_v}\sqrt{P_c - P_e}\sqrt{\rho_l}C_v \tag{6}$$

In steady state, the mass flow through the valve $\dot{m}_v$ must be equal to the mass flow through the compressor $\dot{m}_c$, which can be calculated as the product between the compressor frequency f_{cp}, the compressor inlet volume V_{cp} and the density of the gaseous refrigerant ρ_g.

$$\dot{m}_v = \dot{m}_c = f_{cp}V_{cp}\rho_g \tag{7}$$

The mass flow $\dot{m}_c$ is essentially the product between a constant and the evaporator pressure P_e, when the system is in steady state (P_e is proportional to ρ_g). However, this is only true if the compressor speed is held constant. Equation 6 can also be simplified if it is assumed that the fluctuations in the square root of the difference in pressure is negligible small and that the density of the liquid refrigerant is constant. Combining Equation 6 and 7 with simplifications, gives a steady state equation for the evaporator pressure P_e with variable OD

$$P_e = cOD^{1+\epsilon_v} \tag{8}$$

where c is a further collection of constants. A first order filter is now introduced, see Equation 9, since the outer loop has to be slower than the inner loop for stability. This can be handled by choosing the time constant τ appropriately.

$$\frac{P_e(s)}{OD^{1+\epsilon_v}(s)} = \frac{c}{\tau s + 1} \tag{9}$$

The gain c in the simplified expression is very dependent on the working point and on the characteristics of the given refrigeration system. Therefore, an adaptive update of the constant c is introduced, in order to better estimate the pressure. Furthermore, the value of epsilon is not critical as long as c is fairly accurate. In practice, reasonable performance is expected with $-0.5 < \epsilon_v \leq 0$.

By continuously calculating the variance of the output temperature, while slowly increasing the OD signal, it is possible to detect the point when the evaporator is close to being fully flooded. This was also discussed in Section III and the point is used as a fix point to find a good estimate of the gain c^* in the fix point, by using Equation 8, since OD is known along with the pressure at the fix point P_e^*. The pressure is not measured directly but can be calculated based the measured evaporator output temperature T_o^* and a predetermined offset temperature T_{off} as

$$P_e^* = PDewT(T_o^* - T_{off}) \tag{10}$$

where the refrigeration equation software package RefEqns by Morten Juel Skovrup has been used, however, there are many other software packages that can do the conversion. Figure 3 shows a plot of the evaporator pressure P_e, while OD is gradually increased in open loop on the air conditioning system shown in Figure 1(a).

The dot marks the identified fix point, where the evaporator is nearly flooded. The estimated linear pressure $\hat{P}_e$ based on the estimated gain c is also shown in the figure. It is undesirable to change the value of the gain c instantly in closed loop, since this could result in unstable behavior. The MIT rule is therefore used to adapt the gain c slowly and it is defined as (see e.g. [4]):

$$J = \frac{1}{2}e^2 \tag{11}$$

$$\frac{d\theta}{dt} = -\gamma\frac{\partial J}{\partial\theta} = -\gamma e\frac{\partial e}{\partial\theta} \tag{12}$$

where J is an objective function to be minimized, e is the error, θ is the adjustable parameter to be adapted and γ is the adaption gain.

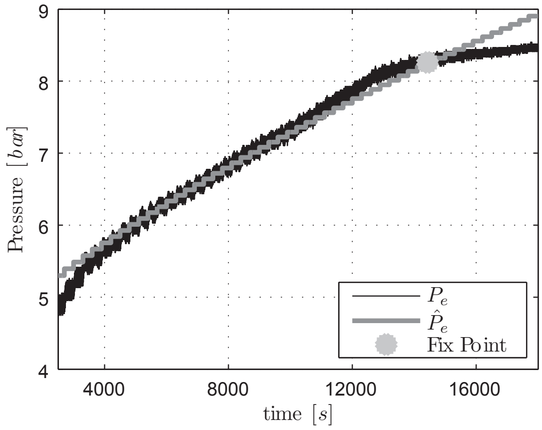

Fig. 3. Measured evaporator pressure during an OD sweep and resulting linear estimated pressure based on the gain c, found in the marked fix point.

The MIT rule can be interpreted as a gradient method for minimizing the error and in the case of adapting the gain c we have

$$\theta = c \tag{13}$$

$$e_c = c - c^* \tag{14}$$

$$\frac{dc}{dt} = -\gamma e_c \tag{15}$$

since the partial derivative of e_c is equal to 1. The gain c^* is the gain obtained at the last fix point and the gain c is the current gain.

Only the adaption gain γ has to be chosen. In general a small γ means slow convergence and a large γ means fast convergence and possibly instability. However, it is hard to say in general how γ influences time variant systems. In the tests on the refrigeration systems γ has been chosen small and thus conservatively. Another possibility would be to use the normalized MIT rule, which would lead to less sensitivity towards signal levels or one could use Lyapunov stability theory to adapt the gain c, and most likely obtain faster adaption and stability guarantees.

VI. Startup Procedure

All parameters in the controller can be determined based on two open loop tests. The OD signal is increased slowly in the first test, while the outlet temperature T_o is measured and its variance is calculated. The test can be stopped when the variance plot shows a clear peak and has decreased to a low level again. The result on each of the test systems is presented in Figure 4 and 5.

The variance levels σ^2_{low} and σ^2_{high} are set to

$$\sigma^2_{high} = \frac{1}{2}max(\sigma^2) \tag{16}$$

$$\sigma^2_{low} = \frac{3}{4}\sigma^2_{high}) \tag{17}$$

where $max(\sigma^2)$ is the highest variance during the OD sweep.

A temperature offset T_{off} is required in Equation 10 to determine the gain c and thus the evaporator pressure. This temperature offset accounts for the temperature difference

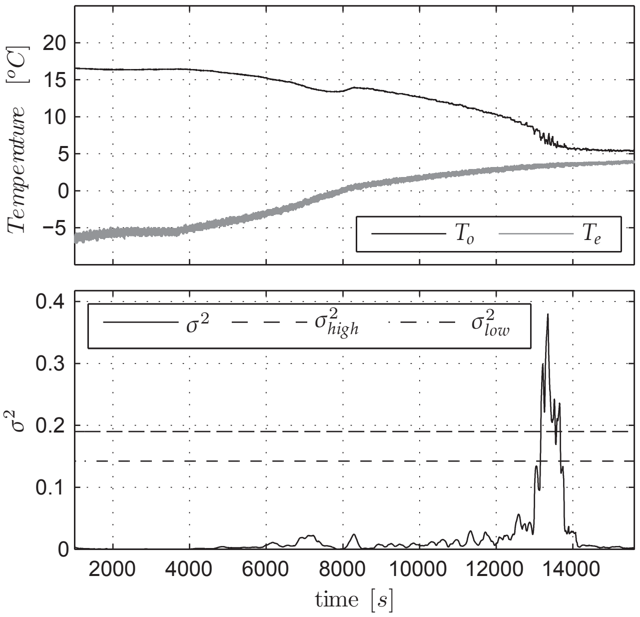

Fig. 4. Evaporator outlet temperature and variance during an *OD* sweep on the air conditioning system.

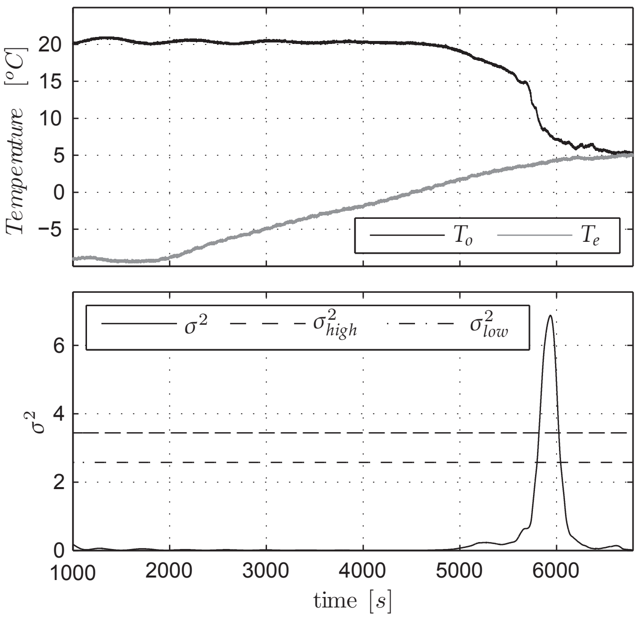

Fig. 5. Evaporator outlet temperature and variance during an *OD* sweep on the refrigeration system.

between the outlet temperature T_o^*, when the high variance threshold σ^2_{high} is reached and an estimate of the evaporation temperature. This estimate is set to be the lowest outlet temperature measured during the *OD* sweep test and gives $T_{off} = T_o^* - min(T_o)$. A start guess of the gain c is then obtainable from Equation 8 and 10. The choice of exponent *epsilon* is not that critical and can in most cases be set to 0, since the gain c is adapted.

The second open loop test is a small upward step in *OD* at low superheat, while T_a or T_w is close to T_e, which is considered as a worst case operating point. This test is used to tune the PI controller based on Ziegler-Nichols tuning with quarter decay ratio, see e.g. [12]. The transfer function of the PI controller is defined as

$$D(s) = k_p\left(1 + \frac{1}{T_I s}\right) \tag{18}$$

$$k_p = \frac{0.9}{RL} \tag{19}$$

$$T_I = \frac{L}{0.3} \tag{20}$$

where R is the slope of the reaction curve and L is the lag obtained from the step test. The PI controller is tuned at an operating point, where the temperature and refrigerant flow is low, which gives the highest system gain. This gives a conservative controller and ensures that the system is stable at all other operating points. The selected worst case operating point is supported by e.g. [13]. The slope R was measured to be -8.08 and -0.95, for the air conditioning system and refrigeration system, respectively, and the lag L was 23.6 and 27.6. These parameters can also be used to determine a suitable value for the reference decrease rate and the time constant τ, since these measures gives an indication of how fast/slow the system is. During the tests presented in Section VII, the reference decrease rate and reference step size was set to 3/1000 and 3, respectively, and τ was set to 30 seconds.

VII. Test Results

Figure 6 shows the result from a test of the controller on the air conditioning system. The estimated superheat $\hat{T}_{sh}$ follows the reference well and the reference is slowly decreased and then stepped back each time the variance gets too high, which indicates low superheat. The measured superheat T_{sh}, using a pressure sensor, is shown for comparison and the difference between the estimated and measured superheat gets smaller as the estimate of the gain c is adjusted.

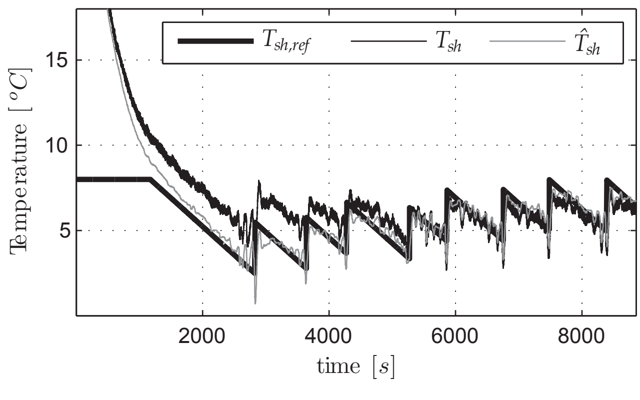

Fig. 6. Closed loop test results on the air conditioning system.

A similar test was conducted on the air conditioning system, where the load was changed by blowing air from the hot room to the cold room. This caused a sudden rise in ambient temperature and thus a change in the load. Figure 7 shows that this disturbance is handled by the controller.

Figure 8 finally shows the result from a test of the controller on the refrigeration system. A change in load was also made in this test, by changing the temperature set point in the water tank with the water heater shown in Figure 1(b).

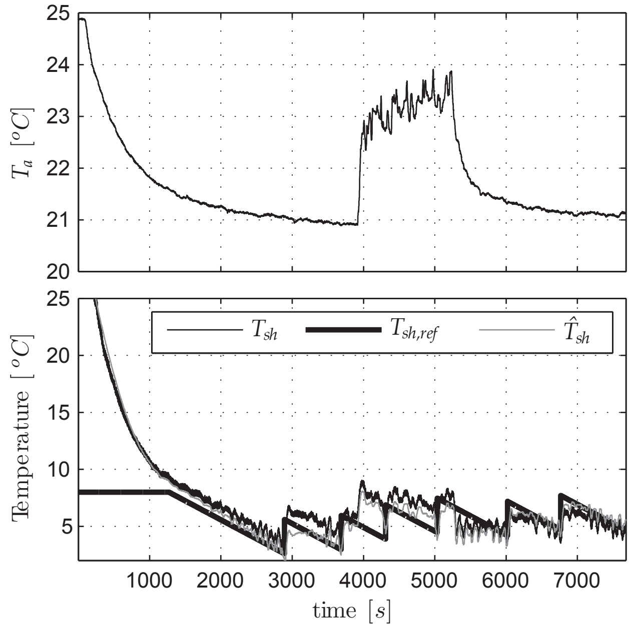

Fig. 7. Closed loop test results on the air conditioning system with a sudden change the in ambient air temperature.

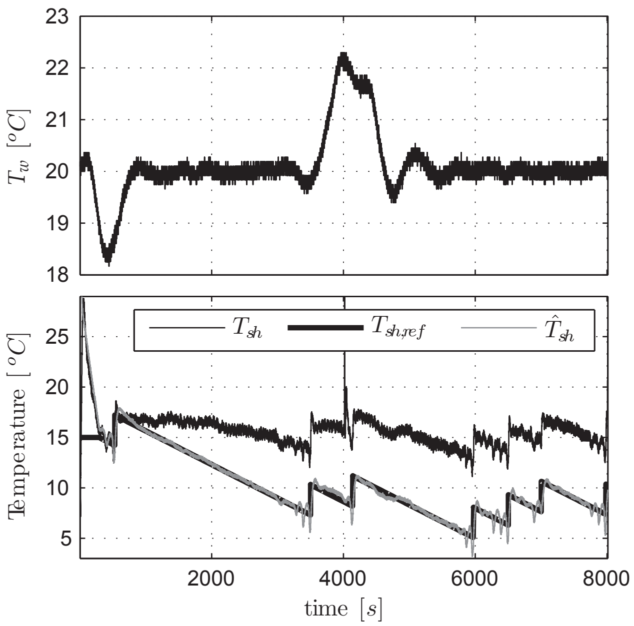

Fig. 8. Closed loop test results on the refrigeration system with a sudden change in the water temperature.

The estimated superheat follows the reference superheat and is stepped back each time the variance gets to high, as anticipated. However, there is approximately a 5 degree temperature offset between the estimated and measured superheat. This is because the variance starts to increase a little earlier in closed loop, and the temperature offset T_{off} was estimated in open loop. The T_{off} estimate could be improved by allowing a small overflow in closed loop. However, if comparing the actual superheat of about 15 degree with Figure 5, then this superheat corresponds to a working point just before the steep slope, which happens over 2-3 quantizations in the valve *OD*. Controlling the superheat to a point on the middle of the slope is quite difficult and the obtained superheat is close to optimal.

The PI controller parameters are chosen conservatively in a situation with low flow and temperature. The controller response time could possibly be improved by limiting the operating range of the system or by adding some kind of gain scheduling. However, the gain scheduling should only be based on the information given by the evaporator outlet temperature measurement. Feed forward, when a step in the reference is made, could also improve the controller.

VIII. Conclusion

Evaporator superheat control is important in order to optimize the heat transfer coefficient in refrigeration systems and to prevent compressor wear. The superheat is conventionally obtained by subtracting the evaporation temperature, given by a pressure sensor, from the temperature at the evaporator outlet. In this paper we have shown that the pressure sensor can be saved by looking at the variance in the outlet temperature, which have shown to increase at low superheat. Results from tests on two different refrigeration systems indicate that the proposed controller, using qualitative system knowledge, can control the evaporator superheat to a low level giving close to optimal filling of the evaporator, with only one temperature sensor. No a priori model knowledge was used and it is anticipated that the method is applicable on a wide variety of refrigeration systems.

References

[1] Ibrahim Dincer and Mehmet Kanoglu. *Refrigeration Systems and Applications*. Wiley, 2nd edition, 2010.

[2] John E. Seem. A New Pattern Recognition Adaptive Controller with Application to HVAC Systems. *Automatica*, 34(8):969–982, 1998.

[3] Karl J. Åström and Tore Hägglund. *Automatic Tuning of PID Controllers*. Instrument Society of America, 1988.

[4] Karl J. Åström and Björn Wittenmark. *Adaptive Control*. Addison-Wesley Publishing, 2nd edition, 1995.

[5] Henrik Rasmussen, Claus Thybo, and Lars F. S. Larsen. Automatic Tuning of the Superheat Controller in a Refrigeration Plant. *7th Portuguese Conference on Automatic Control, Lisboa, Portugal*, 2006.

[6] Qiang Bi, Wen-Jian Cai, Qing-Guo Wang, Chang-Chieh Hang, Eng-Lock Lee, Yong Sun, Ke-Dian Liu, Yong Zhang, and Biao Zou. Advanced controller auto-tuning and its application in HVAC systems. *Control Engineering Practice*, 8(6):633–644, 2000.

[7] Henrik Rasmussen, Claus Thybo, and Lars F. S. Larsen. Nonlinear Superheat and Evaporation Temperature control of a Refrigeration Plant. *IFAC ESC'06 : Energy Saving Control in Plants and Buildings*, 2006.

[8] Matthew S. Elliott and Bryan P. Rasmussen. On reducing evaporator superheat nonlinearity with control architecture. *International Journal of Refrigeration*, 33(3):607–614, May 2010.

[9] Henrik Rasmussen and Lars Finn Sloth Larsen. Nonlinear superheat and capacity control of a refrigeration plant. *17th Mediterranean Conference on Control & Automation*, pages 1072–1077, 2009.

[10] Henrik Rasmussen. Adaptive Superheat Control of a Refrigeration Plant using Backstepping. *International Conference on Control, Automation and Systems*, pages 653–658, 2008.

[11] Xiang-Dong He, Sheng Liu, Harry H. Asada, and Hiroyuki Itoh. Multivariable Control of Vapor Compression Systems. *HVAC&R Research*, 4(3):205–230, 1998.

[12] Gene F. Franklin, J. David Powell, and Abbas Emami-Naeini. *Feedback Control of Dynamic Systems*. Pearson Prentice Hall, 5. edition, 2006.

[13] Dongwon Lim, Bryan P. Rasmussen, and Darbha Swaroop. Selecting PID Control Gains for Nonlinear HVAC&R Systems. *HVAC&R Research*, 15(6):991–1019, 2009.